ABSTRACT

Title of dissertation: A SEARCH FOR LONG-LIVED GLUINOS WITH THE CMS EXPERIMENT DURING BEAM-OFF PERIODS OF THE LARGE HADRON COLLIDER

Kenneth Case Rossato
Doctor of Philosophy, 2011

Dissertation directed by: Professor Sarah Eno
Department of Physics

Many models of new physics include the possibility of a new massive long-lived particle, the existence of which could explain discrepancies between cosmological theories and observations of ^{6}Li and ^{7}Li in the early universe. We search for particles stopping in the CMS detector after production in 7 TeV collisions at the LHC. We look for decays using a specially modified jet trigger, in time periods in which no collisions occur in CMS. In a search interval corresponding to 62 hours of LHC operation, consisting of 10.2 pb^{-1} of integrated luminosity with a peak instantaneous luminosity of 10^{32}cm^{-2}s^{-1}, we observe no significant excess over background. We set a 95% C.L. limit on production of Split-Supersymmetry gluinos over 14 orders of magnitude of gluino lifetime.

A SEARCH FOR LONG-LIVED GLUINOS WITH THE CMS EXPERIMENT DURING BEAM-OFF PERIODS OF THE LARGE HADRON COLLIDER

by

Kenneth Case Rossato

Dissertation submitted to the Faculty of the Graduate School of the
University of Maryland, College Park in partial fulfillment
of the requirements for the degree of
Doctor of Philosophy
2011

Advisory Committee:
Professor Sarah Eno, Chair/Advisor
Professor Andris Skuja
Professor Rabindra N. Mohapatra
Assistant Professor Peter Shawhan
Professor Michael C. Laskowski, Dean's Representative

Dedication

To my grandmother, Marie Rossato.

Acknowledgments

My greatest thanks go to my advisors Sarah Eno and Andris Skuja for their support, encouragement, and patience, without which this document would never have been produced.

Contributions to this document come from members of the CMS Stopped Gluino analysis group: Dr. Sarah Eno, Dr. Andris Skuja, and myself (University of Maryland); Dr. Chris Hill (Ohio State University); Dr. Jim Brooke (University of Bristol, England); Dr. Fedor Ratnikov (Karlsruhe University, Germany); and Dr. Arno Heister (Boston University). New contributing members include Ethan Cowan and Dr. Jeffrey Temple (University of Maryland).

Thanks to support from the University of Maryland High Energy Physics CMS team: Dinko Ferencek, Malina Kirn, Dr. Ellie Lockner, Dr. Drew Baden, Dr. Sarah Eno, Dr. Andris Skuja, Dr. Jeffrey Temple, Dr. Nicholas Hadley, Dr. Richard Kellogg, and Dr. Shuichi Kunori.

Thanks to the full CMS collaboration, the LHC team, CERN, and its member nations and institutions, without whom there would be no data to analyze.

Thanks to the US Department of Energy for the research grant that supports the University of Maryland's CMS efforts, including this work.

Table of Contents

List of Figures

List of Conventions and Abbreviations

x	horizontal axis, Southward from CMS
y	vertical axis, pointing upwards
z	longitudinal axis, along beam-line, Westward ("Jura"-side) from CMS
r	radial distance, from the origin, in the xy plane
ϕ	phi, azimuthal angle, 0 at the positive x axis, $\frac{\pi}{2}$ at the positive y axis
θ	theta, polar angle, 0 at positive z axis, π at negative z axis
η	eta, pseudorapidity, $\eta = -\ln[\tan(\frac{\theta}{2})]$
central	$\|\eta\| < 1.3$, approximately within the HB bounds
forward	$\|\eta\| > 3$, approximately from the beginning of HF to the beam-line
$i\phi$	phi tower index, in units of $\Delta\phi = \frac{\pi}{36} = 0.087$, beginning with 1 from $\phi = 0$
$i\eta$	eta tower index, in units of $\Delta\eta = 0.087$, beginning with 1 from $\eta = 0$ in the positive direction, and -1 in the negative direction
τ	lifetime

UMD	University of Maryland, College Park
SUSY	Supersymmetry
LSP	Lightest Supersymmetric Particle
NLSP	Next-to-Lightest Supersymmetric Particle
LHC	Large Hadron Collider
BX	Bunch Crossing
IP5	Interaction Point 5
CMS	Compact Muon Solenoid
L1	Level 1 Trigger
HLT	High Level Trigger
HCAL	Hadronic Calorimeter
HB	HCAL Barrel
HE	HCAL Endcap
HO	HCAL Outer
HF	HCAL Forward
HPD	Hybrid Photodiode
QIE	Charge-Integrating Electronics
RBX	Read-out Box
HTR	HCAL Trigger and Read-out Card
DCC	Data Concentrator Card
BPTX	Beam Current Monitor
CMSSW	The official CMS Software package
CRAFT	The "Cosmic Rays At Four Tesla" exercise
C.L.	Confidence Level

Chapter 1

Introduction

1.1 Overview

The search for new particles at colliders presents an extraordinary challenge: the collection of vast amounts of data of which only a minute fraction may come from new physics. Particles produced at a collider as high-energy as the Large Hadron Collider (LHC), where this experiment takes place, are predominantly the well-understood elements of the Standard Model of particle physics. Inelastic quantum chromodynamic (QCD) interactions, for example, are four to five orders of magnitude more common at LHC energy than even the most optimistic scenarios for heretofore unobserved particles.

The challenge, therefore, is to be able to discard observations of these well-understood interactions without discarding those due to comparatively infrequent effects. This is usually performed in two steps: producing and collecting large quantities of data, and inventing algorithms to reject unwanted data (background) while preserving data believed to contain evidence of the physics under study (signal).

Most common methods to discard background involve identifying known high-energy-physics phenomena by identifying spectra of understood effects. This search takes an unusual approach of discarding background by looking for new phenomena in a period expected to be void of collider effects entirely. In many colliders, and

in particular the LHC, there are times in which beam is colliding ("beam-on") and times in which it is not ("beam-off"). Under ideal conditions, no observable effects would occur in beam-off periods.

Particles produced under the Standard Model decay into lighter particles at a rate determined by their masses and couplings, as well as those of any particles temporarily produced to mediate the interaction. Particles decaying to those only slightly less massive than themselves, or those decaying via a very small coupling, take longer to decay than others. Particles that decay via an intermediary particle of comparatively large mass also take longer to decay. The time for such a process to occur is independent of any collider or experimental conditions (although it may be boosted by travel at relativistic velocity), and is randomly drawn from an exponential distribution ($n \propto e^{-t/\tau}$). The parameter τ indicates the average lifetime, as measured in the particle's rest-frame.

All particles produced at the LHC either live sufficiently briefly that they decay before interacting with a particle detector ($t, b, \tau, Z, W^{\pm}$), or are sufficiently light that they are produced at a velocity near enough to c that any detector interactions are timed-in (after a calibration that compensates for time-of-flight and cable lengths) and associated with the original production (μ, K, Λ, π).

Should a particle live long enough and travel slowly enough, it would remain in the detector volume long enough to be observed after its production, potentially in beam-off periods. This thesis is a search for such long-lived particles. We have created a special trigger for the collection of data in beam-off periods in the Compact Muon Solenoid (CMS) experiment, and devised methods to discard remaining

background, which consists predominantly of instrumentation noise and incident cosmic rays.

Though this search can be applied to produce a model-independent result, we consider the optimistic and illustrative specific case of split-supersymmetry (split-SUSY) gluinos. Because they would be produced via strong-force processes, in a hadron collider like the LHC they would be seen in comparatively great quantities (~ 600 pb^{-1} at 7 TeV [46, 47]). Furthermore, nuclear interactions from their strong-color charge could cause great energy losses as they pass through detector material [44], leading a larger fraction of produced gluinos to be observable when they decay.

The documentation of this search is organized as follows: an introduction and motivation, the production equipment (The LHC - Large Hadron Collider), the instrumentation (CMS - Compact Muon Solenoid), the experiment (2010 collision running), the characteristics of the signal and simulation used to so predict, the characteristics of the background, the analysis rules, a statistical examination of data selected by the analysis rules, and conclusions that can be drawn from the results.

1.2 Motivation

1.2.1 The Standard Model

$$\partial_\mu\Big(\frac{\partial\mathscr{L}}{\partial(\partial_\mu\Phi^A)}\Big) = \frac{\partial\mathscr{L}}{\partial\Phi^A} \tag{1.1}$$

Under quantum field theory, unbound wave solutions to a Lagrangian under

the Euler-Lagrange equations of motion (Equation 1.1) can be quantized a second time to provide integer occupancy states to solutions of a given momentum $\Phi^A(\mathbf{k})$. These occupancy states correspond to what are commonly referred to as particles [1]. These particles are created and annihilated only by interactions permitted under their Lagrangian. For a simple complex scalar field, a Lagrangian might be given as the following:

$$\mathscr{L} = (\partial^\mu \phi^\dagger)(\partial_\mu \phi) - m^2 \phi^\dagger \phi - \lambda(\phi^\dagger \phi)^2 \tag{1.2}$$

The first two terms describe the behavior of a free particle of mass m. The last term is an interaction term. It describes a vertex where 4 fields meet, each of which may represent a particle being created or destroyed. The coupling constant λ describes the likelihood for this to occur.

The Standard Model of particle physics relates particles with further quantum numbers (beyond occupancy in a momentum state). These numbers are mostly conserved in interactions. Some, such as electric charge, are "abelian" and have a simple additive relationship at interactions. Others are "non-abelian" and have a more complex relationship.

Spin (S) is a non-abelian quantum number; it represents a range of values a particle may have, from $-S$ to S in intervals of 1, for internal angular momentum. Particles may have integer spin (0, 1, etc.; called "bosons") or half-integer spin (1/2, 3/2, etc.; called "fermions"). As a non-abelian quantity, combination of spin at an interaction is complex and requires a rigorous mathematical treatment (such as that

in [2, Ch. 3 and 6]). One consequence immediately relevant, however, is that the number of fermions at an interaction increases or decreases only by multiples of two.

Fermions obey the Dirac equation. One consequence of this is that they have antiparticles. An antiparticle has the same mass and spin, but opposite values for all other quantum numbers. Fermions in the Standard Model are divided into leptons (3 charged and 3 neutral (neutrinos)), and quarks; and have mass and quantum numbers as in Table 1.1. Quarks also have color charge, a non-abelian quantum number, and have a tendency in nature to form color-neutral bound states ("hadrons") via a process called "hadronization".

The Standard Model Lagrangian is as follows:

$$\mathscr{L} = \sum_f \bar{f}(i\partial\!\!\!/ - m_f)f - \frac{1}{4}A_{\mu\nu}A^{\mu\nu} - \frac{1}{2}W^+_{\mu\nu}W^{-\mu\nu} + m_W^2 W^+_\mu W^{-\mu} \tag{1.3}$$

$$-\frac{1}{4}Z_{\mu\nu}Z^{\mu\nu} + \frac{1}{2}m_Z^2 Z_\mu Z^\mu + \frac{1}{2}(\partial^\mu H)(\partial_\mu H) - \frac{1}{2}m_H^2 H^2 \tag{1.4}$$

$$+eJ^{em}_\mu A^\mu + \frac{g}{\cos\theta_W}(J^3_\mu - \sin^2\theta_W J^{em}_\mu)Z^\mu \tag{1.5}$$

$$-\frac{g}{\sqrt{2}}\Big[\bar{u}_i\gamma^\mu\frac{1-\gamma^5}{2}M^{CKM}_{ij}d_j + \bar{\nu}_i\gamma^\mu\frac{1-\gamma^5}{2}e_i\Big]W^+_\mu + h.c. \tag{1.6}$$

$$-\frac{gm_H^2}{4m_W}H^3 - \frac{g^2m_H^2}{32m_W^2}H^4 \tag{1.7}$$

$$+\mathscr{L}_{HV} + \mathscr{L}_{WWV} + \mathscr{L}_{WWVV} \tag{1.8}$$

$$-\sum_f \frac{gm_f}{2m_W}\bar{f}fH \tag{1.9}$$

$$-\frac{1}{4}G^a_{\mu\nu}G^{\mu\nu}_a \tag{1.10}$$

$$-g_sG^a_\mu\bar{u}_i\gamma^\mu T^a_{ij}u_j - g_sG^a_\mu\bar{d}_i\gamma^\mu T^a_{ij}d_j \tag{1.11}$$

and provides the following features:

- Line 1.3: 12 spin-1/2 fermions f of distinct masses m_f and their antiparticles

Group	Particle	q	e	μ	τ	mass
Lepton	$e^{\pm}$	± 1	∓ 1			511 keV
	ν_e, $\bar{\nu}_e$	0	± 1			< 2 eV
	$\mu^{\pm}$	± 1		∓ 1		106 MeV
	ν_μ, $\bar{\nu}_\mu$	0		± 1		< 2 eV
	$\tau^{\pm}$	± 1			∓ 1	1.78 GeV
	ν_τ, $\bar{\nu}_\tau$	0			± 1	< 2 eV
Quark	d, $\bar{d}$	$\mp 1/3$				~ 6 MeV
	u, $\bar{u}$	$\pm 2/3$				~ 3 MeV
	s, $\bar{s}$	$\mp 1/3$				~ 100 MeV
	c, $\bar{c}$	$\pm 2/3$				~ 1.337 GeV
	b, $\bar{b}$	$\mp 1/3$				~ 4.2 GeV
	t, $\bar{t}$	$\pm 2/3$				171 GeV
Boson	A (γ, photon)	0				0
	$W^{\pm}$	± 1				80.40 GeV
	Z	0				91.187 GeV
	H	0				> 114 GeV
	G (g, gluon)	0				0

Table 1.1: Selected constants for Standard Model particles

$\bar{f}$; a massless spin-1 photon A (henceforth also γ), and spin-1 bosons $W^{\pm}$ of mass m_W

- Line 1.4: a spin-1 boson Z of mass m_Z and a spin-0 boson H of mass m_H (the Higgs boson)
- Line 1.5: Electric charge interaction between fermions and photons, and electrical and neutral weak charge interaction between fermions and the Z boson
- Line 1.6: Weak charge interaction between fermions and the $W^{\pm}$ bosons; divided into the lepton components (ν_i, e_i) that conserve generation number (see Table 1.2), and the quark components (u_i, d_i) that may violate generation number via the CKM matrix
- Line 1.7: Higgs boson self-interactions
- Line 1.8: Electro-weak boson (H, A, $W^{\pm}$, Z) interactions
- Line 1.9: Emission/absorption of Higgs at fermions
- Line 1.10: 8 massless gluons G (henceforth also g) that self-interact at 3- and 4-gluon vertices
- Line 1.11: Strong-force interactions between quarks and gluons

1.2.2 Supersymmetry and Split-SUSY

The Standard Model inasmuch as it predicts and constrains observables has frequently been confirmed [4]. However, theoretical considerations and cosmological

	Generation		
	I	II	III
Lepton	e^-	μ^-	τ^-
	ν_e	ν_μ	ν_τ
Quark	u	c	t
	d	s	b

Table 1.2: Standard Model fermions divided into generational pairs. Particles interact with their partner at a $W^\pm$ boson, with occasional exceptions for the quarks.

observations lead many to believe that the Standard Model is incomplete and that new particles may exist at unprobed energies. The "hierarchy problem" is one such problem: the Higgs mass under the Standard Model is determined by the subtraction of 2 constants on the order of the Planck scale, 10^{30} GeV^2, to result in an term on the order of 10^6 GeV^2 (Equation 1.12). This "fine tuning" is considered extraordinarily unnatural and motivates proposals of new physics at higher mass scales that makes a light Higgs more natural [5].

$$m_H^2 = m_0^2 + \delta m_H^2 \sim m_0^2 - g^2\Lambda^2 \tag{1.12}$$

One such model of new physics is supersymmetry (SUSY). SUSY introduces a new bosonic "superpartner" for each fermion (and vice versa) with the same quantum numbers except spin, which differs by 1/2 (Table 1.3 describes these superpartners, their names, and notation). This results in a cancellation in corrections to the Higgs mass, so that it no longer has a term quadratic in the Planck scale Λ. SUSY

introduces an additional quantum number R that distinguishes superpartners from the original lower-mass particle. In theories in which R-parity is conserved, SUSY particles must increase or decrease by multiples of 2 at vertices (like fermions).

Superpartners include partners to the fermions: "squarks", "selectrons", "smuons", "staus", and "sneutrinos"; all of which have a spin of zero under the Minimum Supersymmetric Standard Model (MSSM). The massive fermions have 2 partners each to match the number of degrees of freedom (Dirac fermions have 4, complex scalar fields have 2 each).

In the MSSM, the Standard Model Higgs is replaced by 4 scalars, 2 charged and 2 neutral. The partners to the neutral electro-weak bosons (h_u^0, h_d^0, γ, Z) are called "neutralinos", of which there are four ($\tilde{\chi}_i^0$), although due to a potentially non-diagonal mass matrix, none is presumed to correspond to a particular Standard Model particle.

Similarly, the 4 charged electro-weak bosons ($h_u^+, h_d^-, W^\pm$) are paired with 2 pairs of "charginos" ($\tilde{\chi}_i^\pm$). Again, the mass eigenbasis of the charginos does not necessarily correspond to that of the charged electro-weak bosons.

Finally, the supersymmetric partner of a gluon is a "gluino" ($\tilde{g}$).

R-parity conservation, if true, implies that all SUSY particles decay into at least one other SUSY particle. Since the lightest SUSY superpartner has no lighter superpartner to decay to, it must therefore be stable. This is called the LSP (lightest supersymmetric particle), and is under many models a neutralino ($\tilde{\chi}_1^0$). This could be a candidate for dark matter currently suggested by astronomical observations.

"Split-supersymmetry" (split-SUSY) is a variant of supersymmetry in which

Particle	Spin	Superpartner	Name	Spin
q	1/2	$\tilde{q}$	squark	0
e	1/2	$\tilde{e}$	selectron	0
μ	1/2	$\tilde{\mu}$	smuon	0
τ	1/2	$\tilde{\tau}$	stau	0
ν	1/2	$\tilde{\nu}$	sneutrino	0
h_u^0, h_d^0	0	$\tilde{\chi}_i^0$	neutralino	1/2
γ	1	$\tilde{\chi}_i^0$	neutralino	1/2
Z	1	$\tilde{\chi}_i^0$	neutralino	1/2
h_u^+, h_d^-	0	$\tilde{\chi}_i^\pm$	chargino	1/2
$W^\pm$	1	$\tilde{\chi}_i^\pm$	chargino	1/2
g	1	$\tilde{g}$	gluino	1/2

Table 1.3: Supersymmetric partners of Standard Model particles in the Minimum Supersymmetric Standard Model (MSSM) [5].

the squarks are much heavier than the other superpartners. As a result, gluino decay is suppressed by a very high squark mass ($\tilde{g} \to \tilde{q}q \to \tilde{\chi}_1^0 qq$), making gluinos meta-stable.

The subject of this thesis is a search for the signal produced by decays of split-SUSY gluinos ($\tilde{g}$).

1.2.3 Other Standard Model Extensions

Other extensions to the Standard Model produce some phenomenology similar to split-SUSY: a heavy meta-stable particle that may stop and decay within the CMS detector apparatus at the LHC during beam-off crossings. Even within the previously discussed MSSM, some research has shown parameter ranges that may result in long-lived staus [6].

Another SUSY model predicting potentially long-lived particles is "Gauge Mediated Supersymmetry Breaking" (GMSB). In GMSB it is proposed that ordinary gauge (electro-weak, strong) interactions break the symmetry between particles and their superpartners, rather than gravity, as in mSUGRA, the most common SUSY model with a supersymmetry-breaking mechanism. As a result, a graviton superpartner (called "gravitino") becomes the LSP, and the next-to-lightest supersymmetric particle (NLSP) decays primarily to its Standard Model partner and a gravitino. This decay may be suppressed by a very weak coupling constant (F^{-1}, where F is the scale of supersymmetry breaking), causing this superpartner to be potentially long-lived [7].

Beyond SUSY, "hidden valley" scenarios [8, 9] and some grand unified theories where decay is suppressed by dimension 5 or 6 operators [10] may also predict heavy long-lived particles.

1.2.4 Cosmological Evidence

Astronomical observations also provide motivation into the search for long-lived particles. Models of nucleosynthesis during the Big Bang suggest inconsistencies with observations of ^{6}Li and ^{7}Li isotopes produced during the early universe. The abundance could be reconciled with the existence of a particle with lifetime on the order of 100-1000 seconds [11, 12, 13].

1.2.5 DØ Search

The DØ Collaboration published in 2007 limits on production of split-SUSY gluinos from $p\bar{p}$ collisions at 1.96 TeV center-of-mass energy. From comparison of simulated gluinos at $m_{\tilde{g}} = 200$, 300, 400, and 500 GeV, and 410 pb^{-1} to data from the Tevatron (1.96 TeV $p\bar{p}$ synchrotron, 1987-present) at Fermilab, Batavia, IL, the collaboration was able to exclude the existence of split-SUSY gluinos of $m_{\tilde{g}} < 270$ GeV [14]. Figure 1.1 shows cross-section limits as a function of $m_{\tilde{g}}$ for 3 different gluino lifetimes.

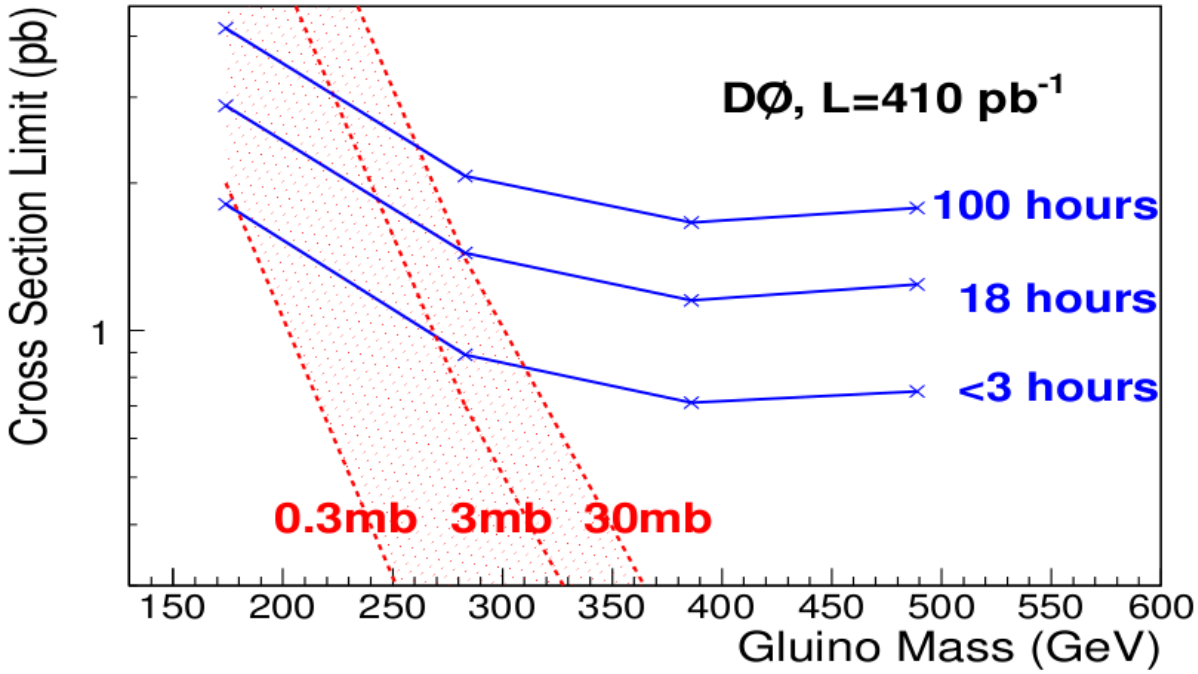

Figure 1.1: The most competitive pre-existing cross-section limit on stopped gluinos, from the DØ Collaboration. Blue text is lifetime. Assumes $m_{\chi_1^0} = 50$ GeV

Chapter 2

The Large Hadron Collider

2.1 Overview

The Large Hadron Collider at the European Organization for Nuclear Research (CERN), Geneva, Switzerland, is a 27 kilometer circumference synchrotron storage ring designed to collide proton bunches at center-of-mass energy up to 14 TeV. The LHC was designed to collide protons at a rate as high as $10^{34}\text{cm}^{-2}\text{s}^{-1}$ [18], a luminosity that results in a rate of top-quark pair production as high as 8.5 per second [15], and $Z/W^{\pm}$ production as much as 3 orders of magnitude higher [16].

The LHC began running in September 2008 but experienced a serious failure 9 days later that delayed subsequent startup until November 2009. The LHC began collisions at injection energy (900 GeV) and, following a winter shutdown, began its physics program at 7 TeV, running from March to November 2010.

The LHC, as a synchrotron, accelerates its beams via an electrostatic radio-frequency (RF) kicker system. Time-varying RF standing waves are generated in a sinusoidal cavity, and the system is timed so that particles experience positive potential during their stay in the system. This implies the necessity to bunch the beam, so that no protons will experience negative voltage periods. The phenomenon of "phase-stability" [3, p.341] is exploited to concentrate bunches to a 2.5 ns sub-section of a 25 ns period.

Size of gap, in bunches	Number of gaps per orbit
8	27
38	8
39	3
119	1

Table 2.1: Size and quantity of beam-gaps in the nominal bunch LHC bunch structure.

Not every 25 ns bucket in each beam has a proton bunch; there are gaps. The largest of these gaps, at the end of nominal cycle, leaves enough time for the LHC beam dump magnets to switch on, so that beam doesn't traverse this region during an intermediate magnetic state and travel into walls or equipment.

Other periodic gaps are in place due to analogous considerations in the LHC pre-accelerators: the Proton Synchrotron (PS) and associated Booster (PSB), and the Super Proton Synchrotron (SPS) (see Figure 2.1). These are smaller rings and thus contain fewer bunches than necessary to completely fill the LHC. As trains of bunches are injected from the PS into the SPS, and then from the SPS into the LHC, a gap is included with sufficient length to accommodate the injection-system magnet rise-time between each pair of accelerators. The combination of multiple cycles from each machine results in a complex nominal bunch structure with numerous gaps of varying sizes shown in Figure 2.2 and described in Table 2.1.

Other bunching schemes may be necessary for temperature and other practical considerations, and are documented in [21]. Bunching schemes for start-up

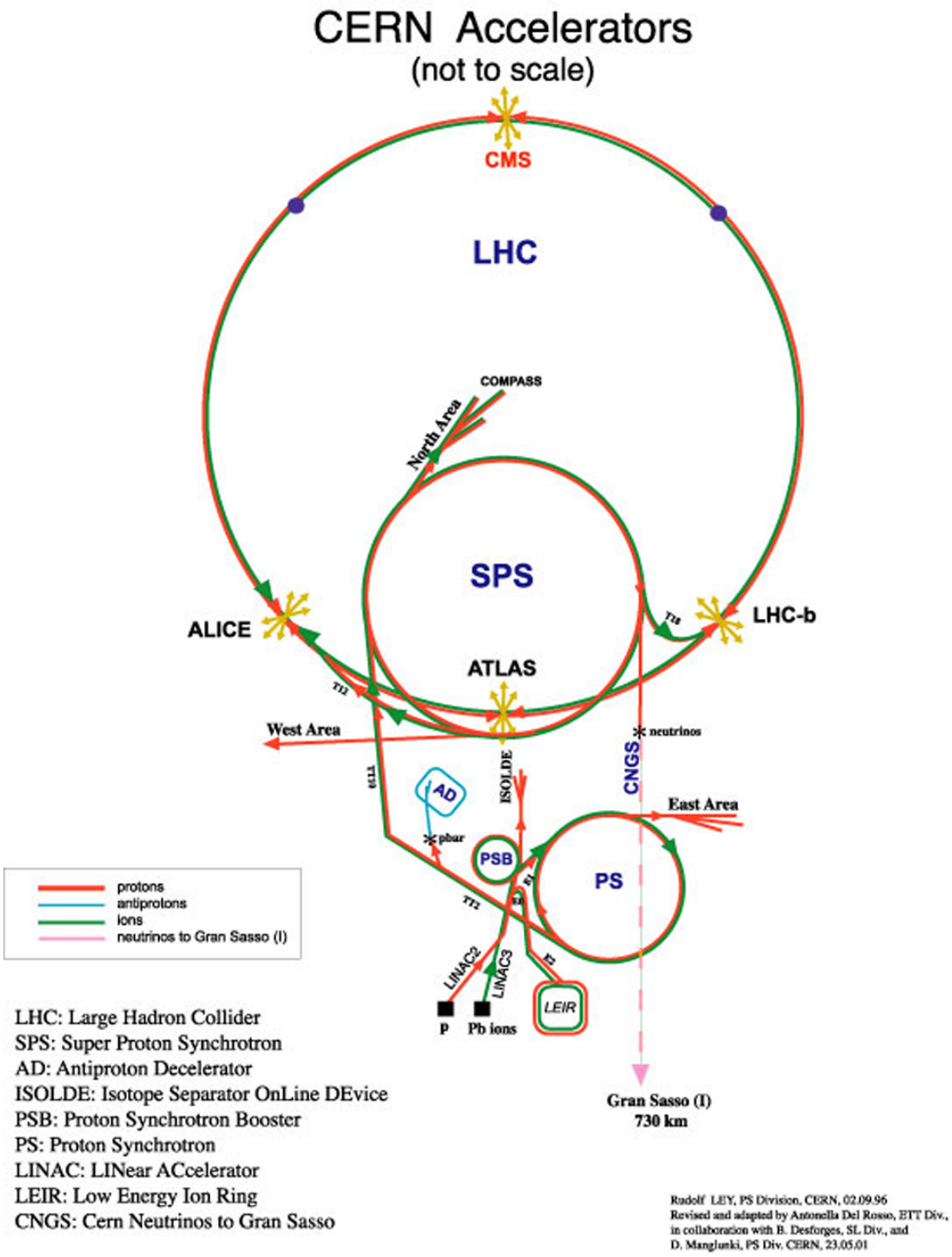

Figure 2.1: The CERN accelerators and experimental regions (courtesy CERN)

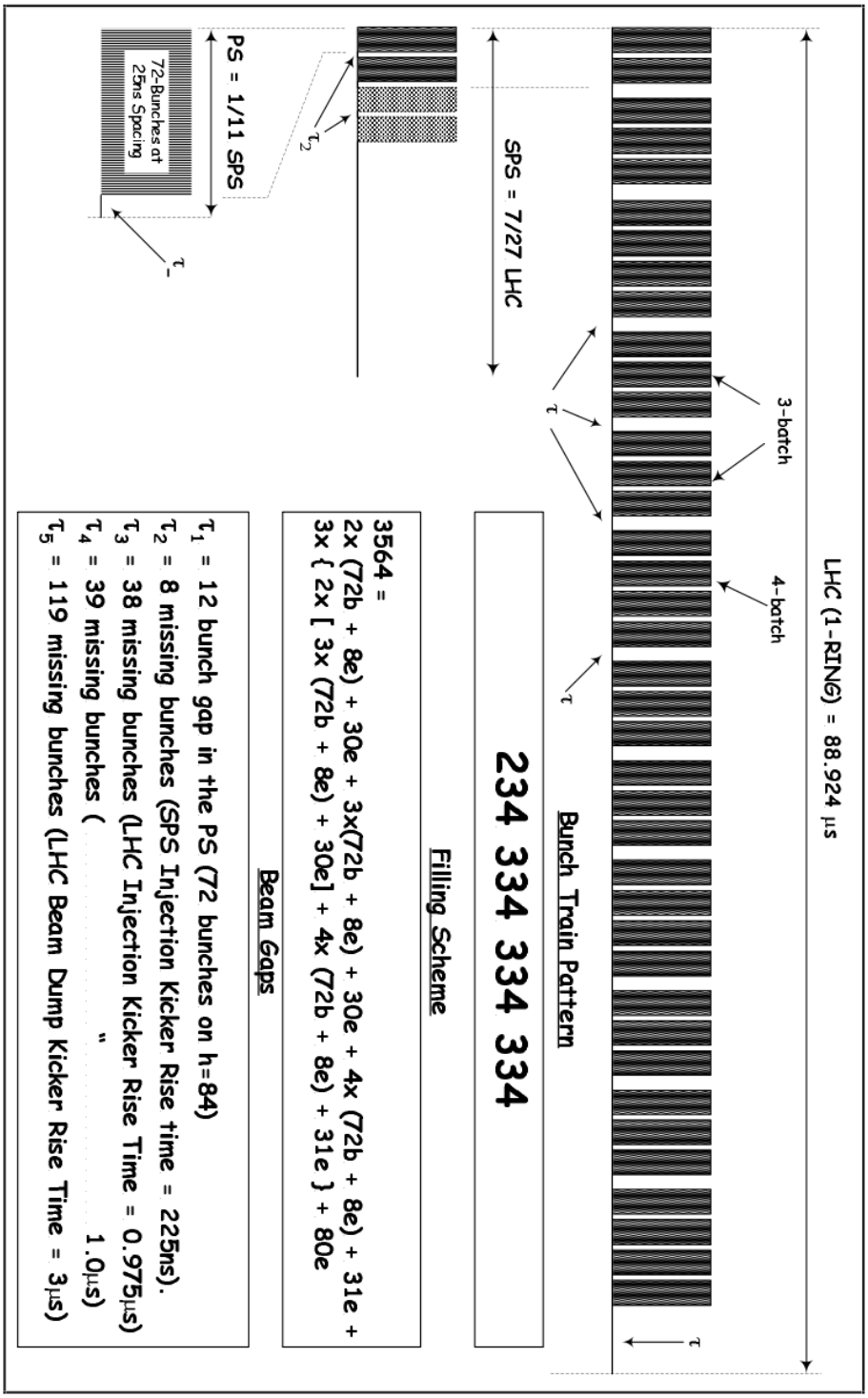

Figure 2.2: The nominal LHC beam filling scheme, from [25].

conditions are much more limited and documented in [26] and [27].

2.2 The Proton Synchrotron Complex

The Proton Synchrotron Complex is composed of two accelerators: the Proton Synchrotron (PS) and the lower energy Proton Synchrotron Booster (PSB). These two accelerators together have the responsibility of bunching the beam to its final 25 ns. spacing along with task of accelerating to an output energy of 25 GeV. Both are accomplished by time-varying RF standing waves.

The PSB has 4 independent rings which operate on the 1st harmonic of the natural RF wavelength, bunching protons via phase-stability into a single bunch before releasing them to the PS. These 4 bunches are timed so that their arrivals coincide with the proper phases of a higher harmonic wave in the PS.

The PSB/PS system can accommodate a number of filling schemes. The nominal one consists of 6 bunches on a 7th harmonic wave (leaving one empty bunch). The purpose of the empty bunch is to leave a region that can be disturbed by the rise-time of the injection magnets for the SPS.

The bunches that occupy the Proton Synchrotron at this point are not the final 25 ns bunches that we will see in the LHC. They are split twice before being released to the SPS. First, the bunches are split three ways by adiabatically varying the RF wave from the 7th harmonic to the 21st. Then, the synchrotron is ramped up to its output energy (25 GeV). Finally the bunches are split again, this time four ways, by similarly adjusting the wave harmonic. These bunches are now the final 25

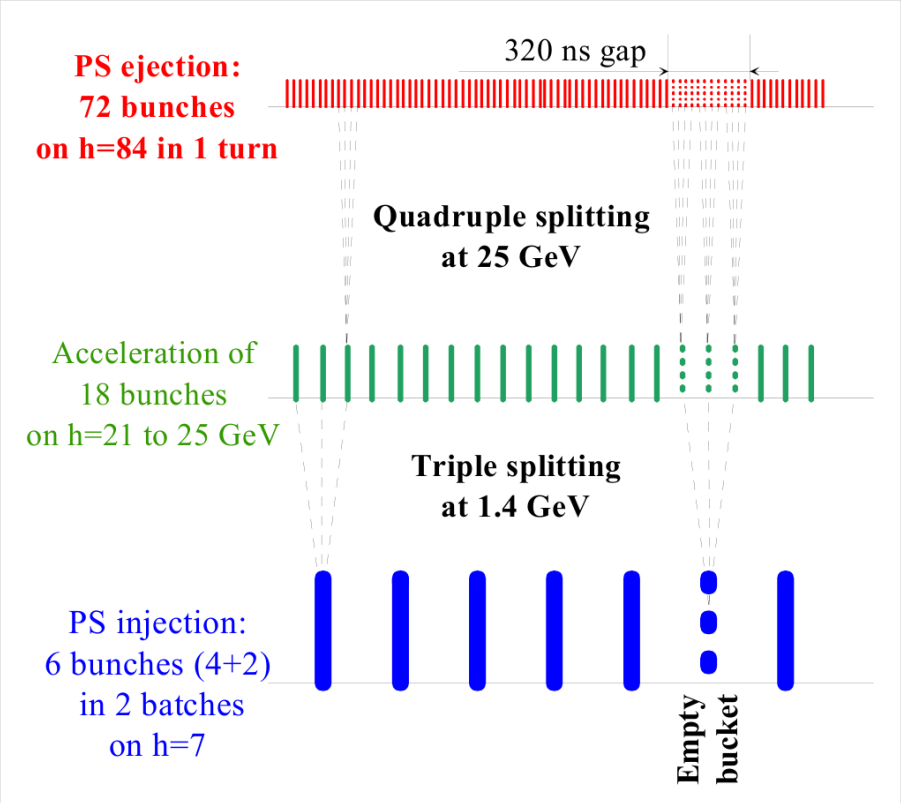

Figure 2.3: The derivation of 25ns proton bunches in the Proton Synchrotron complex

ns bunches, and the original empty bunch has become a continuous 320 ns period of empty space. This process can be seen in Figure 2.3 [21].

2.3 The Super Proton Synchrotron

The Super Proton Synchrotron (SPS) is the next stage of proton preacceleration. The SPS is filled with bunches from the Proton Synchrotron, but due to the larger size, the SPS requires multiple (3 or 4) runs of the PS before it is completely filled. After being filled, the SPS ramps up to its maximum energy of 450 GeV and injects the bunches into the LHC.

The SPS, as a former collider, was fitted with experimental areas to the north

and to the west. As a result of LHC modifications, the west area was closed fully and converted into the clockwise LHC injection site. An area to the east was opened, and now houses a neutrino source in addition to being the counter-clockwise injection site. Neutrinos are generated by diverting a small selection of the proton beam and colliding it with bulk matter. All particles produced as a result of the collision are removed except for the neutrinos, which continue on in the direction of Gran Sasso, Italy, for neutrino oscillation experiments. This project (called CERN Neutrinos to Gran Sasso, or CNGS) is roughly analogous to current neutrino oscillation experiments at the Soudan mine in Minnesota, USA, using neutrinos generated at FNAL [23].

2.4 The Large Hadron Collider

The Large Hadron Collider (LHC) is the last stage in the proton journey. Preaccelerated bunches from the SPS arrive at 450 GeV into two distinct, counter-rotating storage rings that are then ramped up to a final 7 TeV. Collisions occur at 4 of 8 evenly spaced interaction regions in the synchrotron, each of which is equipped with a detector system for reconstruction of the physics of the collision. The other 4 interaction regions hold facilities for maintenance of the beam, including a dumping facility for when the beam is no longer desired (typically because luminosity has fallen below acceptable levels) [18].

2.4.1 The LHC as a Synchrotron

The LHC is built in tunnels that approximate a circular layout. It has eight equally-spaced approximately-500-m. "long straight sections", which house the interaction regions. Between these straight sections are arcs, each of which contains 23 approximately 100 m. long "cells".

A cell contains primarily the magnets used for bending and focusing. Each cell is composed of two nearly identical "half-cells". In each half-cell are 3 main superconducting bending dipoles which can be operated from 0.54 to 8.33 T [19], and one main focusing quadrupole whose orientation alternates between half-cells to achieve a "strong focusing" effect [3, p.341]. Smaller, ring-specific quadrupole and higher-order magnets are also in place for finer corrections [18].

2.4.2 The Interaction Regions

The long straight sections contain the eight interaction regions of the LHC. Each region serves a specific purpose, for either studying collisions or performing maintenance on the beam.

2.4.2.1 ATLAS

Interaction region 1 houses "a torroidal LHC apparatus", a.k.a. ATLAS. This is a general-purpose physics detector, and one of two designed to receive the highest luminosity for pp collisions, with a β at the interaction point of 0.55 m [17]. This experiment competes with the similar CMS detector in interaction region 5, and dif-

fers primarily in the arrangement of detector magnets (ATLAS has a small solenoid inside its calorimeters, and torroids in its muon system. CMS has a single large solenoid outside its calorimeters). ATLAS is also larger in size (twice the length and approximately 1.5 times the radius) [28].

2.4.2.2 ALICE

ALICE, standing for "a large ion collider experiment", is a detector system located in interaction region 2. ALICE's purpose is to study Pb/Pb collisions during the heavy-ion running cycles, though it will take proton data as well. The β for ALICE is dependent on run mode: it will receive low luminosity during proton runs due to a β of 10, and it will receive high luminosity during heavy-ion runs with a β of 0.5 m [17] [30].

2.4.2.3 Longitudinal Momentum Cleaning

Quadrupoles in the magnet arcs focus beam position, but since Liouvilles theorem requires that area in phase-space remain constant, beam momentum will suffer as a result. A system of collimators in IR3 and IR7 remove beam that is sufficiently far from nominal. The apparatus in IR3 is responsible for cleaning beam momentum in the longitudinal direction (along the beam path).

2.4.2.4 RF and Beam Instrumentation

Interaction region 4 contains the RF kicker system that is responsible for accelerating the beams. It also houses varying types of beam-monitoring equipment.

2.4.2.5 CMS

The "compact muon solenoid" (CMS) is located in interaction region 5. CMS is a high-luminosity, general-purpose physics detector, with a β at the interaction point of 0.55 m [17]. CMS competes with the similarly designed ATLAS as described above [29], and is used for the result presented in this thesis.

2.4.2.6 Beam Dump

Interaction region 6 is the location of the beam dumping system, which is a series of magnets designed to safely direct beam out of the synchrotron and into the earth. Beam is typically dumped when it is no longer desired due to luminosity losses, but it can be dumped for other reasons (emergencies, etc).

2.4.2.7 Betatron Cleaning

Transverse momentum cleaning (also known as "betatron" cleaning) occurs in interaction region 7. Collimators of optimized apertures stop beam particles with excessive transverse travel paths. This section differs from the longitudinal momentum cleaning in IR3 by having optics optimized for nominal- (on-) momentum particles.

2.4.2.8 LHC-b

The last interaction region houses the LHC-b detector, a low-luminosity bottom-meson physics experiment. Due to the higher rate of production of its physics goals, LHC-b doesn't require as high luminosity as the other experiments, and in fact such luminosity often causes difficulty in reconstruction due to a higher rate of unrelated "pile-up". The β at the interaction point is adjustable from 1 to 50 meters, depending on current beam conditions [17]. As luminosity at the other experiments rises, LHC-b will lower its β to attain its lower luminosity goal [31].

2.5 Beam Cycle and Luminosity Losses

With RF equipment compensating for energy losses, the LHC would ideally run its beams forever. Unfortunately, the collisions slowly lose luminosity as the beam loses particles because of a number of factors. Scattering between the beams at interaction points is the leading source of this loss. Also, beams can scatter off of the remaining gas at rest in the vacuum chambers. Finally, there is innate coulomb repulsion within a beam packet itself. With these sources combined, luminosity dies away over a time-span of approximately 14.9 hours [18], after which time the beam must be dumped and new beam must be injected.

The time it takes to fill the LHC with protons is dependent on the cycle time of each accelerator in the chain. The LHC takes 12 cycles of SPS fills, each of which will take 3-4 cycles of PS fills. The total time for this process is 20 minutes. Including LHC ramp-down, beam dumping, and brief equipment checks, turn-around time is

estimated at 70 minutes. Practical experience at HERA, however, indicates that the real turn-around time may be as high as 6 times that value, leading to a run cycle that is just an hour or two short of a 24-hour day [18].

2.6 Commissioning the LHC

In June of 2007 it was announced that the LHC would suffer a delay due to the failure in tests of certain magnets provided by Fermilab [32]. Subsequent schedules planned for first beam in the LHC in mid-May 2008, beginning a series of stages that would commission the machine and eventually bring it to its design luminosity. In September 2008 first collisions were achieved, although as a result of further equipment failures, 9 days later the LHC was severely damaged, delaying future runs.

In November 2009 collisions resumed at the injection energy of 900 GeV center-of-mass. A 7 TeV physics program began in March 2010 that lasted until November 2010, this energy being chosen so as to minimize risk of further damage by the mechanism responsible for the September 2008 failure. A heavy-ion run followed this physics run, after which the LHC was shutdown for maintenance.

Chapter 3

The Compact Muon Solenoid

3.1 Overview

The Compact Muon Solenoid (CMS) collects data from LHC collisions at Interaction Point 5 (IP5) on the LHC ring (see Figure 2.1). CMS consists of an approximately cylindrical detector, 15m in diameter by 21.5m in length, centered at the interaction point, built around a 3.8 Tesla superconducting magnet. The detector is itself composed of constituent subdetectors, arranged in concentric rings in the central regions (see Figures 3.1 and 3.2). In addition to the description provided here, the design of CMS is described very thoroughly in a publication authored by the CMS collaboration [35].

Particles produced at IP5 travel through CMS subdetectors depending on their particle type (Figure 3.3). Electrons and photons shower quickly, producing a cascade of lower-energy photons and electron-positron pairs and depositing that energy in CMS's electromagnetic calorimeter (ECAL, $PbWO_4$ crystal), after traveling through the much-less-dense pixel and silicon-strip tracking chambers. Strongly-interacting particles (K, π, Λ, n, p) undergo a similar shower process, but mostly contained within the hadronic calorimeter (HCAL) positioned after the ECAL. Finally, muons are sufficiently massive not to be stopped by the ECAL, but not strongly interacting and thus do not shower in the HCAL. They travel through the entire CMS

detector volume, causing responses in CMS's three muon-detector systems (Figure 3.4).

Detector response is measured by on-detector electronics in the CMS cavern, and off-detector electronics in a parallel service cavern, before being packaged into digital payloads, collected, and recorded on above-ground computers.

CMS employs a two-level trigger to select events from the 40 MHz collision rate to be saved for analysis. The first level (L1) is entirely in hardware, and collects information from the calorimeters and muon systems, marks events with decisions from a collection of algorithms, and allows events to continue if one of the algorithms they pass is on the configurable L1-accept list. This reduces the event rate to approximately 100 kHz. Then a software high-level-trigger (HLT) analyzes the entire event content and makes decisions to pare down the rate to 100 Hz [35, Ch.8].

L1 algorithms are implemented in hardware and are thus difficult to adjust. The menu of accepted L1 decisions can be configured, however, to accommodate increasing event rates from increasing LHC luminosity. L1 algorithms can also be "pre-scaled", allowing a defined fraction for an algorithm to continue, in the case that the events are useful but excessively frequent. HLT algorithms can be adjusted at will (although the algorithm must run sufficiently quickly to prevent unprocessed data from accumulating, a process that could result in data loss) and are tuned to produce maximum useful physics results for a given luminosity. The menu of accepted HLT algorithms is also configurable at run-time.

CMS data is monitored in multiple control rooms, including (at the time of this

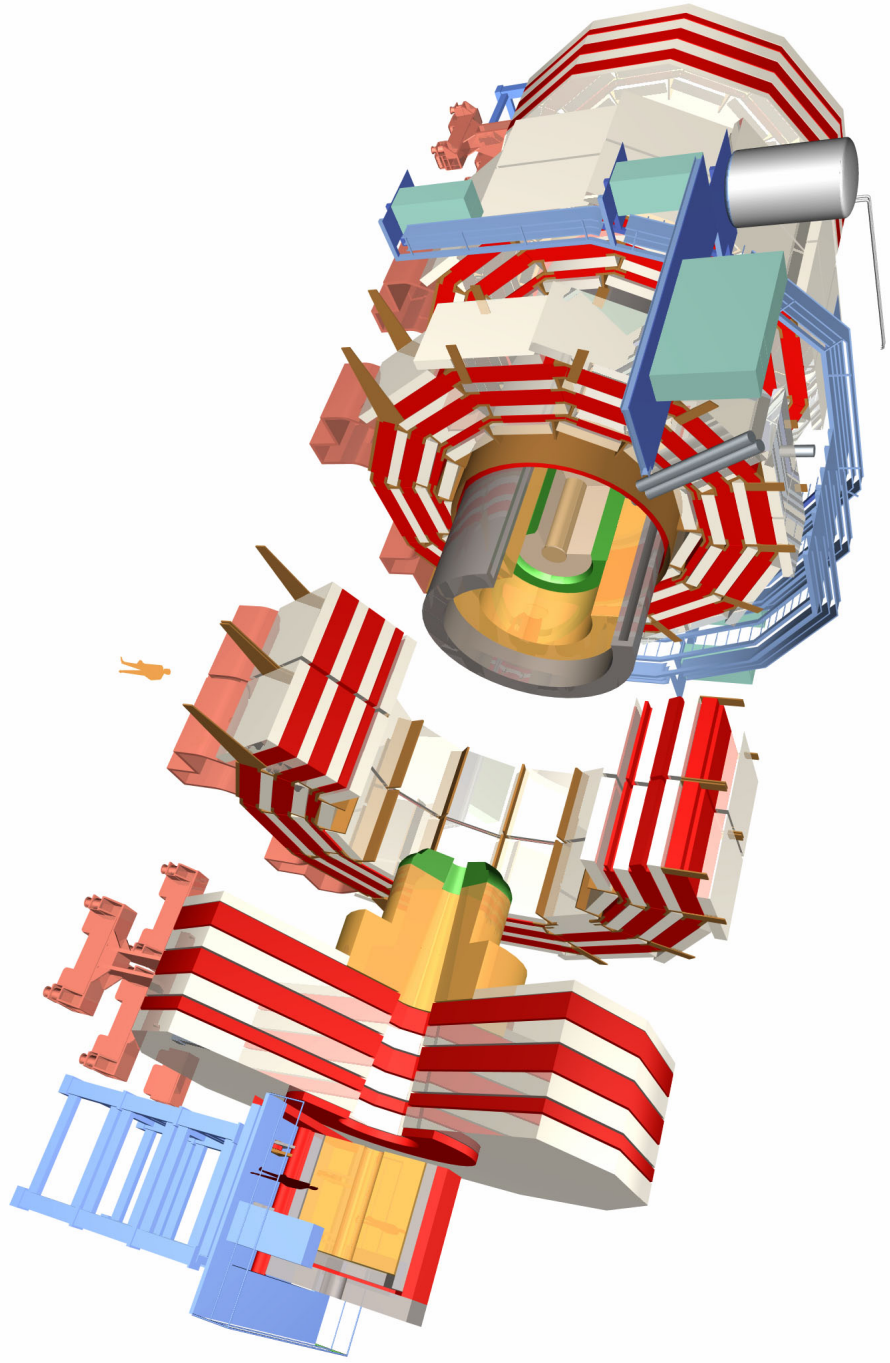

Figure 3.1: A scale schematic of the CMS detector with portions cut-away, movable rings detached to show detail

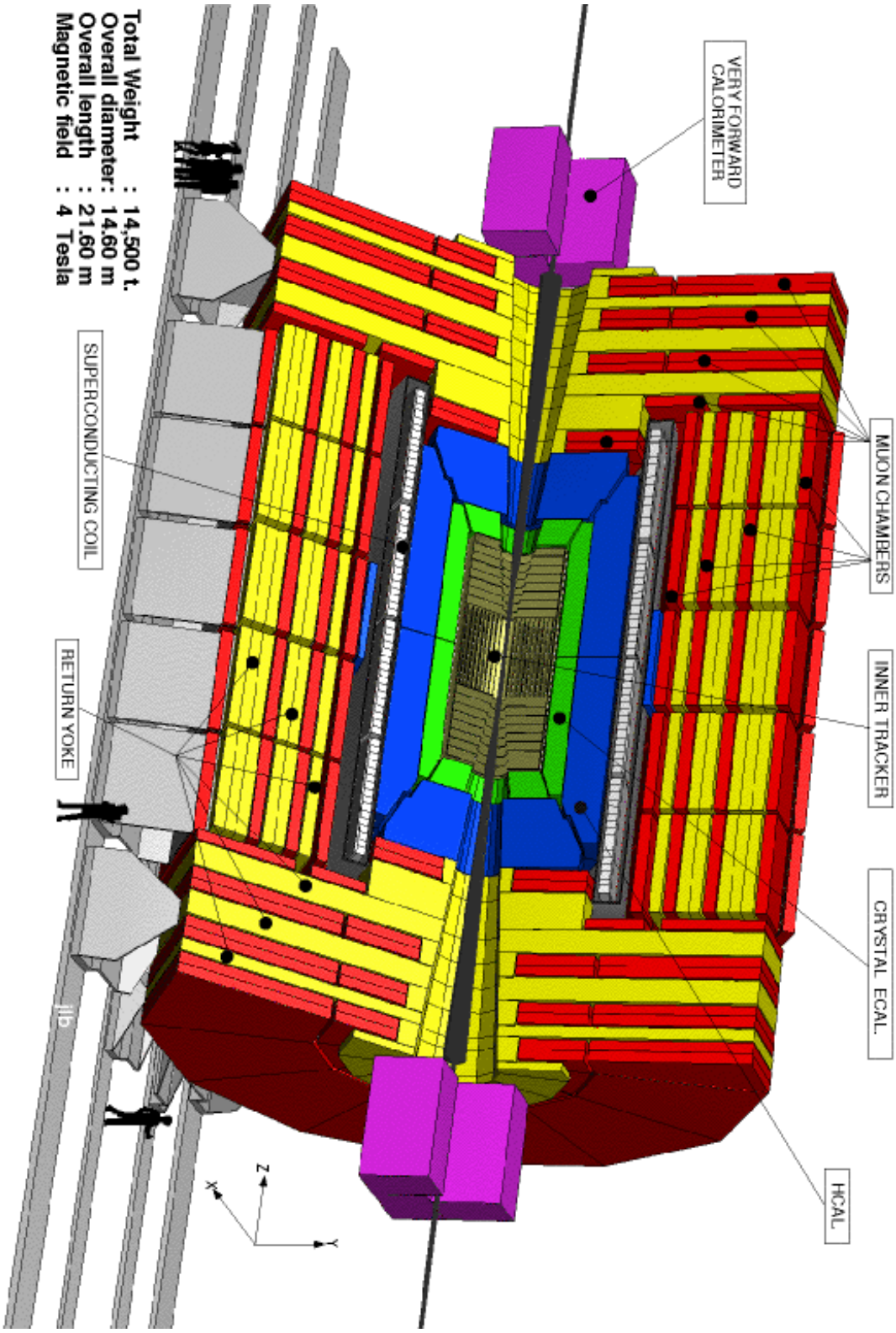

Figure 3.2: A cut-away schematic of the CMS detector, from the CMS Technical Proposal

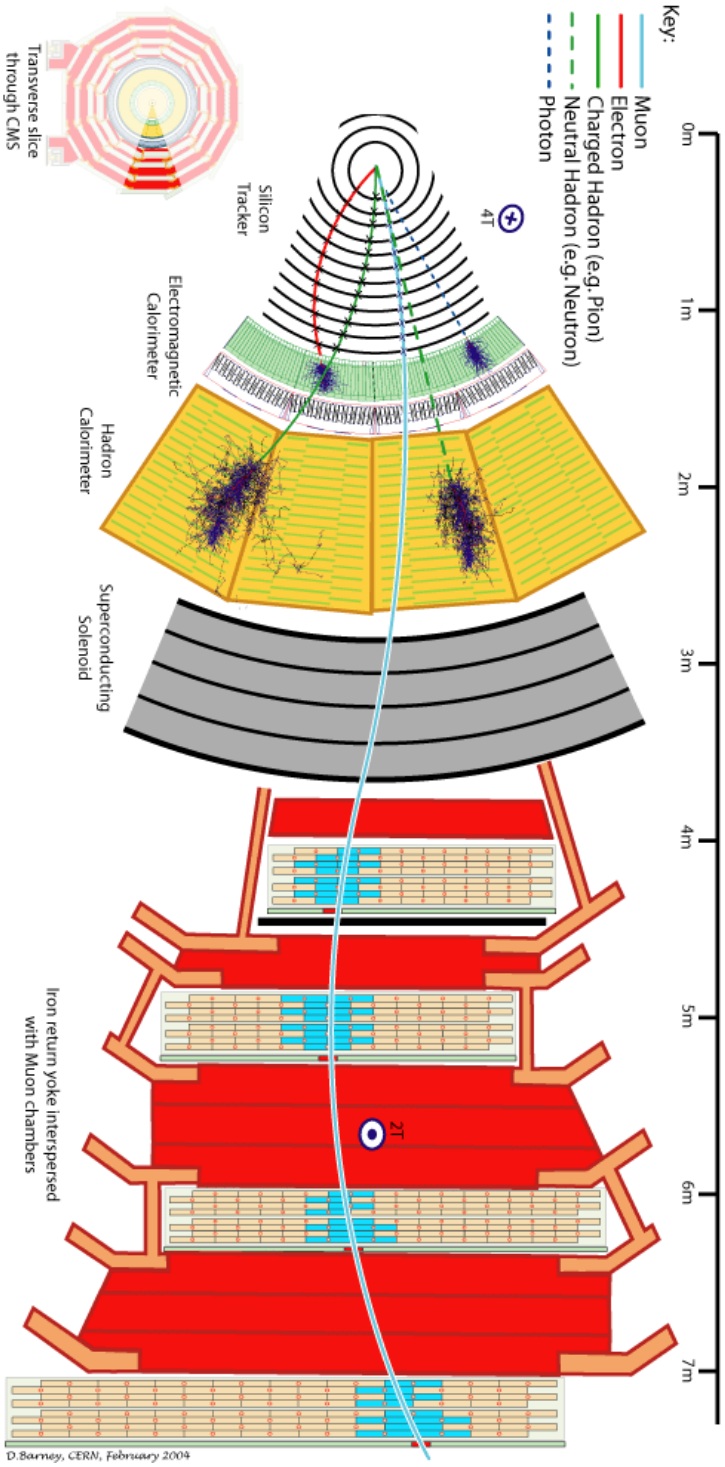

Figure 3.3: Ideal particle paths through central CMS detectors, and corresponding response

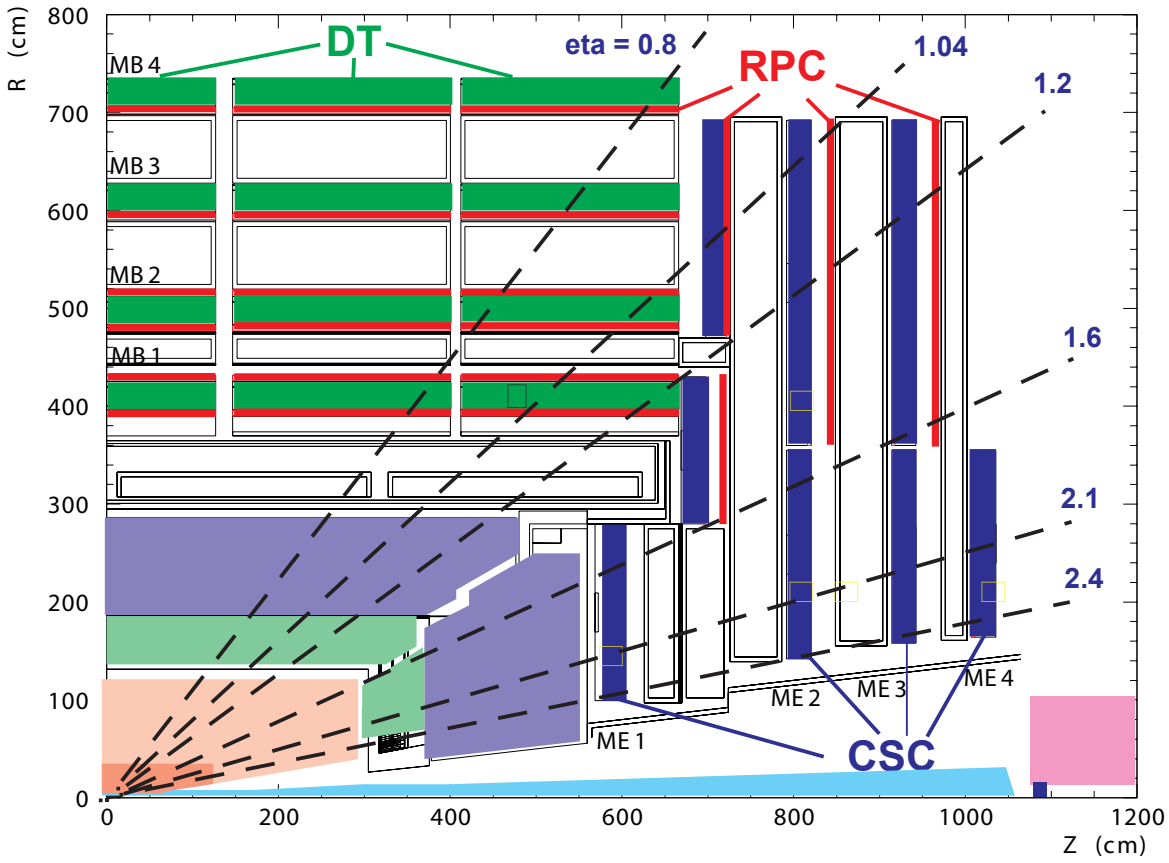

Figure 3.4: An r-z view of the CMS detectors (quarter cross-section), with muon detectors labeled

writing) an above-ground control room in SX5 (above CMS), the "CMS Center" in the primary CERN campus in Meyrin, Switzerland, and the LHC remote operations center in Wilson Hall, Fermilab (Batavia, IL). These control rooms contain banks of computers for debugging and monitoring of individual subdetectors, as well as global data quality monitoring (DQM), trigger, magnet, and data acquisition (DAQ) operations.

3.2 Subdetectors

For the purpose of this analysis, data from the hadronic calorimeter and muon systems are used. The hadronic calorimeter provides a large massive location for long-lived particles to stop, as well as instrumentation to measure the energy of their decay. The muon systems provide a veto against cosmic rays that may produce noise in the hadronic calorimeter via a hard bremsstrahlung process.

3.2.1 The Hadronic Calorimeter

The hadronic calorimeter (HCAL) can be divided into four main subdetectors (but has other parts as well, beyond the scope of this document). The data for this search comes from the HCAL Barrel (HB), which spans to slightly beyond $|\eta| < 1.3$. There is also the HCAL Endcap (HE) which overlaps at the end of HB and provides coverage beyond it; the HCAL Outer (HO), a thin layer in the barrel region beyond the magnet; and the HCAL Forward (HF) in the forward region ($|\eta| > 3$). HB, HE, HF and HO are pictured in Figure 3.5.

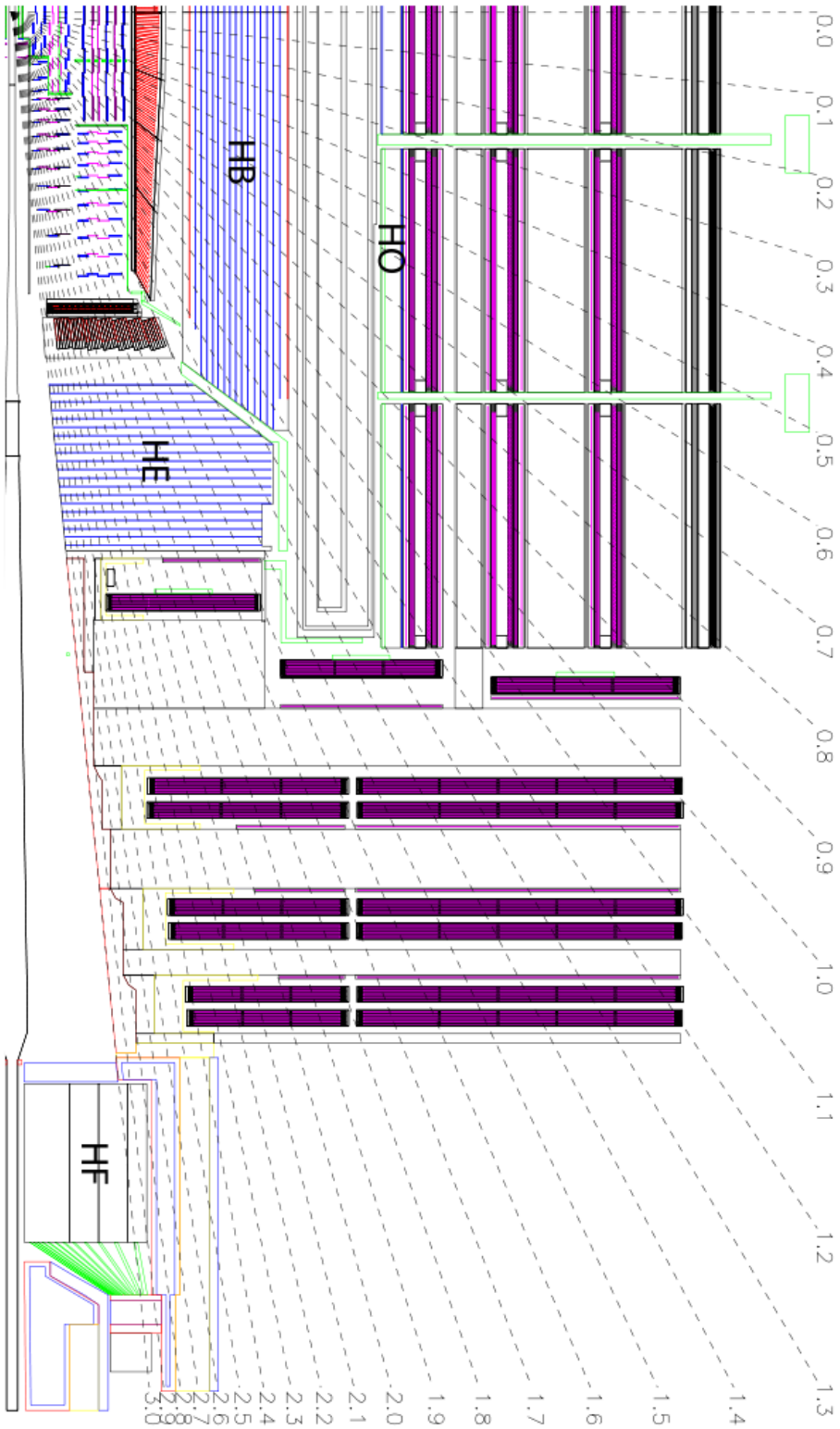

Figure 3.5: Layout of the HCAL subdetectors (quarter cross-section, η labels on dashed lines)

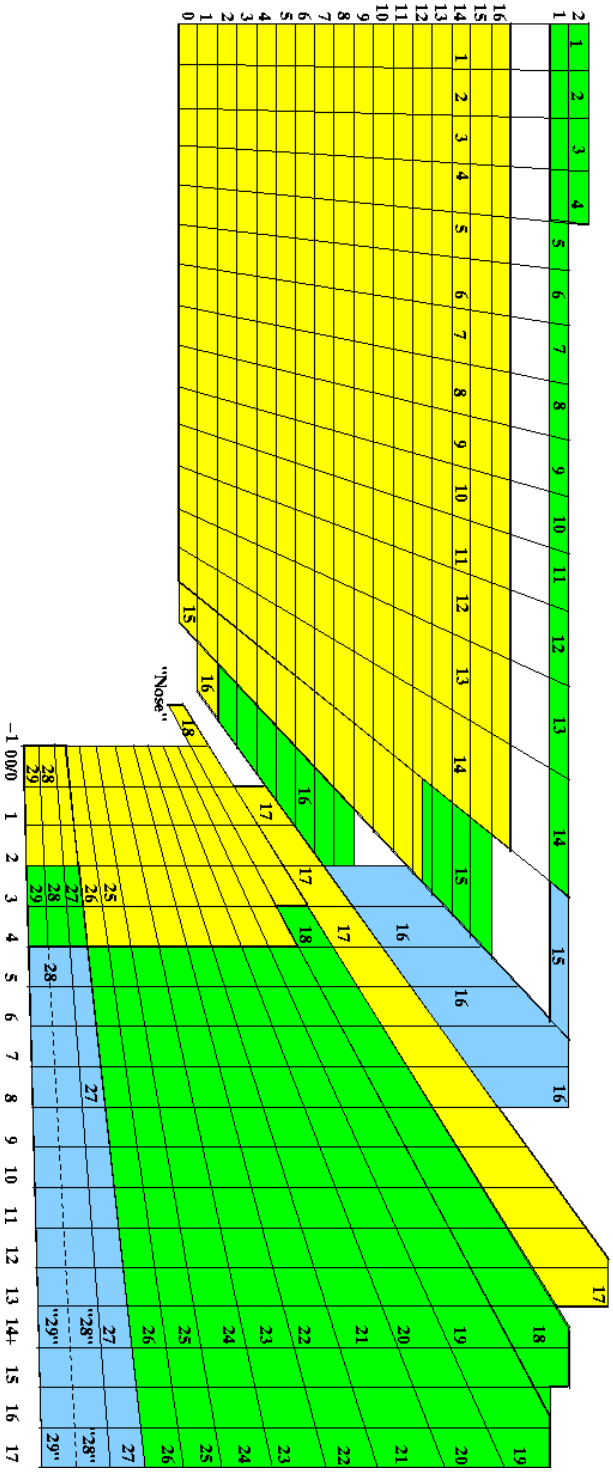

Figure 3.6: The segmentation of the HB and HE subdetectors (quarter cross-section, r-z axes, angular segmentation of $\Delta\eta = 0.087$ per line)

HB is composed of alternating layers of brass (50.5-75.0 mm thick, depending on depth) and plastic scintillator tiles (3.7mm thick for inner tiles, 9mm for outer). HB brass is 70% copper, and 30% zinc, with a radiation length of 1.49 cm and an interaction length of 16.42 cm [35, Ch.5].

The tiles are placed perpendicular to the r direction, forming rectangular towers of 17 tiles $\Delta\phi = 0.087$ by $\Delta\eta = 0.087$ wide. The light in the scintillators of each tower are optically summed. Tower index is hereafter referred to as $i\phi$ and $i\eta$, beginning at 1 from the 0 position of ϕ and η respectively. There is no center tower in η; $i\eta = 1$ borders $i\eta = -1$ at $\eta = 0$ (tower segmentation illustrated in Figure 3.6).

The process of conversion of light into electric charge is often achieved via a photomultiplier tube (PMT). Collected light is directed onto photocathodes coated with alkalai metals, where it liberates electrons via the photoelectric effect. Liberated electrons cascade through a series of dynodes at increasing potential, resulting in a multiplication of the original charge. The end result is a detectable electric current at the output dynode [3, p.358-360].

HCAL uses hybrid photodiodes (HPD) to convert HB scintillator light into electric current. An HPD operates by the normal process of charge liberation on a photocathode, but then liberated electrons are accelerated onto a silicon diode surface, where the incident electron energy is dissipated in the excitement of silicon valence electrons. The advantage of this process over ordinary PMTs is mechanical simplicity and increased stability within magnetic fields [33, 34].

The light from each tower is collected along a wavelength-shifting-fiber to clear

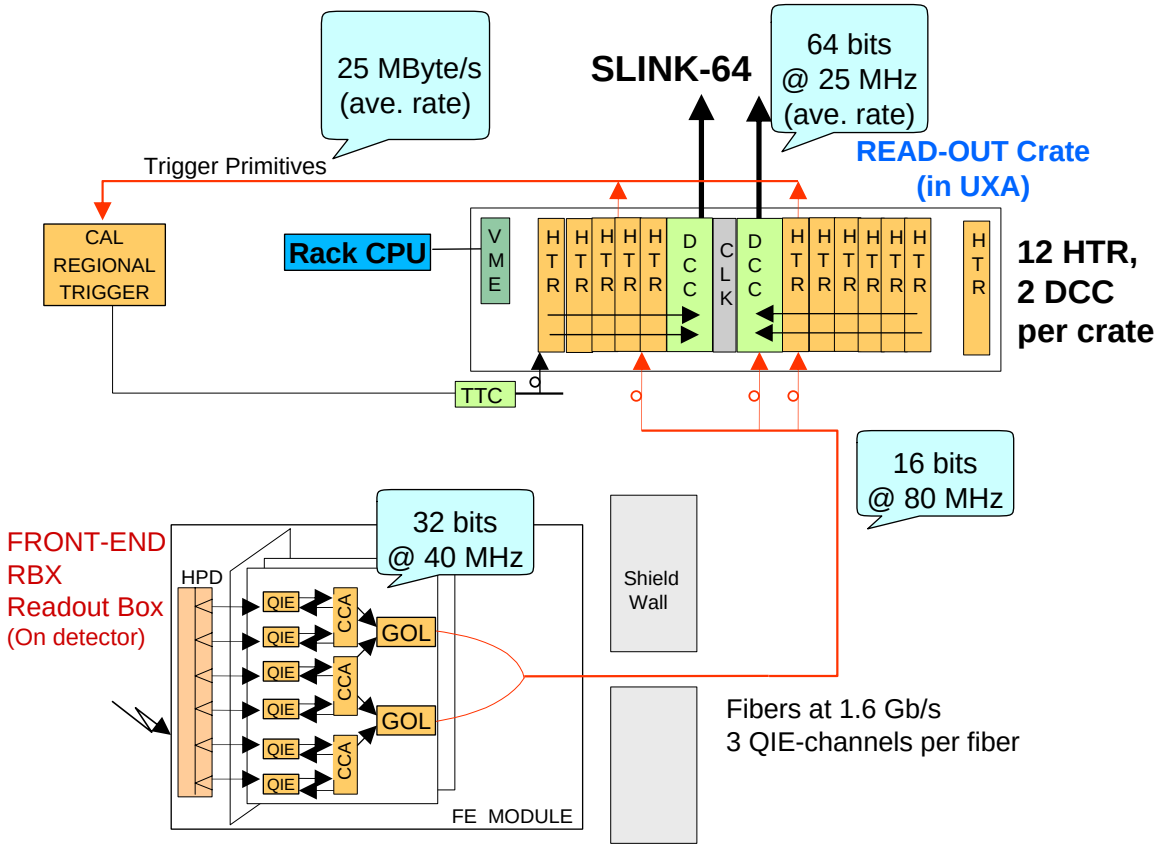

Figure 3.7: Schematic of the HCAL electronics

fibers before interfacing with an HPD. The fibers from up to 18 towers each connect to a pixel arranged in a honeycomb layout on a single HPD (Figure 3.8), and are converted into electric current. The electrical signal (again, one per pixel), is carried to on-detector electronics (schematic: Figure 3.7).

The electrical signal is collected by one of four capacitors on a charge-integrating electronics (QIE) board, and digitized on a multi-linear scale (Figure 3.9) by an 8-bit analog-to-digital converter. The capacitor is then rotated out so that it has sufficient time to discharge before its next use.

The digitized signal is packaged and sent by optical fiber to off-detector elec-

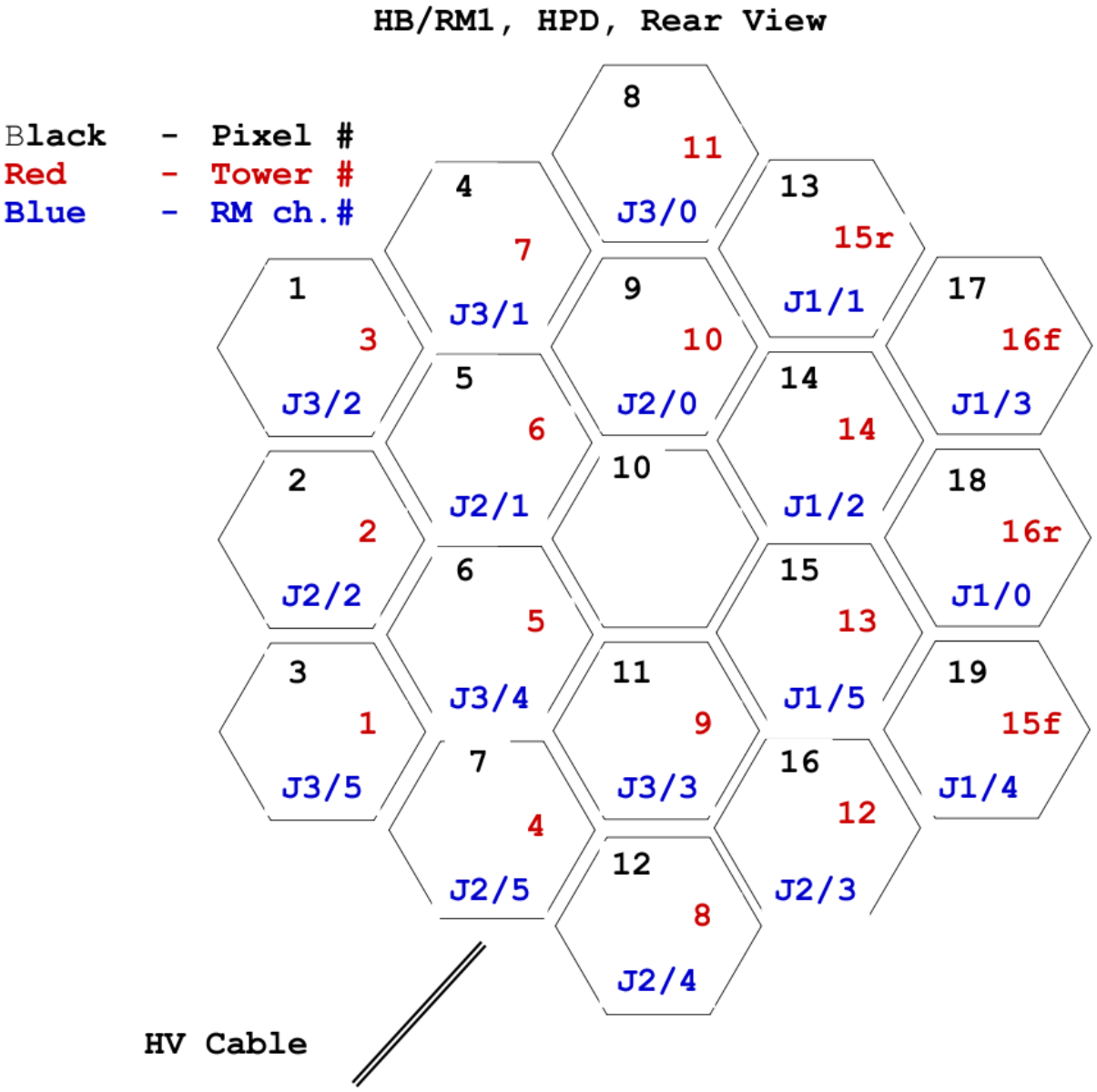

Figure 3.8: Example layout of tower fibers on HPD pixels

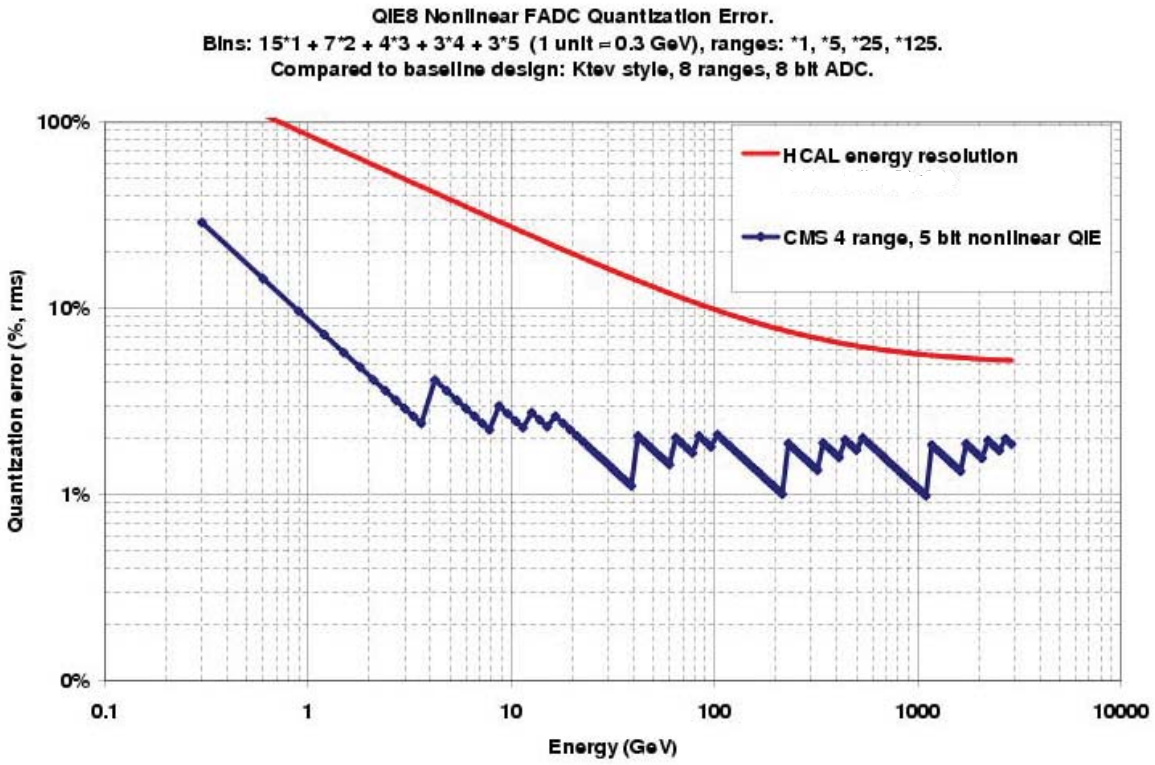

Figure 3.9: Quantization effects of the multi-linear scale of the HB analog-to-digital converters

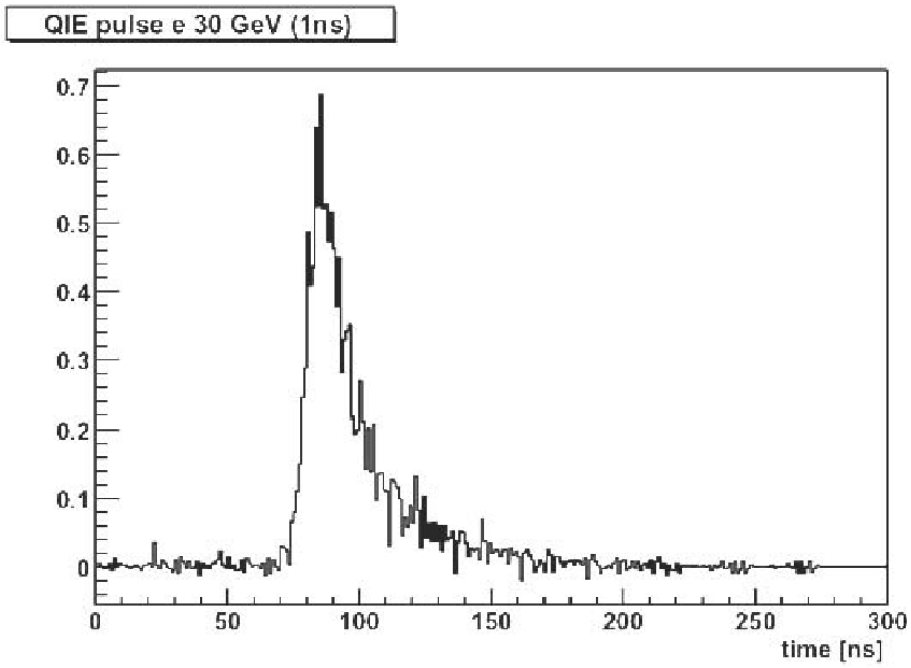

Figure 3.10: A measured pulse of scintillator light characteristic of HB, HE, and HO, taken at a QIE ASIC by a 1 ns sampling-rate oscilloscope

tronics, beginning with HCAL Trigger and Readout (HTR) boards, where it is both sent onward to the L1 trigger system, and saved in the event of a L1 accept decision. If an event is selected by the L1 trigger, data from 10 consecutive 25ns bunches (each called a "time-slice" of data) are selected such that the triggering bunch is placed 4^{th}. This selection of data is packaged and forwarded to Data Concentrator Cards where the aggregated digital payload is packaged and formatted to be written to disk or tape (for permanent use, or later testing by the HLT).

A raw HCAL hit is composed of 10 time-slices because energy deposited in the plastic scintillator material causes a pulse of light with a well-defined shape of duration approximately 4 bunches. The greatest energy time-slice (also called the "peak") is preceded by a "front porch", a rapid warm-up of light. The subse-

quent time-slices resemble an exponential fall-off, making the over-all curve slightly poissonian in appearance (Figure 3.10).

The QIE ADCs are tuned so that data with zero scintillator light is at a very low value. If the output from an ADC is below a threshold, the data is considered "zero" and will not be delivered from the HTRs to the DCCs after a trigger. This is known as "zero suppression" and keeps the size of the event payload sufficiently low that high rates of data can be taken without overloading the data acquisition paths.

Anomalous data appears in the absence of beam at a rate of approximately 3 Hz in our HLT jet path. The causes of this data are diverse and discussed in Chapter 6, however one main cause is data that does not originate from physical scintillator pulses, and instead is caused by unintended behavior of the electronics.

3.2.1.1 Jet Reconstruction

Unbound gluons and quarks (and their supersymmetric counterparts squarks and gluinos) resulting from particle interactions are not observable. Particles with color charge undergo a process of hadronization as they travel through the detector, popping new particles out of the vacuum to produce color-neutral states. The result is a shower of particles, primarily pions, as the particles enter the sensitive regions of CMS. This shower is tightly collimated, and can be characterized as a single object, known as a "jet" [3, p.46-47].

To reconstruct jets responsible for deposits of energy within the CMS electro-

magnetic and hadronic calorimeters, a process of consolidating data from multiple sources is undertaken.

First each raw HCAL hit is reconstructed into a "RecHit". The ADC data is linearized and the expected value corresponding to zero-scintillator-light (the "pedestal") is subtracted. Total energy is then derived by applying calibration constants to a sum of time-slices within the pulse. The time of the pulse is calculated relative to the trigger, and the energy and time are recorded in an output RecHit object.

Electromagnetic Calorimeter data is joined with HCAL RecHits from all HCAL subdetectors to form "CaloTowers", an object describing energy at a single $(i\eta, i\phi)$ pair. A collection of CaloTowers completely describes the distribution of deposited energy across η and ϕ coordinates across CMS. Data may be excluded from the construction of towers on the basis of several quality flags [36].

From a collection of CaloTowers, jets are reconstructed. There are several algorithms for reconstructing jets in CMSSW: Iterative Cone, Midpoint Cone, SISCone, and fast-k_T [37], and more recently anti-k_T [38]. Iterative Cone, which is used to produce the data used in this analysis, is a comparatively simple algorithm that is based on searching in cones around "seeds", CaloTowers considered in order of decreasing energy.

For each seed (of minimum energy 1 GeV), the algorithm searches for a cone such that all inputs are within a radius $\sqrt{\Delta\eta^2 + \Delta\phi^2} \leq R$ from the cone center, where R is a configurable parameter (0.5 for this analysis). This cone minimizes the difference between the geographic center and the sum of the 4-vectors of the

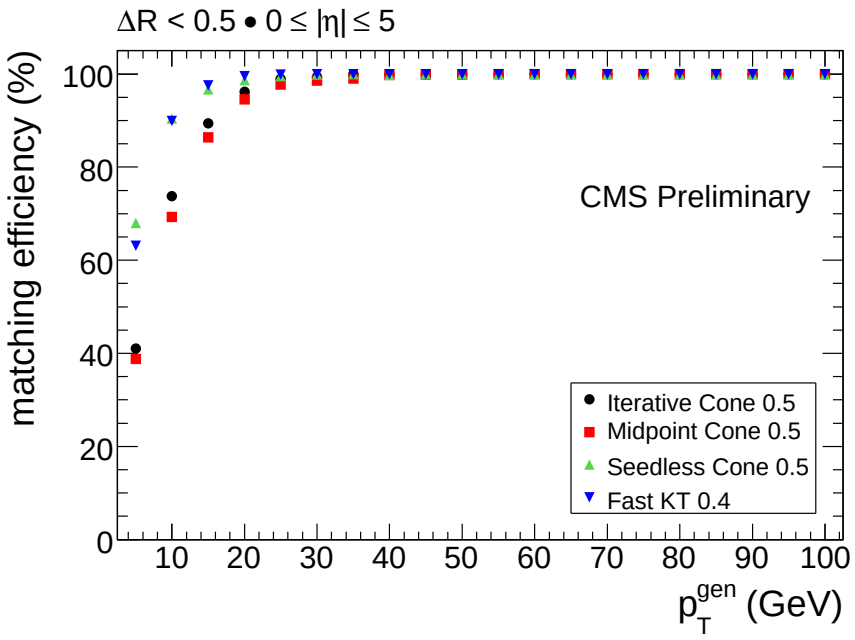

Figure 3.11: Jet-matching efficiency for various jet algorithms

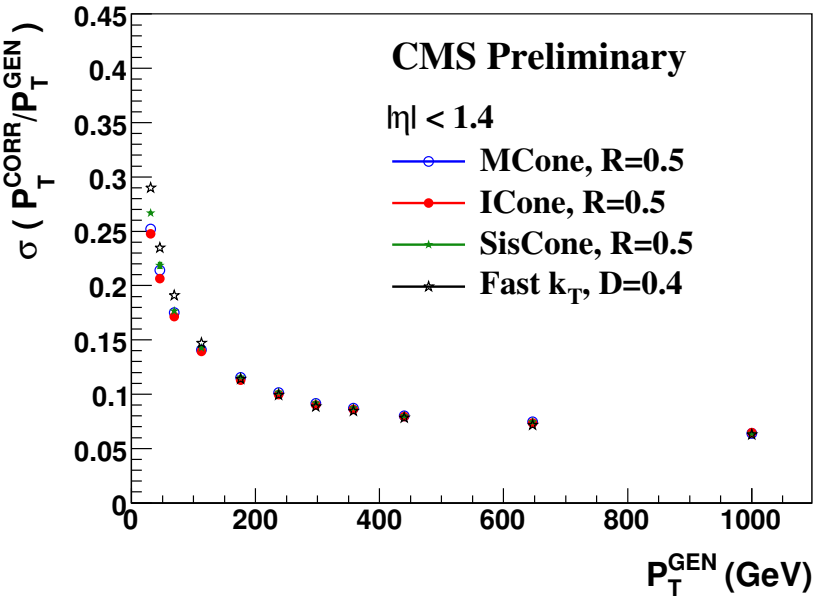

Figure 3.12: Jet energy resolution for various jet algorithms

constituent towers. If the difference is within a tolerance, jet variables are computed and recorded, and the inputs are removed from further consideration as jet components or seeds. Performance of this algorithm is shown in Figures 3.11 and 3.12 [37, p1].

3.2.1.2 HF Luminosity Monitoring

The forward HCAL subdetector, HF, is used to calculate LHC beam luminosity delivered to IP5. HF consists of quartz fibers embedded in steel absorber plates, to better deal with the occupancies expected in the forward regions that HF measures ($3 < |\eta| < 5$). Read-out is via photomultiplier tubes and digitized with RBXes and HTRs in a manner similar to HB [35].

HF has an independent path for collecting data for luminosity in time periods during which CMS is collecting data and periods during which it is not. This data provides input for two algorithms which can produce an initial estimate of CMS luminosity in near-real-time. A more accurate offline method is used for this analysis. The offline method is based on a serious of cuts to eliminate non-collision backgrounds, including a coincidence requirement of energy deposits in both η-sides of HF. All methods produce a count of events which scales linearly with luminosity. The determination of this scaling factor is presented alongside further details of the luminosity measurement process in [39].

3.2.2 The Muon Systems

The muon system is a collection of three detectors: the drift tubes (DT) in the barrel region, the cathode strip chambers (CSC) in the end-cap region, and the resistive plate chambers (RPC) in both (labelled in Figure 3.4). This system is sensitive to the path of traversing charged particles, particularly muons since they are unlikely to have been stopped by detector material.

While the muon system is designed to be efficient for muons originating from the center of CMS [35, Ch.7], it is also a good detector of external cosmic rays (Figure 3.13) [40]. CMS software can reconstruct path segments of incident particles, including cosmic rays, which by their nature do not necessarily travel through the beam-line. This capability provides a useful veto for cosmic ray events which interact with the hadronic calorimeter, mimicking desired signal.

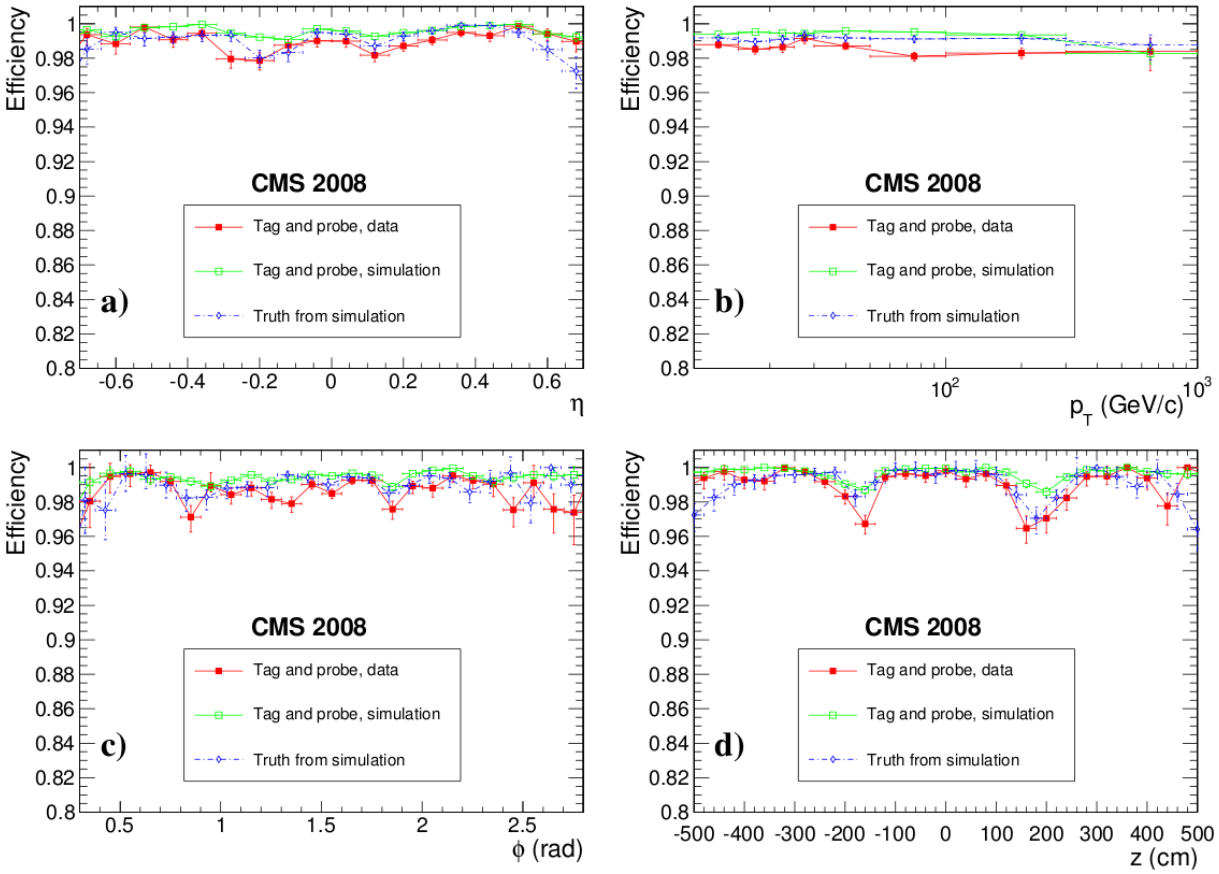

Figure 3.13: Muon efficiency as a function of the variables of the muon entry point to the detector. Reconstruction efficiency is for 1-leg CosmicSTA standalone muons.

Chapter 4

The Experiment

This search follows data taken during the 2010 LHC pp physics run at 7 TeV center-of-mass energy. 10.2 pb^{-1} of data was taken with a peak luminosity of $10^{32}\text{cm}^{-2}\text{s}^{-1}$. The combined data amounts to a running time of 62 hours.

The data for this search was acquired by looking for energy deposits left by long-lived particles in the hadronic calorimeter. A level-1 trigger was configured to look for jets of energy 10 GeV or higher in coincidence with an absence of beam in CMS. A high-level-trigger was configured to look for events passing this L1 trigger with a jet in the central region ($|\eta| < 1.3$) of energy 20 GeV or higher. This restricts jet signal to the Hcal Barrel (HB) region, which reduces the necessary understanding of instrumentation noise. The signal is produced centrally and thus is not reduced very much by this cut.

The HLT also applied very loose instrumentation cuts to reduce data rate to a manageable amount:

- For each HPD whose summed energy of hits is above "hpdSpikeEnergy" (see Table 4.1), the event is rejected if neither of its neighbors is above "hpdSpikeIsolationEnergy".

- For each RBX whose summed energy of hits is above "rbxSpikeEnergy", the event is rejected if the lowest energy HPD within the RBX is less than

HLT Parameter	Value
hpdSpikeEnergy	10.1 GeV
hpdSpikeIsolationEnergy	1.1 GeV
rbxSpikeEnergy	40.0 GeV
rbxSpikeUnbalance	0.21

Table 4.1: Parameters for the instrumentation noise filter in the high-level-trigger

"rbxSpikeUnbalance" times the energy of the highest HPD within the RBX.

Chapter 5

Signal: Simulation and Characteristics

5.1 Overview

To study approaches for distinguishing signal from background we produce the best available estimate of the behavior of the hypothesized signal. We do this in multiple steps that track signal particles (split-SUSY gluinos) from production to decay and detector response, resulting in files of processed data that very closely resemble that which would come out of the regular data-taking process.

The simulation process of signal is factored into distinct stages. First, pair production of split-SUSY gluinos is simulated at the interaction point, and the attributes of the emerging particles are set. Then, the travel of those particles is tracked through the detector and any gluinos that come to rest within the detector volume are recorded. For these stopped gluinos, the decay process of gluino into neutralino and jets is simulated, and the travel and interaction of those resultant particles with the detectors is simulated. Finally detector response is simulated and the digitized results are saved to disk, and processed with the same software used to process collision data.

A further stage of the simulation randomly distributes the time of the stopped-gluino decays so that the profile in multiple timing variables can be studied. Many gluinos that would otherwise be detected by our analysis decay during time periods

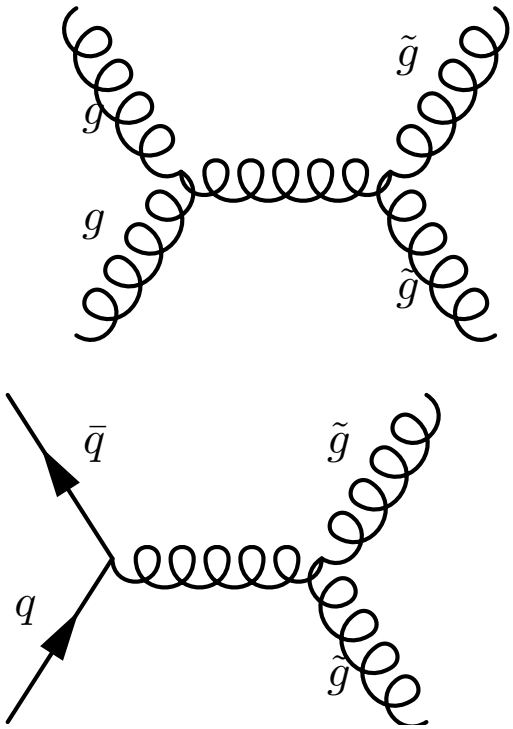

Figure 5.1: Leading Feynmann diagrams of gluino production at the LHC

we are unable to use, either because of a simultaneous beam collision (a "beam-on" bunch), because the CMS hardware is not recording data, or because of analysis rules that help prevent contamination with excessive noise.

5.2 Production

PYTHIA is a publicly-available software tool used to simulate many particle physics processes [41]. In the case of signal production, we run PYTHIA to simulate the $gg \to \tilde{g}\tilde{g}$ and $q\bar{q} \to \tilde{g}\tilde{g}$ via virtual gluon processes (Figure 5.1) in pp collisions of center-of-mass energy of 7 TeV (our environment at the LHC).

PYTHIA can simulate the behavior of many particle types, including gluinos, based on customizable parameterizations of models like Supersymmetry. However,

for the sake of generalization and convenience, we instruct the program to create gluinos with infinite lifetime, so that we can factorize this step from the remaining ones. We further instruct PYTHIA to create gluinos with masses scanning from 200 to 900 GeV, so that we can study many possible points in the space of the split-SUSY model.

Since gluinos carry color charge, it is also necessary to simulate the hadronization of gluinos into "R-hadrons" (so named because of the R-charge of supersymmetric particles, assumed conserved for the purposes of this analysis). The PYTHIA team has published additional routines, PYRHAD and PYGLRF, which were used to accomplish this step [41, Sec.8.7.9]. The resulting hadron states are baryon-like ($\tilde{g}qqq$) and meson-like ($\tilde{g}q\bar{q}$). There are large uncertainties on the hadronization process, and especially on the fraction of neutral baryons produced.

5.3 Detector Traversal and the Cloud Model

GEANT4 is a publicly-available software tool used to simulate the interaction of energetic particles with ordinary matter, particularly the materials commonly found in particle-physics detectors, so that the path of simulated particles can be propagated from an originating position and momentum [42]. We use GEANT4 in this case to extrapolate the path of R-hadrons formed from gluinos from production points to stopping points, if they stop in the detector volume at all.

GEANT4 can be configured to simulate many physical interaction models of particles with matter. For the purposes of this analysis, a "cloud"-model originat-

ing from [44] is used to simulate the effects of R-hadronization energy losses from interactions with the detector material. Strong-force interactions can cause hadron state flipping in the R-hadron (since an interaction can never leave a bare colored gluino), and each of such interactions carries with it an opportunity to deposit energy in the material. Figure 5.2 shows the percentage of R-hadrons stopping in the detector volume for this model, as well as for models with only electromagnetic (EM) force contributions (Figure 5.3, as described by [4, Ch.27]), and models where the R-hadron is constrained to change to a neutral baryon whenever a strong interaction with the detector occurs. Given the amount of uncertainty surrounding hadron states of gluinos and their interactions, these models represent less-optimistic scenarios that can be considered in lieu of the cloud-model, which should be considered hypothetical in the absence of actual gluinos to measure.

The location of stopping points (Figures 5.4 and 5.5) very roughly correlate with the mass-density of components of the CMS detector. Primarily, many gluinos stop within the hadronic calorimeter and within the iron magnet return yoke components interspersed within the central muon system.

$$E = \frac{mc^2}{\sqrt{1-\beta^2}} \tag{5.1}$$

Figure 5.2 also shows the relationship between gluino mass and stopping efficiency. Equation 5.1 gives the basic kinematic relationship between mass and energy. For a given distribution of energy E in a particle production, a higher mass particle will be produced with a lower distribution of velocity β. Since slower particles are easier to stop, higher gluino masses result in higher stopping efficiencies.

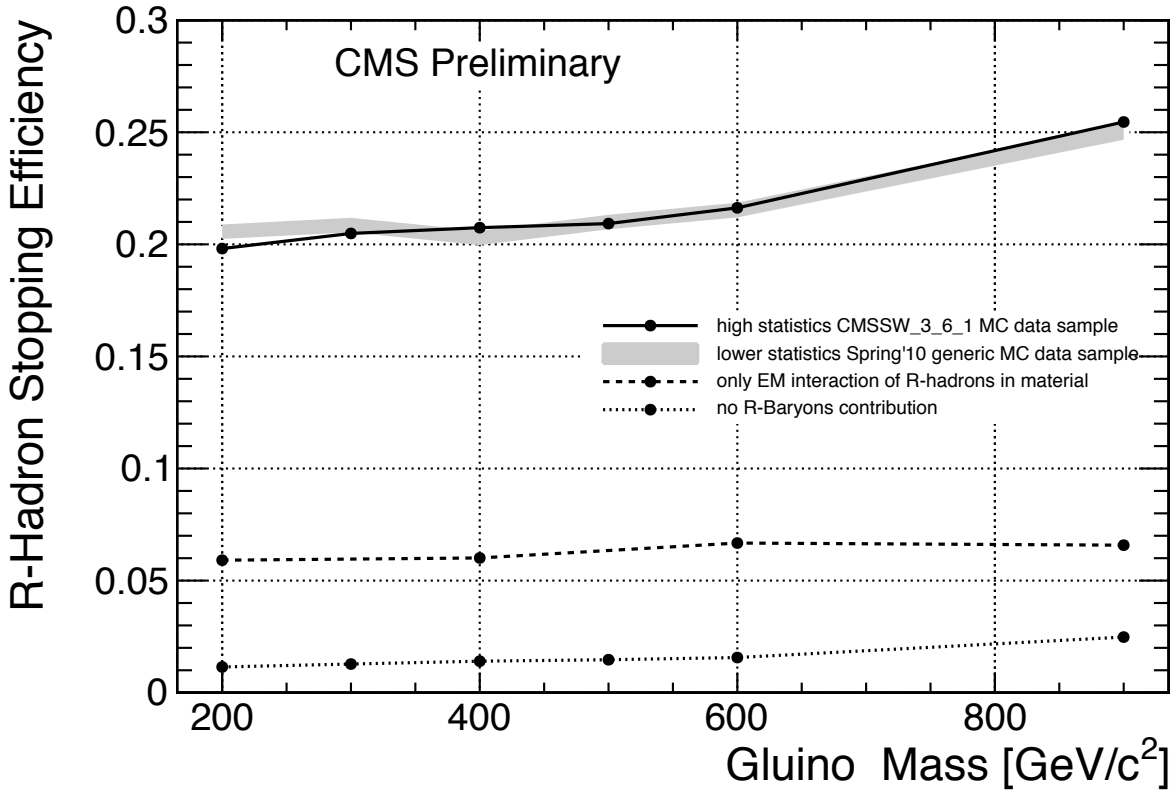

Figure 5.2: The probability of gluinos to stop within the CMS detector volume for multiple interaction models

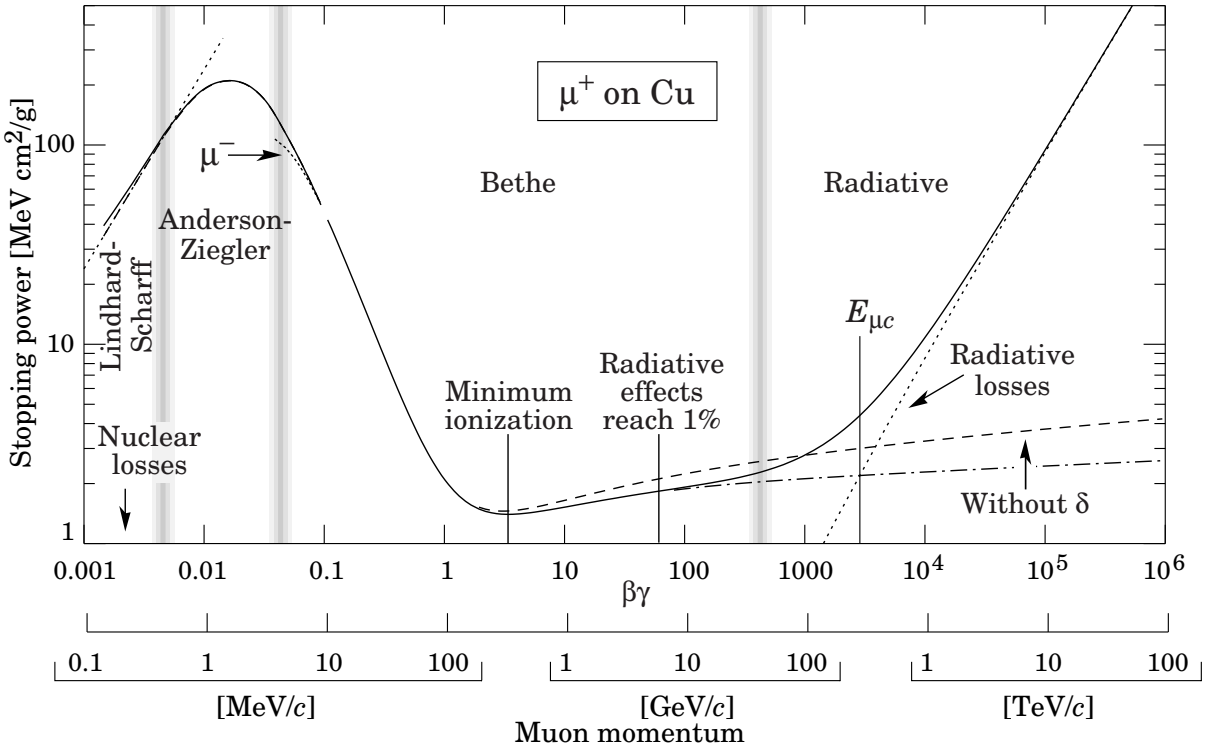

Figure 5.3: Energy loss for positive muons in copper as a function of $\beta\gamma$.

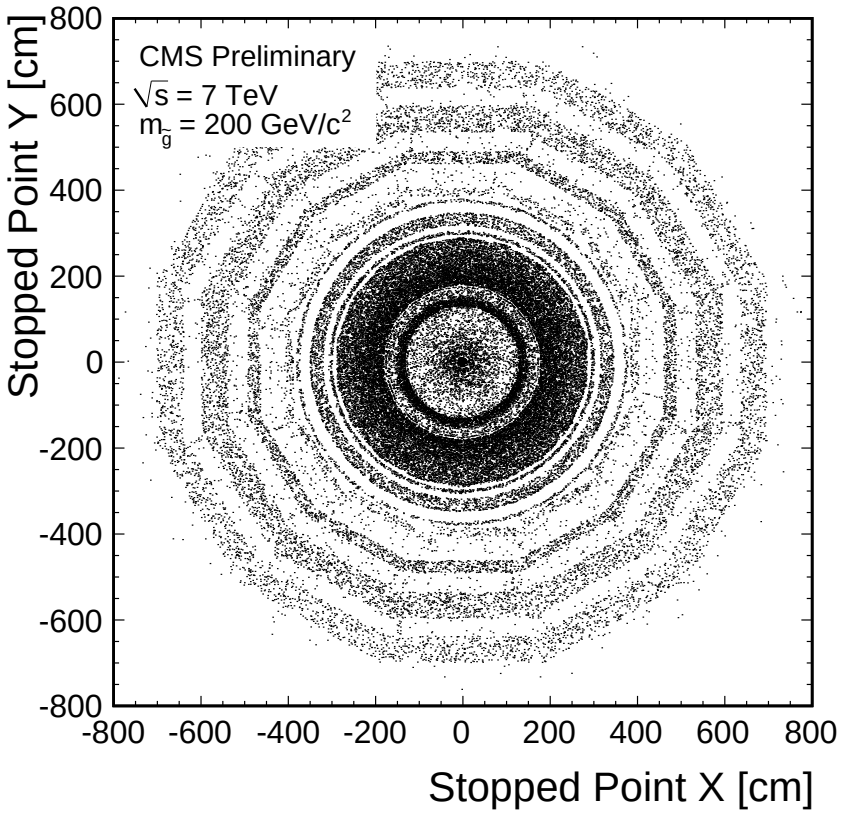

Figure 5.4: xy view of locations of stopped gluinos within the CMS detector volume

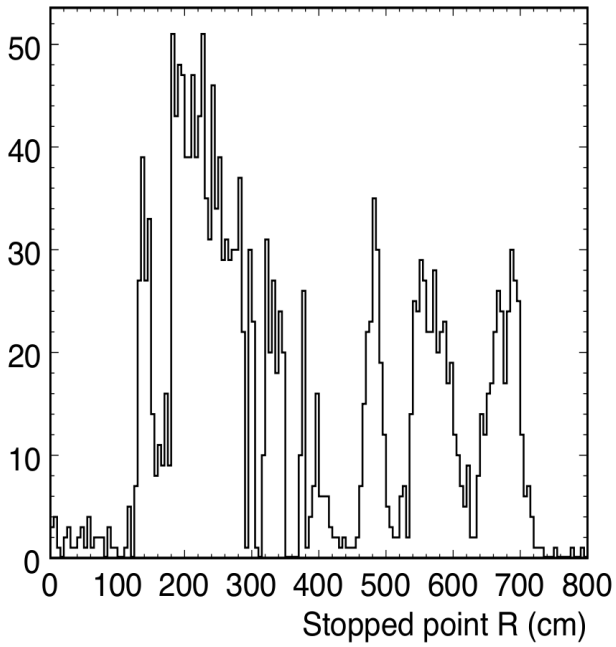

Figure 5.5: r distribution of stopping points of gluinos within CMS

5.4 Decay

PYTHIA is now used to simulate the decay of gluinos within R-hadrons that stop within the detector volume. We simulate the two leading processes (Figure 5.6):

$$\Delta_{\tilde{g}}^{++} \rightarrow \tilde{g}u(uu) \rightarrow g\tilde{\chi}_1^0 u(uu)$$

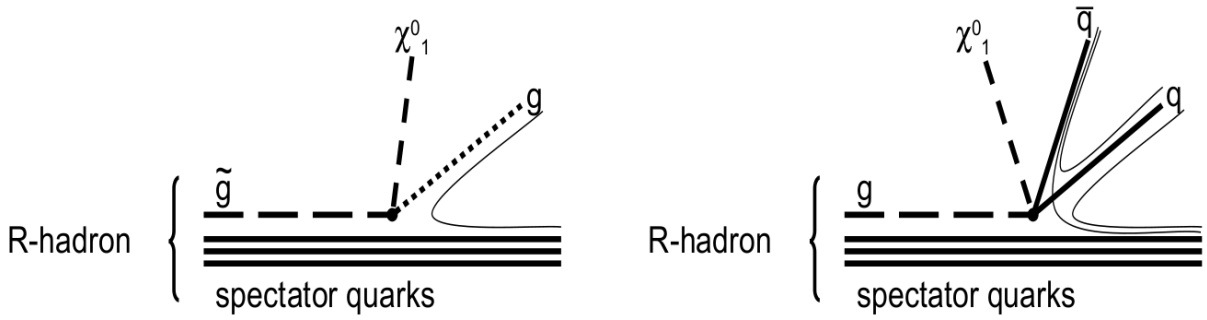

Figure 5.6: The mono- and di-jet decay modes of R-hadrons

$$\Delta_{\tilde{g}}^{++} \rightarrow \tilde{g}u(uu) \rightarrow q\bar{q}\tilde{\chi}_1^0 u(uu)$$

Neutralino mass is scanned for each gluino mass to produce a wide range of resultant available energy for jets coming out of the decay point.

5.5 CMSSW

CMSSW is a CMS-collaboration-internal software suite for processing CMS data [43]. CMSSW data consists of ROOT files formated with a consistent directory structure. The "Event" substructure of CMSSW ROOT files contains one or more collections of custom-defined C++ classes corresponding to various types of objects, for example HCAL hits, muon tracks, and reconstructed electrons. The bulk of CMSSW code is in a large number of independently compiled C++ plug-ins, which loops over provided events, takes a subset of custom classes as input, and either adds derived information to the event (an "EDProducer"), returns a true/false result to a test (an "EDFilter"), or produces results to be saved to external plots or data files (an "EDAnalyzer"). "Event Setup" modules provide detector conditions information such as a magnetic field map, or HCAL calibration, valid for the time the data originates from.

PYTHIA, GEANT4, and ROOT are included in distributions of the CMSSW suite, although stored independently from the collaboration-specific code and accessed via wrapper interfaces. Versions of PYTHIA, GEANT4, and ROOT are standardized on for a given CMSSW version.

For the purpose of this analysis, we use CMSSW to simulate detector response

to simulated decays, and to process that data into higher-level objects, such as calorimetry towers and muon tracks. Many of these higher-level objects are produced as a matter of course in the process of standard data-taking and processing, and we favor these standard objects over our own production of these objects whenever possible.

5.6 Timing

The timing stage of the simulation is independent of the physical production, decay, and material-interaction model. The simulation calculates, for a given lifetime of a long-lived particle and the conditions within the LHC, the relative likelihood to detect a particle in a given non-collision bunch. The results from the other stages are used to translate these results into absolute numbers of decays, and given such information as input, the timing simulation will also distribute these decays randomly according to the likelihood it calculates for each time location.

The simulation begins with an arbitrarily large number of signal events, and assigns the production of each one randomly according to provided instantaneous luminosity information. This can be actual luminosity information from the CMS luminosity group for the running of the LHC in a given period, or a hypothetical model. Each particle is assigned to a particular luminosity section, a period of 2^{18} orbits, which is the granularity of the available information for LHC running.

Then the simulation randomly determines the decay time of each particle by drawing a number from an exponential distribution, with the input lifetime used as

the decay constant. This decay time is added to the production time to determine when the particle would be observed.

This time is then checked to see if it is in a sensitive period according to the timing rules. Using an input nominal bunch structure as a basis, these rules check for proximity to colliding bunches, unpaired bunches, and bunches close-but-not-colliding with bunches in the opposite beam. The timing rules used for this analysis are further discussed in Chapter 7.

Trigger rules can also be simulated.

The result is then rescaled so that the total number of events simulated sum according to the following formula:

$$N = t\sigma L\epsilon_{Stopping}\epsilon_{Analysis}$$

where t is the time of the run, σ is the production cross-section, L is the luminosity, $\epsilon_{Stopping}$ is the probability of a produced particle stopping within the detector boundaries, $\epsilon_{Analysis}$ is the probability of the decay of a stopped particle passing trigger and analysis rules that separate signal from noise.

The timing simulation likewise determines the effect of timing factors on the sensitivity to background; however it is assumed that the occurrence of background events is flat with respect to time, since background is largely independent of any beam effects (see Chapter 6), greatly simplifying the steps required.

The results of the third phase can be summarized by the so-called "timing efficiency", that is, the probability that timing factors will not exclude an event from being detected. This factor is model independent except for lifetime and can

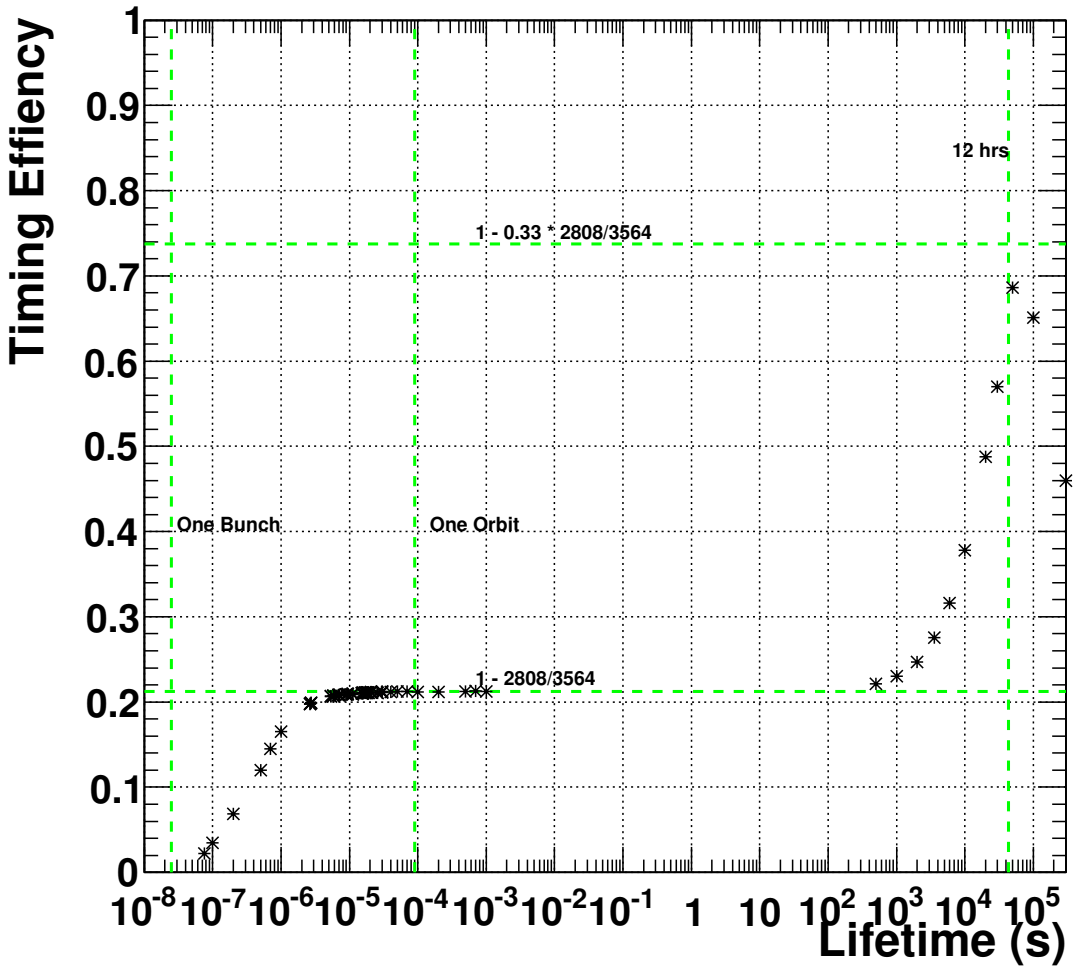

Figure 5.7: The effects of filling scheme and running cycle on sensitivity

be used in conjunction with the results of the other stages. Alternately this stage of the simulation can run pseudoexperiments to determine a number of detected signal and background for a particular hypothetical analysis.

Figure 5.7 shows several features in timing efficiency for a hypothetical running situation (nominal LHC full filling scheme, 8 hours on, 16 hours off). First, for lifetimes well below 10^{-7}s, particles aren't sufficiently long-lived to decay away from their collision bunch crossing. All collision bunch crossings are excluded from our

analysis, as a source of excessive noise.

The second feature is the plateau at efficiency of 0.212. As lifetime approaches the length of the orbit, decays occur randomly within the bunch structure. The result is an efficiency that approaches the ratio of empty bunches to total bunches within an orbit.

Eventually the run stops. Particles with lifetimes in minutes and greater start to decay more and more after the end of the run. All bunches in this region are sensitive, since there are no collisions taking place. At some point CMS stops recording data, and the longest lived particles decay more frequently after that point, resulting in the drop-off at the end of the plot.

The contrast of a flat distribution (for the background) and an exponential one (signal) suggests the design of a time cut-off after which background events dominate and should be ignored. By maximizing the expression $s/\sqrt{b}$, the optimum window after possible production can be determined to be 1.256 times the lifetime. This factor will be used in the final analysis.

Chapter 6

Background Characteristics

6.1 Overview

This search gets its data from periods without collisions. Therefore, backgrounds can be studied even before activation of the LHC. On several occasions CMS recorded data in conditions similar to those in which collisions were expected to take place. In 2008 and 2009 CMS took long-term runs to observe cosmic rays and test the detector, and then in 2010 CMS took data to test detector readiness in advance of collisions. All this data provides inspiration and direction for analysis rules, and then provides a source to draw from to perform the final measurement of background rate.

Since the strategy for this search is to look for deposits in the hadronic calorimeter that cause a high-level jet trigger to fire, background consists of anything that causes the spontaneous appearance of a jet-like object in the absence of collisions. There are two sources that do this in the absence of circulating beam: hard bremsstrahlung from a cosmic muon in the hadronic calorimeter, and noise within the instrumentation of HCAL electronics. With circulating beam, halo effects, beam-gas collisions, and non-colliding bunches may also contribute.

Noise Type	Frequency ± Stat. Uncertainty
Cosmic Bremsstrahlung	16.3% ± 0.3%
HPD (CT method)	47.3% ± 0.4%
HPD (E frac. method)	31.7% ± 0.4%
RBX	4.6% ± 0.1
Remainder	0.1% ± 0.02%

Table 6.1: Relative frequency of observed noise types in low luminosity (10^{26}cm^{-2}s^{-1}) running. Systematic uncertainty is roughly 23% (from 8.3).

6.2 Non-Beam-Related Background

Further information in this section on HCAL-instrumentation-related noise and cosmic muon effects in the hadronic calorimeter was developed in collaboration with the CMS HCAL team and published in [36].

The relative frequency of events in the HLT path caused by the mechanisms below is given in Table 6.1.

6.2.1 Cosmic Bremsstrahlung

Events originating from cosmic muon activity within the HCAL (example Figure 6.1) can be rejected by vetoing events that identify one or more muon travelling through the muon system. Any muon that has a reconstructable path through CMS, even those not originating from the beam-line, are identified and recorded by the standard CMS reconstruction path, allowing us to reject them.

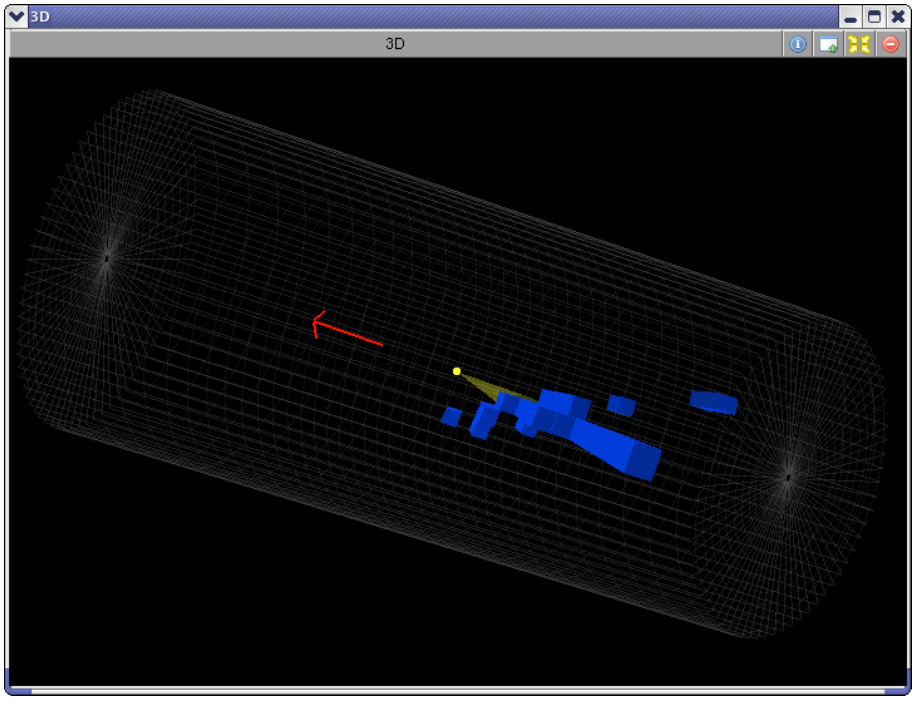

Figure 6.1: An example muon bremsstrahlung event in the CMS hadronic calorimeter.

6.2.2 Instrumentation Noise

6.2.2.1 HPD Noise

The largest contribution of events by far to our sample set is noise caused by the discharge of a Hybrid Photodiode. HPD noise is recognizable because it appears as an energy deposit in most, if not all, 18 channels connected to an HPD without signal in the other HPDs. The channels in an HB HPD correspond to a row of towers in a single $i\phi$ on one η side, and so can be quickly identified.

Two methods were used to isolate HPD noise in Table 6.1. The first labels an event as HPD noise if the five largest HB energy deposits are in the same HPD. The second labels an event as HPD noise if the first method fails and 90% or more of the energy deposited in HB was deposited in the same HPD.

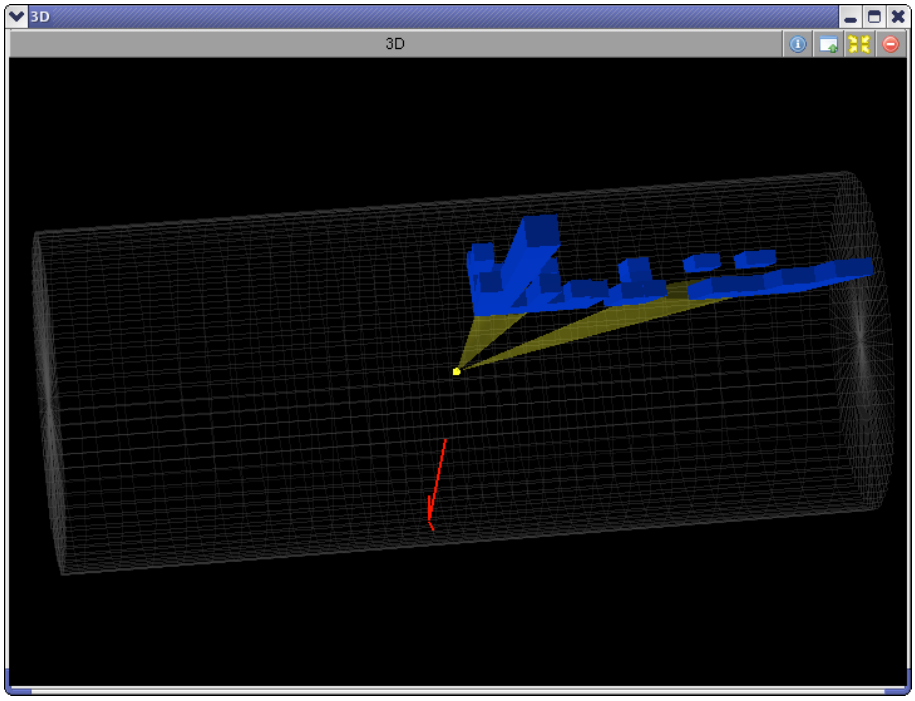

Figure 6.2: An example RBX noise event in the CMS hadronic calorimeter

6.2.2.2 RBX Noise

The remaining cause of events within the sample studied had a large number of hits in the read-out box of greatest energy (example Figure 6.2). Read-out boxes package together the digitization electronics for fibers from 4 HPDs, and appear to have a common source of abnormal behavior, resulting in a sudden appearance of an energy deposit in these HPDs. This can manifest as a large number of hits appearing in the highest energy RBX.

6.3 Beam-Related Background

Other events may originate from beam activity but be more difficult to distinguish if they produce physical energy deposits in the HCAL HB without causing

responses in other detectors like cosmic rays do. One test that can be effective is to veto events with a reconstructed vertex in the beam-pipe.

Beam Halo is the distribution of energetic muons running parallel to the beam-line. Halo is caused by protons escaping the beam-line and colliding with magnets, etc., to create a shower of pions, some of which decay to muons. Halo can be identified by the Cathode Strip Chamber muon detectors in the endcaps of CMS. A level-1 trigger tags events containing halo activity.

Non-colliding bunches may also produce unwanted events. Several filling schemes in 2010 contain bunches that do not collide at IP5. Their proximity to other bunches, however, may cause "parasitic" collisions by leaking protons into neighboring bunches and causing unexpected collisions. In the 2010 filling schemes, it is possible without much effect on the amount of data collected to ignore the BXes of these bunches, and their neighbors.

Chapter 7

Analysis

7.1 Overview

The following approach was taken to distinguish between signal and background events in acquired data:

1. Acquire data via a no-collision jet trigger
2. Apply very loose cuts against HPD and RBX noise to reduce HLT to an acceptable rate to write to disk (detailed in Chapter 4)
3. Reject beam background
4. Reject cosmic muon background
5. Reject HPD and RBX noise via jet variables
6. Reject HPD and RBX noise via pulse shape in HCAL raw data
7. Eliminate events not less than 1.256τ after collisions to optimize significance for each lifetime considered

A threshold for removing data is hereafter referred to simply as a "cut". Plots shown in this chapter are referred to as "N-1" if they are plotted after removing events via all cuts other than the one on the displayed variable, with the exception

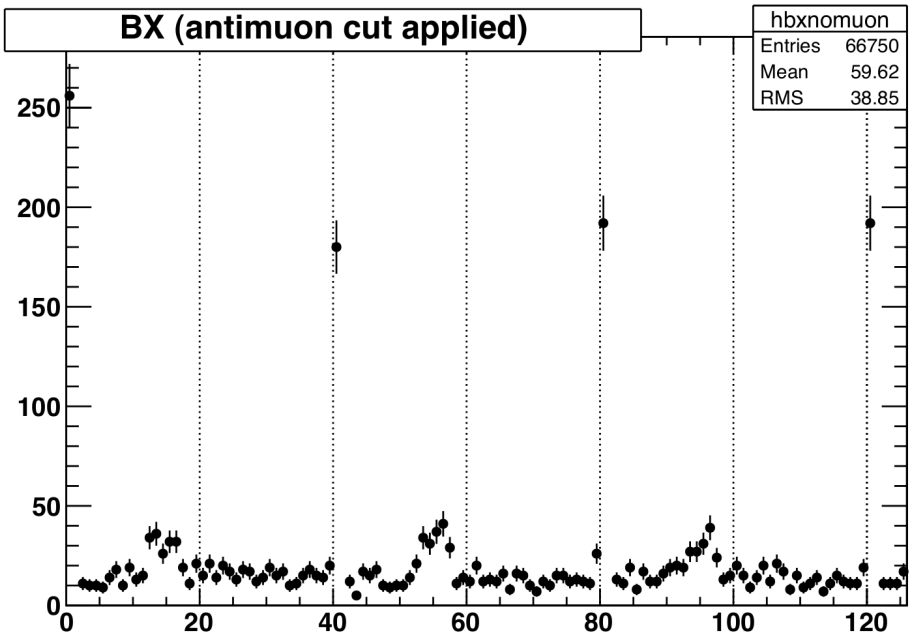

Figure 7.1: A sample distribution of HLT events taken from collision data, showing BXs 1 to 125. Collisions at 1,41,81,... are expected for this sample.

that HCAL raw timing variable cuts are not performed before muon and jet-variable N-1 plots.

7.2 Rejecting Beam Background

Figure 7.1 shows the distribution of BX number for HLT events taken before any beam background rejection is applied. Spikes can be seen preceding expected collisions, demonstrating the existence of significant beam-related background.

To suppress beam-related background, we veto any event in which the beam current monitor (BPTX) detects particles in either beam (events with particles in both are already rejected by the L1 trigger). Proton leakage into neighboring BXes can cause events to appear 1 BX early or late with respect to a collision BX. These events are suppressed by rejecting events within a range $BX - 2$ to $BX + 1$ of a

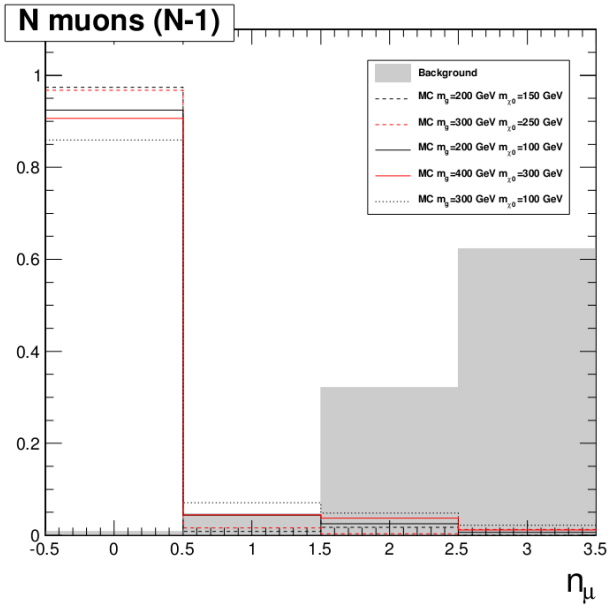

Figure 7.2: N-1 distribution of number of reconstructed muons for MC signal and observed background

collision.

Some LHC filling schemes contain non-colliding bunches and/or "parasitic" collisions 11.25 m before or after the center of the detector. Backgrounds from parasitic collisions with these bunches, beam halo, or beam gas are suppressed by rejecting events falling within $BX-2$ to $BX+1$ of the expected passage of a bunch through CMS.

7.3 Rejecting Cosmic Muons

Cosmic muon events are rejected by rejecting events in which the standard CMSSW reconstruction sequence reconstructs one muon in the "cosmic" collection. This collection is distinct from the usual one in CMSSW which has a restriction on muon vertex (a restriction which would severely reduce the reconstruction efficiency

for cosmic muons). The distribution of the number of muons from gluino monte-carlo and observed background in the low luminosity background sample is shown in Figure 7.2.

7.4 Rejecting HPD and RBX noise via Jet Variables

We restrict our search to the HCAL barrel. Since gluinos tend to be produced centrally due to their high mass, we do not consider events from other subdetectors with little loss of signal efficiency. This enables us to consider noise from instrumentation only associated with the HB and not from the HE and (very different) HF.

We reject jets via specific reconstructed quantities. Energy over 50 GeV is required, to minimize the contribution of fluctuations over our HLT threshold. Furthermore, noise due to minimum-ionizing-particles, such as cosmic muons, is reduced.

We veto events with 90% of the jet energy in 3 or fewer towers, and events with 60% of the energy in 6 or greater towers. This selects events where the jet shape resembles a natural physical response expected from gluino decays, and rejects a large quantity of HPD- and RBX-related noise.

Finally, we eliminate events in which the 5 greatest-energy hits are in the same $i\phi$. This reduces contributions from events in which an HPD discharges, causing spurious charge flashes on its pixels.

Distributions for these variables are shown in Figure 7.3.

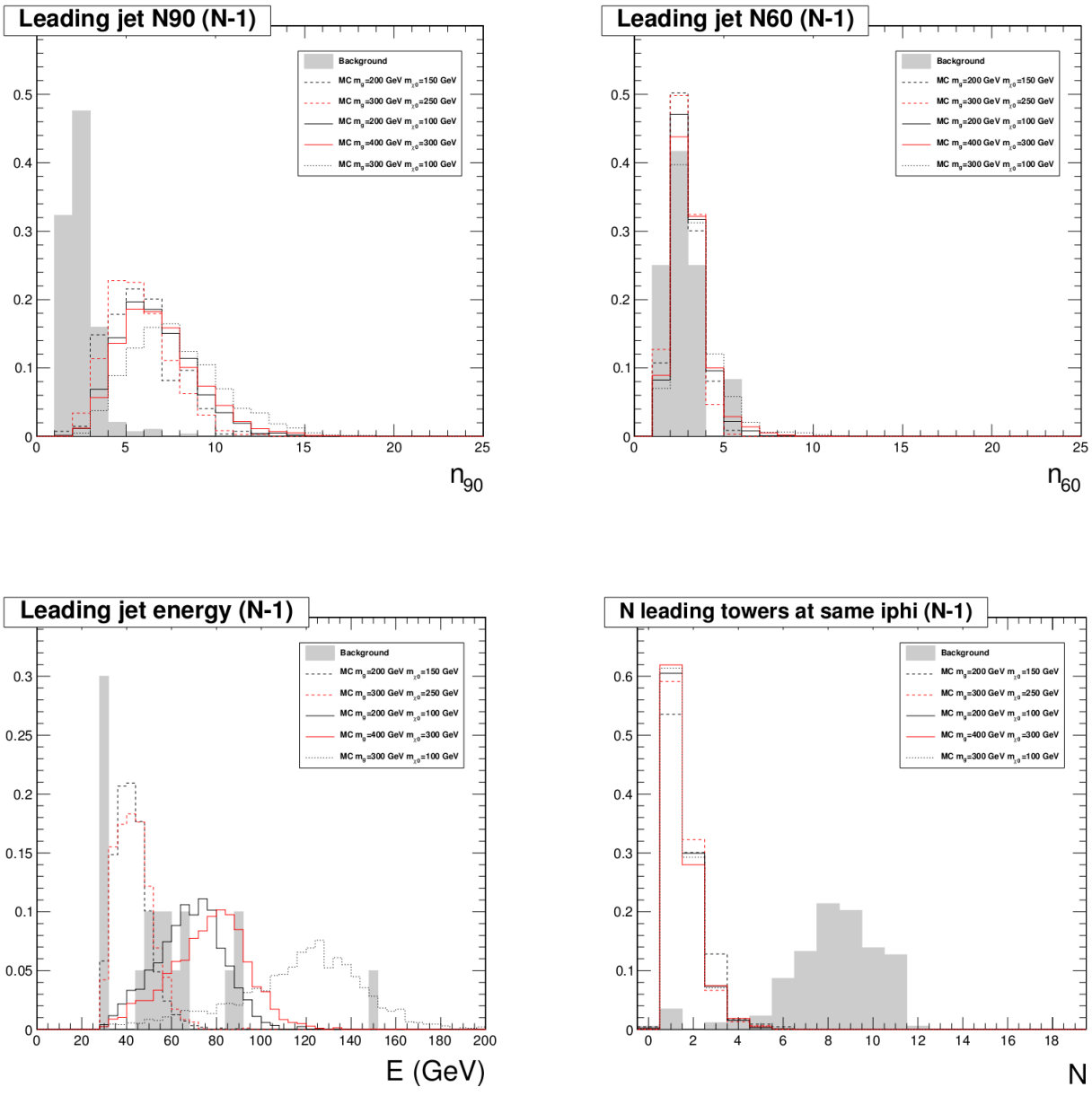

Figure 7.3: N-1 distributions of jet analysis variables in MC signal and observed background

7.5 Rejecting HPD and RBX noise via Pulse Shape

The raw HCAL time-slices of the remaining events are examined. Proper QIE response to a physical interaction with the scintillator material was shown in Figure 3.10. A sample event with properly formed digitization of this signal is visible in Figure 7.4. Common results from bad events caused by undesired activity in the HPD or RBXes can be seen in Figure 7.5.

Signal can be distinguished from background in this case by taking advantage of the rise and fall-off characteristic of the signal pulse shape. Four variables are used:

1. R_1: Ratio of the signal in the time-slice immediately following the peak time-slice to the signal in the peak

2. R_2: Ratio of the signal 2 BXes after the peak to the signal 1 BX after the peak.

3. R_{peak}: Ratio of the peak to the sum of all 10 BXes

4. R_{outer}: Ratio of the sum of all BXes except the peak, the BX prior to the peak, and the two BXes after the peak, to the sum of all 10 BXes

Timing variables for various classes of events can be seen in Figures 7.6, 7.7 and 7.8.

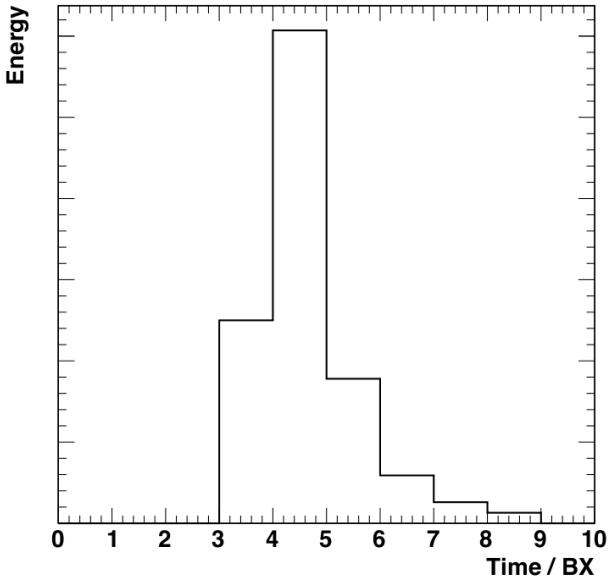

Figure 7.4: Expected HCAL pulse shape for signal

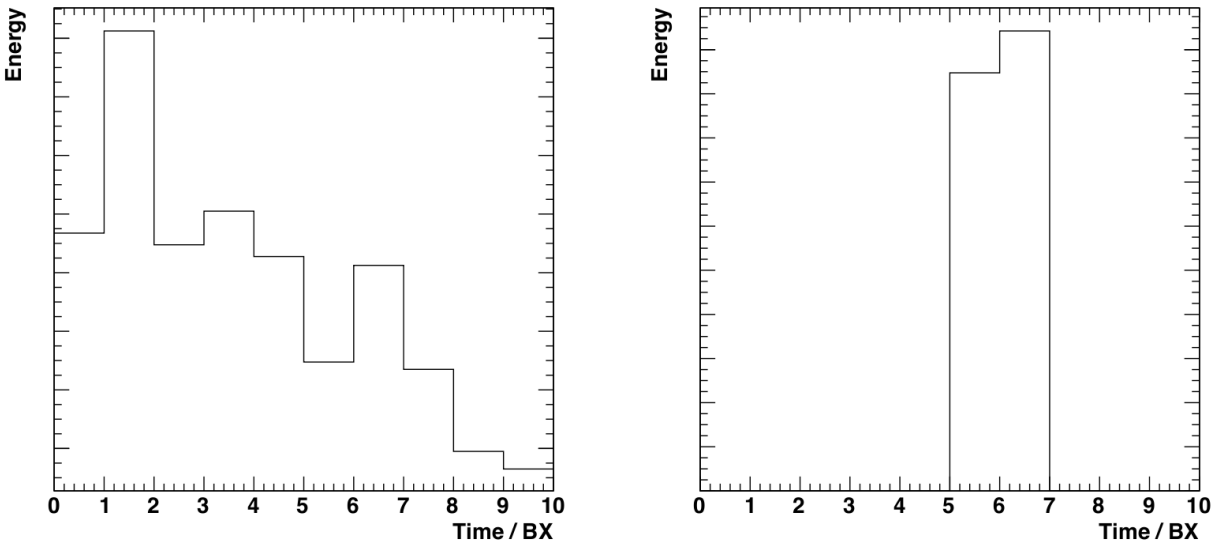

Figure 7.5: Example pulse shapes from bad HPD or RBX events

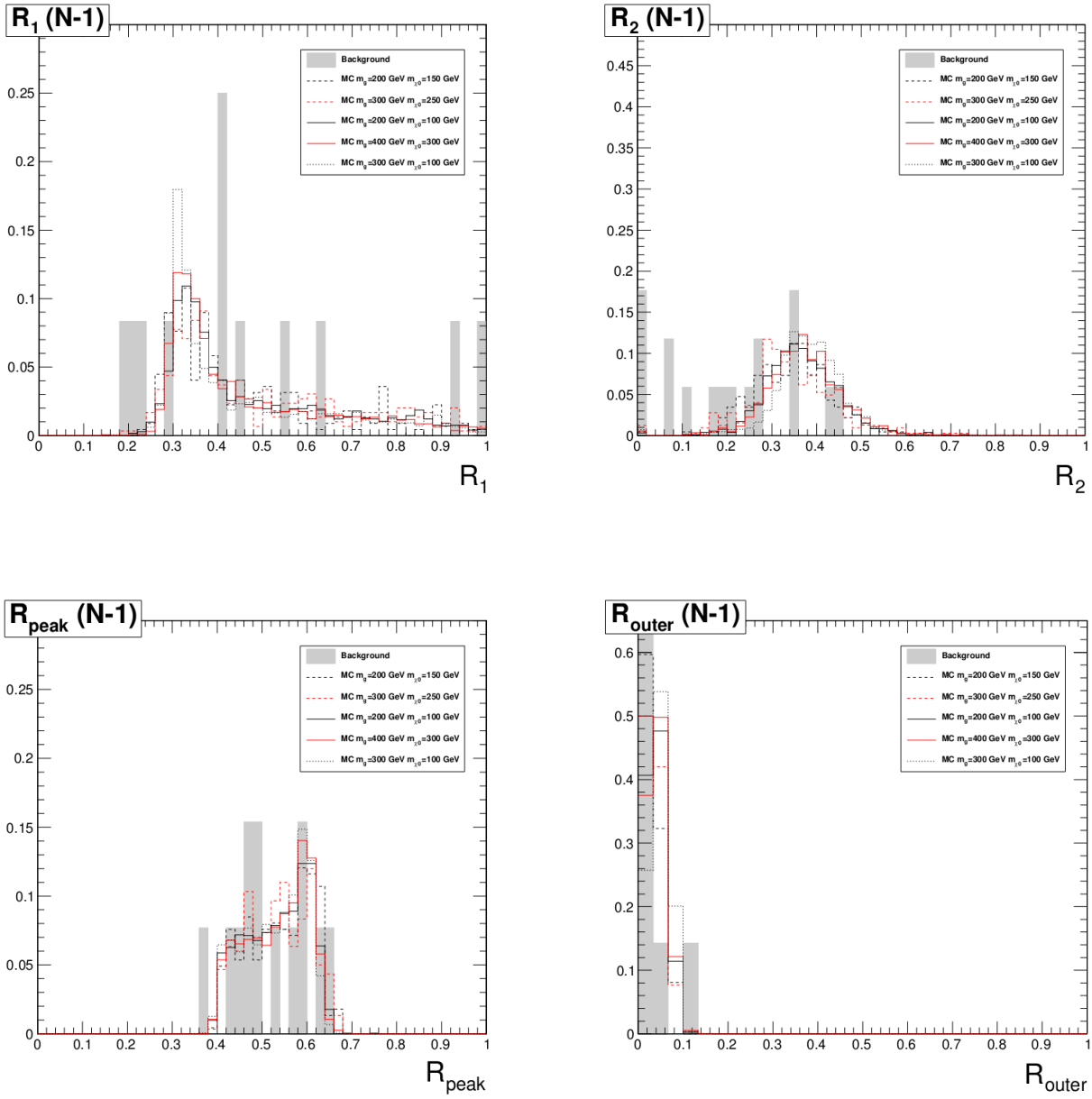

Figure 7.6: Raw signal variable N-1 plots, as defined Section 7.5

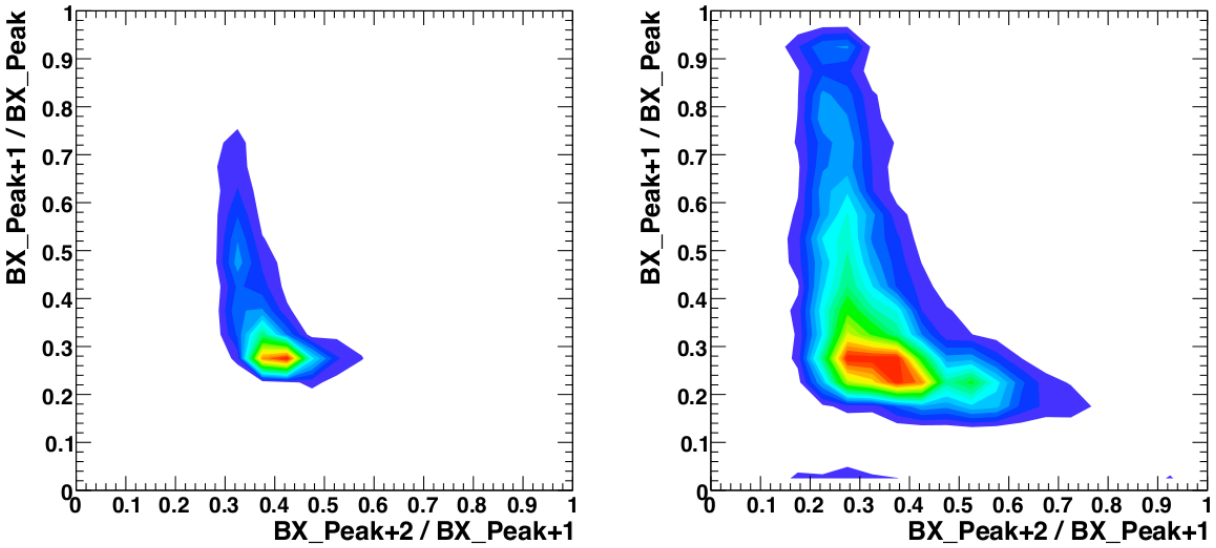

Figure 7.7: Raw signal timing ratios for (a) signal events and (b) high energy cosmic muon events from CRAFT 08

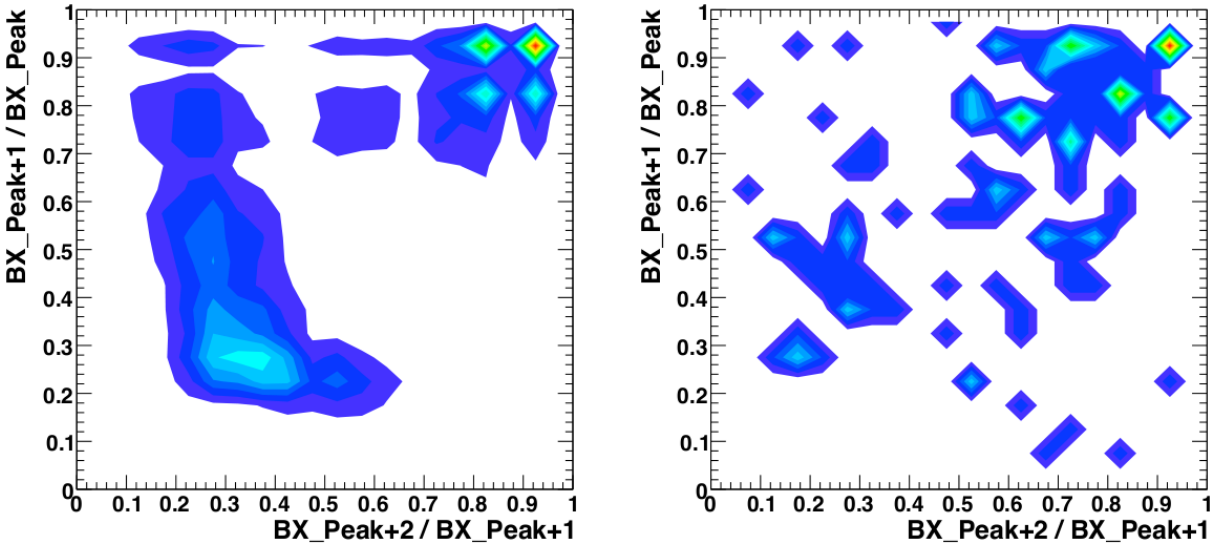

Figure 7.8: Raw signal timing ratios for (c) all jet-triggered events and (d) events after jet shape cuts from CRAFT 08

Cut	BG eff% (cum.)	BG eff% (N-1)
muon veto	67.	1.2
$E_{jet} > 50$ GeV, $\|\eta_{jet}\| < 1.3$	7.6	1.2×10^{-2}
$n_{60} < 6$	7.6	5.4×10^{-3}
$n_{90} > 3$	0.39	1.9×10^{-1}
$n_{iphi} < 5$	0.011	1.3×10^{-1}
$R_1 > 0.15$	0.0091	6.0×10^{-3}
$0.1 < R_2 < 0.5$	0.0060	7.4×10^{-3}
$0.4 < R_{peak} < 0.7$	0.0057	5.7×10^{-3}
$R_{outer} < 0.1$	0.0054	5.7×10^{-3}
Cut	Signal MC eff% (cum.)	Signal MC eff% (N-1)
muon veto	88.0	62.7
$E_{jet} > 50$ GeV, $\|\eta_{jet}\| < 1.3$	68.6	66.2
$n_{60} < 6$	67.6	58.2
$n_{90} > 3$	62.0	62.7
$n_{iphi} < 5$	61.8	57.8
$R_1 > 0.15$	61.8	57.5
$0.1 < R_2 < 0.5$	58.3	60.8
$0.4 < R_{peak} < 0.7$	57.7	58.1
$R_{outer} < 0.1$	57.5	57.7

Table 7.1: Cumulative and N-1 efficiencies for all cuts, with respect to total number of events passing HLT, beam background and standard HCAL noise cuts

Cut	BG rate (Hz)	Signal rate (Hz)
HLT	3.27	1.17×10^{-4}
HBHE filter	1.04	1.15×10^{-4}
BPTX/BX veto	1.03	1.15×10^{-4}
muon veto	6.9×10^{-1}	1.03×10^{-4}
$E_{jet} > 50$ GeV, $\lvert\eta_{jet}\rvert < 1.3$	7.99×10^{-2}	7.99×10^{-5}
$n_{60} < 6$	7.9×10^{-2}	7.89×10^{-5}
$n_{90} > 3$	4.0×10^{-3}	7.24×10^{-5}
$n_{phi} < 5$	1.1×10^{-4}	7.21×10^{-5}
$R_1 > 0.15$	9.4×10^{-5}	7.21×10^{-5}
$0.1 < R_2 < 0.5$	6.1×10^{-5}	6.80×10^{-5}
$0.4 < R_{peak} < 0.7$	5.8×10^{-5}	6.73×10^{-5}
$R_{outer} < 0.1$	5.6×10^{-5}	6.70×10^{-5}

Table 7.2: Background and signal event rates assuming $m_{\tilde{g}} = 300$ GeV, $m_{\tilde{\chi}} = 200$ GeV, and an instantaneous luminosity of $10^{31}\text{cm}^{-2}\text{s}^{-1}$.

7.6 Comparison to Expected Events

This sequence results in a rate of events of 0.000056 Hz, or one every five hours, for background noise. 57.5% of stopped gluino HLT events pass this sequence (Tables 7.1 and 7.2).

The relationship between expected number of events and gluino cross-section is very complicated for this analysis. The number of events is the product of the percentage of productions that stop in the detector, the percentage that pass analysis rules, and the percentage that are visible after beam-related BX cuts, the lifetime-dependent cut, and CMS dead-time (time CMS is not recording events because of errors, planned shutdown, or cycling CMS state). Furthermore, since neither the instantaneous luminosity nor CMS availability are constant over time, these quantities needs to be integrated over time.

In order to determine the number of expected observable decays, the following information is used:

- History of instantaneous luminosity (CMS provides this information averaged over 23.4 second segments, called "luminosity sections")
- Bunch structure of LHC fills
- Time periods of CMS data-taking

This information is fed into a timing simulation to determine a timing-efficiency figure as a function of lifetime, which then provides the final ingredient for the relationship between cross-section and number of expected events:

$$n_s = \sigma \mathcal{L} \epsilon_{Stopping} \epsilon_{Analysis} \epsilon_{Timing}$$

Finally, the expected background is calculated as the following:

$$n_b = rate * t$$

"*Rate*" is measured from a smaller very-low-luminosity ($10^{26}\text{cm}^{-2}\text{s}^{-1}$) sample preceding the search sample. We choose a sample as close in time to the search sample as possible, as the rate of HPD- and RBX-caused events vary over time-scales of months or greater (due to causes unknown but, at the minimum, related to variations in equipment used and voltages applied).

Chapter 8

Results and Conclusions

8.1 Results

After applying the selection criteria to the search sample, we are left with seven events. When we introduce the lifetime-dependent search window, the number of events remaining is shown along background expectation in Table 8.1. Two statistical uncertainties are quoted in this table. The first is the uncertainty of the simulation that calculates timing efficiency, and the second is the statistical uncertainty on the background rate measurement from the low-luminosity background sample.

No significant excess of events was observed. Therefore, we set 95% Confidence Level (C.L.) limits on gluino production as a function of lifetime. We use the CLs procedure documented in [45] to generate an upper limit on the cross-section, accounting for both statistical and systematic uncertainties. Figure 8.1 shows this as a function of lifetime, alongside the theoretical prediction, calculated from [46, 47].

Following the relationship between mass and stopping efficiency predicted from the monte-carlo results in Section 5.3, the corresponding plot of excluded cross-section as a function of gluino mass is calculated and shown in Figure 8.2

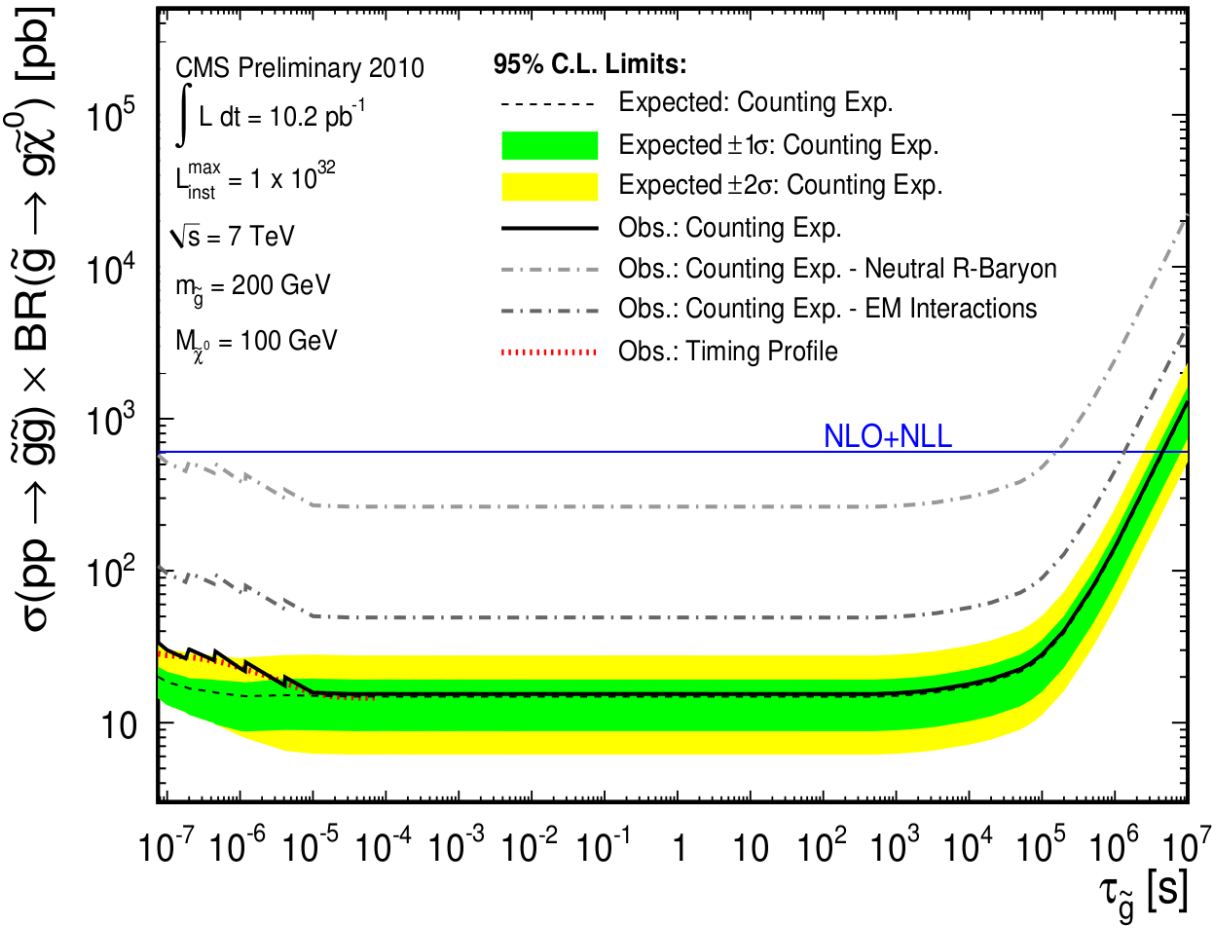

Figure 8.1: Expected and observed 95% C.L. limits on gluino pair production cross-section as a function of gluino lifetime

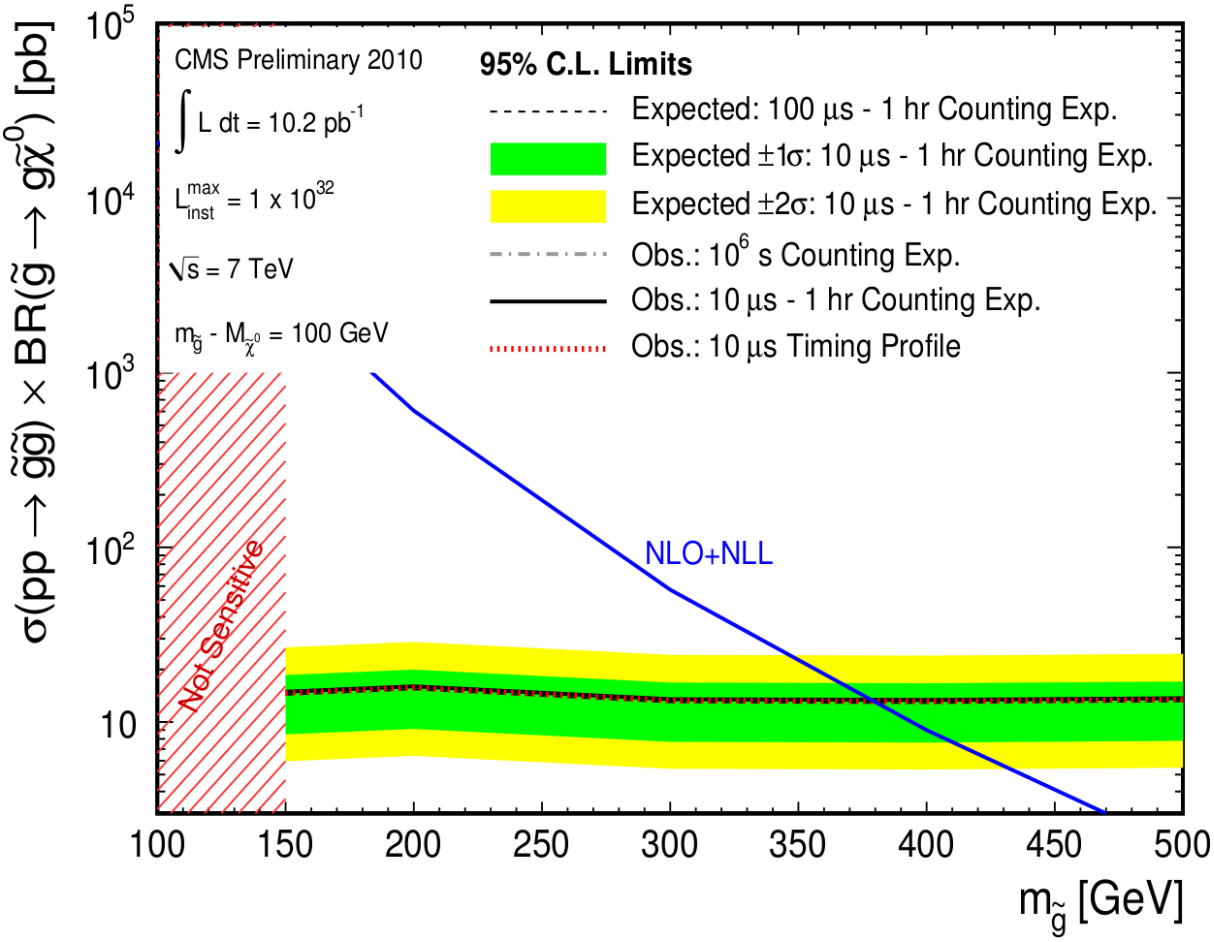

Figure 8.2: Expected and observed 95% C.L. limits on gluino pair production cross-section as a function of gluino mass

Lifetime	$L_{eff}(pb^{-1})$	Expected Bg ($\pm$ stat)	Observed
75 ns	3.3	$0.9 \pm 0.1 \pm 0.2$	3
100 ns	3.6	$0.9 \pm 0.1 \pm 0.2$	3
1 μs	5.8	$2.5 \pm 0.2 \pm 0.3$	5
10 μs	8.4	$6.4 \pm 0.4 \pm 1.4$	7
30 μs - 10^3 s	8.5	$6.4 \pm 0.4 \pm 1.4$	7
10^4 s	7.4	$6.4 \pm 0.4 \pm 1.4$	7
10^5 s	4.7	$6.4 \pm 0.4 \pm 1.4$	7
10^6 s	0.9	$6.4 \pm 0.4 \pm 1.4$	7
10^7 s	0.1	$6.4 \pm 0.4 \pm 1.4$	7

Table 8.1: Results of analysis of the search period for selected τ

8.2 Systematic Uncertainty

Systematic uncertainty is minimized by the design of the experiment. Background is measured directly, in detector conditions as close to identical to the search window as obtainable. Systematic uncertainty on the background rate is dominated by the reliability of this noise background estimate, and is determined from the range of values of the square points in Figure 8.3 (measured background rates in multiple low-luminosity runs) to be 23%.

Jet energy scale also contributes to systematic uncertainty. For a jet-energy-scale uncertainty of $\pm$10%, we calculate a 7% effect on cross-section limit. Finally, there is an estimated 11% uncertainty on the luminosity.

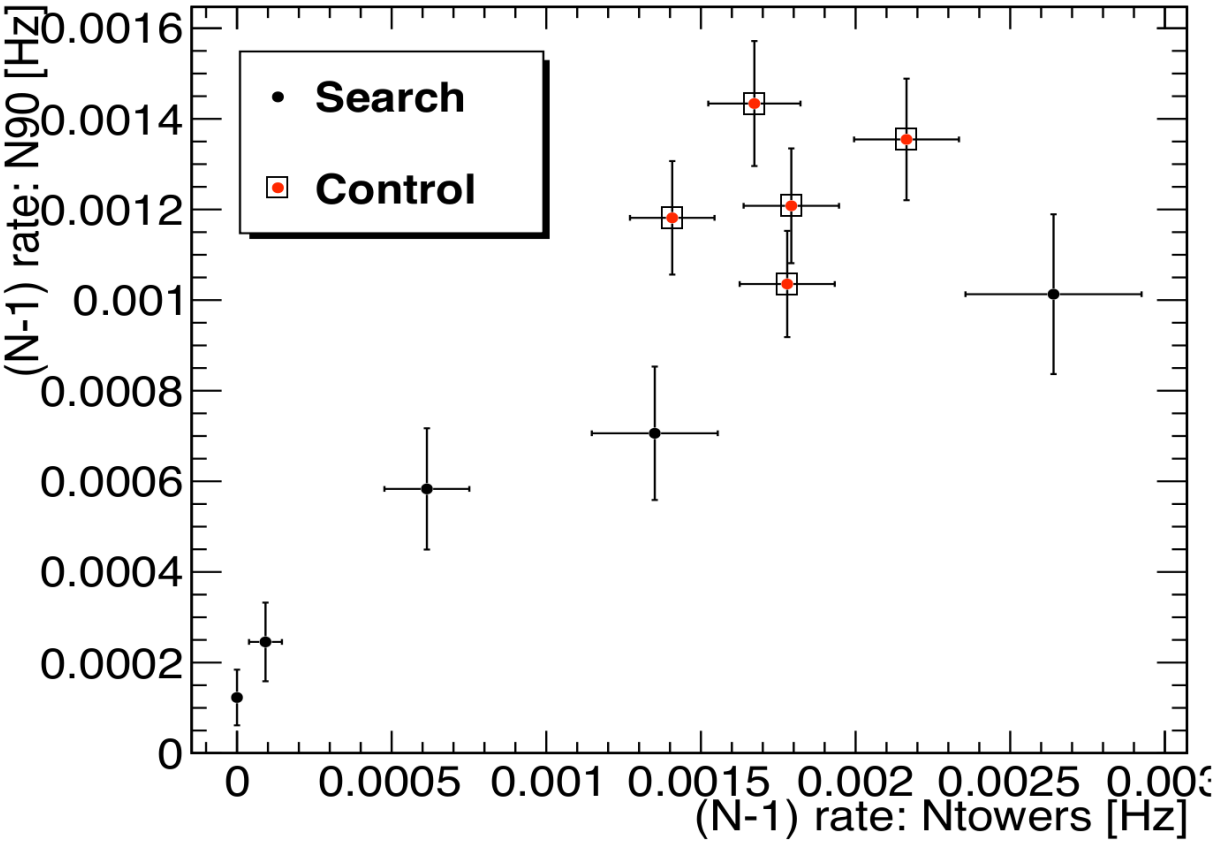

Figure 8.3: Measured background rates after N-1 cuts on n_{90} and n_{iphi}, showing stability of each in a sequence of runs.

Sources of Systematic Error	Fractional Uncertainty
Theoretical Uncertainty on Stopping Efficiency	see Figure 8.1
Jet Energy Scale Uncertainty	7%
Luminosity Uncertainty	11%
Uncertainty on Background Rate	23%

Table 8.2: Dominant sources of systematic uncertainty

Any model-dependent result also carries a much more substantial systematic uncertainty since the signal yield is dependant on the stopping probability. The GEANT4 simulation used to derive the stopping efficiency implements models for both electromagnetic and nuclear interaction (NI) energy loss mechanisms. Whereas the EM model has been extremely well tested in previous experiments, and is based on known physics, the R-hadron "cloud model" used for NI has never been tested and is based on speculative physics extrapolated from low-energy QCD. Moreover, there are alternative models [48] in which R-hadrons preferentially become neutral after NI. While we think both the neutral R-hadron and EM only models are pessimistic scenarios, in Figure 8.1 we present limits employing each of these models. The range spanned by these three curves represents the uncertainty on the limit due to the stopping model.

Systematic uncertainties are summarized in Table 8.2.

8.3 Lifetime Fit Analysis

Figure 8.1 also includes a 95% C.L. exclusion limit for a method referred to as "Timing Profile". This method involves a more complex analysis using the distribution of the observed events in time. Since a gluino decays with exponential distribution after its productions, one expects for a given lifetime the decays to follow a predictable distribution as a function of bunch crossing within an orbit. Rather than restricting events to a window of 1.256τ following collision bunches, we vary τ using the statistical suite RooStats [49] and calculate the statistical likelihood of a signal hypothesis versus that of a background with constant distribution in time. This method uses no background prediction and thus lacks the corresponding systematic uncertainty, but instead has a larger statistical uncertainty due to the additional degrees of freedom. The obtained limit is overlaid on Figure 8.1.

A sample signal distribution for this lifetime-fitting method is depicted in Figure 8.4.

8.4 Conclusion and Prospectus

In this thesis we demonstrated the results of a search for long-lived gluinos which have stopped in the Compact Muon Solenoid detector after being produced in 7 TeV *pp* collisions from CERN's Large Hadron Collider. We looked for the subsequent decay of these particles during time intervals where there were no *pp* collisions in the Compact Muon Solenoid experiment. In a dataset with a peak instantaneous luminosity of $1 \times 10^{32}\text{cm}^{-2}\text{s}^{-1}$, an integrated luminosity of up to

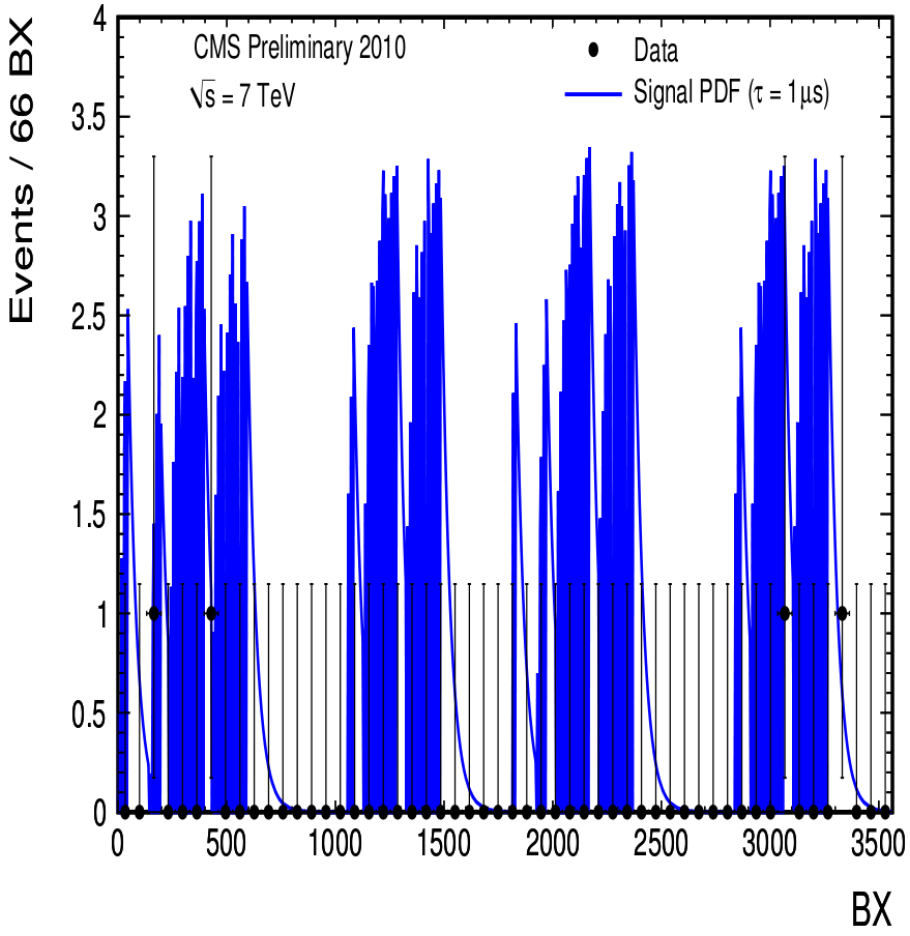

Figure 8.4: 4 events observed in a data sample with 248×248 LHC filling structure, overlaid on a decay profile for a 1 μs lifetime hypothesis

10.2 pb^{-1}, and a search interval corresponding to 62 hours of LHC operation, no significant excess above background was observed. In the absence of a signal, we set a limit at 95% C.L. on gluino pair production over 14 orders of magnitude of gluino lifetime. For a mass difference $m_{\tilde{g}} - m_{\tilde{\chi}_1^0} > 100$ GeV, assuming BR($\tilde{g} \to g\tilde{\chi}_1^0$) = 100%, we are able to exclude lifetimes from 10 μs to 1000 s for $m_{\tilde{g}} \leq 378$ GeV. This result extends existing limits from the Tevatron [14]. This result is consistent with the complementary exclusion provided by the direct HSCP search [50].

We expect better mass limits and lower cross-section reach from this method as LHC luminosity and energy increase in 2011. As luminosity increases and the bunch structure becomes more filled, methods to identify beam-related backgrounds will become more important. However, if background remains flat with respect to time, we can expect statistical significance of results to grow roughly as $s/\sqrt{b} = (L * t)/\sqrt{t} = L\sqrt{t}$, linearly proportional to instantaneous luminosity, which is faster than the rate of growth of traditional analyses (where background is also luminosity-dependent). We can thus expect the increase in machine performance in 2011 to be especially beneficial to this analysis and its results.

Appendix A

The CMS Collaboration

As of Nov. 26, 2010

Yerevan Physics Institute, Yerevan, Armenia

V. Khachatryan, A.M. Sirunyan, A. Tumasyan

Institut für Hochenergiephysik der OeAW, Wien, Austria

W. Adam, T. Bergauer, M. Dragicevic, J. Erö, C. Fabjan, M. Friedl, R. Frühwirth, V.M. Ghete, J. Hammer[1], S. Hänsel, C. Hartl, M. Hoch, N. Hörmann, J. Hrubec, M. Jeitler, G. Kasieczka, W. Kiesenhofer, M. Krammer, D. Liko, I. Mikulec, M. Pernicka, H. Rohringer, R. Schöfbeck, J. Strauss, A. Taurok, F. Teischinger, W. Waltenberger, G. Walzel, E. Widl, C.-E. Wulz

National Centre for Particle and High Energy Physics, Minsk, Belarus

V. Mossolov, N. Shumeiko, J. Suarez Gonzalez

Universiteit Antwerpen, Antwerpen, Belgium

L. Benucci, L. Ceard, K. Cerny, E.A. De Wolf, X. Janssen, T. Maes, L. Mucibello, S. Ochesanu, B. Roland, R. Rougny, M. Selvaggi, H. Van Haevermaet, P. Van Mechelen, N. Van Remortel

Vrije Universiteit Brussel, Brussel, Belgium

V. Adler, S. Beauceron, F. Blekman, S. Blyweert, J. D'Hondt, O. Devroede, A. Kalogeropou-

los, J. Maes, M. Maes, S. Tavernier, W. Van Doninck, P. Van Mulders, G.P. Van Onsem, I. Villella

Université Libre de Bruxelles, Bruxelles, Belgium

O. Charaf, B. Clerbaux, G. De Lentdecker, V. Dero, A.P.R. Gay, G.H. Hammad, T. Hreus, P.E. Marage, L. Thomas, C. Vander Velde, P. Vanlaer, J. Wickens

Ghent University, Ghent, Belgium

S. Costantini, M. Grunewald, B. Klein, A. Marinov, D. Ryckbosch, F. Thyssen, M. Tytgat, L. Vanelderen, P. Verwilligen, S. Walsh, N. Zaganidis

Université Catholique de Louvain, Louvain-la-Neuve, Belgium

S. Basegmez, G. Bruno, J. Caudron, J. De Favereau De Jeneret, C. Delaere, P. Demin, D. Favart, A. Giammanco, G. Grégoire, J. Hollar, V. Lemaitre, J. Liao, O. Militaru, S. Ovyn, D. Pagano, A. Pin, K. Piotrzkowski, L. Quertenmont, N. Schul

Université de Mons, Mons, Belgium

N. Beliy, T. Caebergs, E. Daubie

Centro Brasileiro de Pesquisas Fisicas, Rio de Janeiro, Brazil

G.A. Alves, D. De Jesus Damiao, M.E. Pol, M.H.G. Souza

Universidade do Estado do Rio de Janeiro, Rio de Janeiro, Brazil

W. Carvalho, E.M. Da Costa, C. De Oliveira Martins, S. Fonseca De Souza, L. Mundim, H. Nogima, V. Oguri, W.L. Prado Da Silva, A. Santoro, S.M. Silva Do Amaral, A. Sznajder, F. Torres Da Silva De Araujo

Instituto de Fisica Teorica, Universidade Estadual Paulista, Sao Paulo, Brazil

F.A. Dias, M.A.F. Dias, T.R. Fernandez Perez Tomei, E. M. Gregores[2], F. Marinho,

S.F. Novaes, Sandra S. Padula

Institute for Nuclear Research and Nuclear Energy, Sofia, Bulgaria

N. Darmenov[1], L. Dimitrov, V. Genchev[1], P. Iaydjiev[1], S. Piperov, M. Rodozov, S. Stoykova, G. Sultanov, V. Tcholakov, R. Trayanov, I. Vankov

University of Sofia, Sofia, Bulgaria

M. Dyulendarova, R. Hadjiiska, V. Kozhuharov, L. Litov, E. Marinova, M. Mateev, B. Pavlov, P. Petkov

Institute of High Energy Physics, Beijing, China

J.G. Bian, G.M. Chen, H.S. Chen, C.H. Jiang, D. Liang, S. Liang, J. Wang, J. Wang, X. Wang, Z. Wang, M. Xu, M. Yang, J. Zang, Z. Zhang

State Key Lab. of Nucl. Phys. and Tech., Peking University, Beijing, China

Y. Ban, S. Guo, W. Li, Y. Mao, S.J. Qian, H. Teng, B. Zhu

Universidad de Los Andes, Bogota, Colombia

A. Cabrera, B. Gomez Moreno, A.A. Ocampo Rios, A.F. Osorio Oliveros, J.C. Sanabria

Technical University of Split, Split, Croatia

N. Godinovic, D. Lelas, K. Lelas, R. Plestina[3], D. Polic, I. Puljak

University of Split, Split, Croatia

Z. Antunovic, M. Dzelalija

Institute Rudjer Boskovic, Zagreb, Croatia

V. Brigljevic, S. Duric, K. Kadija, S. Morovic

University of Cyprus, Nicosia, Cyprus

A. Attikis, R. Fereos, M. Galanti, J. Mousa, C. Nicolaou, F. Ptochos, P.A. Razis,

H. Rykaczewski

Academy of Scientific Research and Technology of the Arab Republic of Egypt, Egyptian Network of High Energy Physics, Cairo, Egypt

Y. Assran[4], M.A. Mahmoud[5]

National Institute of Chemical Physics and Biophysics, Tallinn, Estonia

A. Hektor, M. Kadastik, K. Kannike, M. Müntel, M. Raidal, L. Rebane

Department of Physics, University of Helsinki, Helsinki, Finland

V. Azzolini, P. Eerola

Helsinki Institute of Physics, Helsinki, Finland

S. Czellar, J. Härkönen, A. Heikkinen, V. Karimäki, R. Kinnunen, J. Klem, M.J. Kortelainen, T. Lampén, K. Lassila-Perini, S. Lehti, T. Lindén, P. Luukka, T. Mäenpää, E. Tuominen, J. Tuominiemi, E. Tuovinen, D. Ungaro, L. Wendland

Lappeenranta University of Technology, Lappeenranta, Finland

K. Banzuzi, A. Korpela, T. Tuuva

Laboratoire d'Annecy-le-Vieux de Physique des Particules, IN2P3-CNRS, Annecy-le-Vieux, France

D. Sillou

DSM/IRFU, CEA/Saclay, Gif-sur-Yvette, France

M. Besancon, M. Dejardin, D. Denegri, B. Fabbro, J.L. Faure, F. Ferri, S. Ganjour, F.X. Gentit, A. Givernaud, P. Gras, G. Hamel de Monchenault, P. Jarry, E. Locci, J. Malcles, M. Marionneau, L. Millischer, J. Rander, A. Rosowsky, I. Shreyber, M. Titov, P. Verrecchia

Laboratoire Leprince-Ringuet, Ecole Polytechnique, IN2P3-CNRS, Palaiseau, France

S. Baffioni, F. Beaudette, L. Bianchini, M. Bluj[6], C. Broutin, P. Busson, C. Charlot, L. Dobrzynski, R. Granier de Cassagnac, M. Haguenauer, P. Miné, C. Mironov, C. Ochando, P. Paganini, S. Porteboeuf, D. Sabes, R. Salerno, Y. Sirois, C. Thiebaux, B. Wyslouch[7], A. Zabi

Institut Pluridisciplinaire Hubert Curien, Université de Strasbourg, Université de Haute Alsace Mulhouse, CNRS/IN2P3, Strasbourg, France

J.-L. Agram[8], J. Andrea, A. Besson, D. Bloch, D. Bodin, J.-M. Brom, M. Cardaci, E.C. Chabert, C. Collard, E. Conte[8], F. Drouhin[8], C. Ferro, J.-C. Fontaine[8], D. Gelé, U. Goerlach, S. Greder, P. Juillot, M. Karim[8], A.-C. Le Bihan, Y. Mikami, P. Van Hove

Centre de Calcul de l'Institut National de Physique Nucleaire et de Physique des P ticules (IN2P3), Villeurbanne, France

F. Fassi, D. Mercier

Université de Lyon, Université Claude Bernard Lyon 1, CNRS-IN2P3, Institut de Physique Nucléaire de Lyon, Villeurbanne, France

C. Baty, N. Beaupere, M. Bedjidian, O. Bondu, G. Boudoul, D. Boumediene, H. Brun, N. Chanon, R. Chierici, D. Contardo, P. Depasse, H. El Mamouni, A. Falkiewicz, J. Fay, S. Gascon, B. Ille, T. Kurca, T. Le Grand, M. Lethuillier, L. Mirabito, S. Perries, V. Sordini, S. Tosi, Y. Tschudi, P. Verdier, H. Xiao

E. Andronikashvili Institute of Physics, Academy of Science, Tbil-

isi, Georgia

V. Roinishvili

RWTH Aachen University, I. Physikalisches Institut, Aachen, Germany

G. Anagnostou, M. Edelhoff, L. Feld, N. Heracleous, O. Hindrichs, R. Jussen, K. Klein, J. Merz, N. Mohr, A. Ostapchuk, A. Perieanu, F. Raupach, J. Sammet, S. Schael, D. Sprenger, H. Weber, M. Weber, B. Wittmer

RWTH Aachen University, III. Physikalisches Institut A, Aachen, Germany

M. Ata, W. Bender, M. Erdmann, J. Frangenheim, T. Hebbeker, A. Hinzmann, K. Hoepfner, C. Hof, T. Klimkovich, D. Klingebiel, P. Kreuzer[1], D. Lanske[†], C. Magass, G. Masetti, M. Merschmeyer, A. Meyer, P. Papacz, H. Pieta, H. Reithler, S.A. Schmitz, L. Sonnenschein, J. Steggemann, D. Teyssier

RWTH Aachen University, III. Physikalisches Institut B, Aachen, Germany

M. Bontenackels, M. Davids, M. Duda, G. Flügge, H. Geenen, M. Giffels, W. Haj Ahmad, D. Heydhausen, T. Kress, Y. Kuessel, A. Linn, A. Nowack, L. Perchalla, O. Pooth, J. Rennefeld, P. Sauerland, A. Stahl, M. Thomas, D. Tornier, M.H. Zoeller

Deutsches Elektronen-Synchrotron, Hamburg, Germany

M. Aldaya Martin, W. Behrenhoff, U. Behrens, M. Bergholz[9], K. Borras, A. Cakir, A. Campbell, E. Castro, D. Dammann, G. Eckerlin, D. Eckstein, A. Flossdorf, G. Flucke, A. Geiser, I. Glushkov, J. Hauk, H. Jung, M. Kasemann, I. Katkov, P. Katsas, C. Kleinwort, H. Kluge, A. Knutsson, D. Krücker, E. Kuznetsova, W. Lange,

W. Lohmann[9], R. Mankel, M. Marienfeld, I.-A. Melzer-Pellmann, A.B. Meyer, J. Mnich, A. Mussgiller, J. Olzem, A. Parenti, A. Raspereza, A. Raval, R. Schmidt[9], T. Schoerner-Sadenius, N. Sen, M. Stein, J. Tomaszewska, D. Volyanskyy, R. Walsh, C. Wissing

University of Hamburg, Hamburg, Germany

C. Autermann, S. Bobrovskyi, J. Draeger, H. Enderle, U. Gebbert, K. Kaschube, G. Kaussen, R. Klanner, B. Mura, S. Naumann-Emme, F. Nowak, N. Pietsch, C. Sander, H. Schettler, P. Schleper, M. Schröder, T. Schum, J. Schwandt, A.K. Srivastava, H. Stadie, G. Steinbrück, J. Thomsen, R. Wolf

Institut für Experimentelle Kernphysik, Karlsruhe, Germany

J. Bauer, V. Buege, T. Chwalek, W. De Boer, A. Dierlamm, G. Dirkes, M. Feindt, J. Gruschke, C. Hackstein, F. Hartmann, S.M. Heindl, M. Heinrich, H. Held, K.H. Hoffmann, S. Honc, T. Kuhr, D. Martschei, S. Mueller, Th. Müller, M. Niegel, O. Oberst, A. Oehler, J. Ott, T. Peiffer, D. Piparo, G. Quast, K. Rabbertz, F. Ratnikov, M. Renz, C. Saout, A. Scheurer, P. Schieferdecker, F.-P. Schilling, G. Schott, H.J. Simonis, F.M. Stober, D. Troendle, J. Wagner-Kuhr, M. Zeise, V. Zhukov[10], E.B. Ziebarth

Institute of Nuclear Physics "Demokritos", Aghia Paraskevi, Greece

G. Daskalakis, T. Geralis, S. Kesisoglou, A. Kyriakis, D. Loukas, I. Manolakos, A. Markou, C. Markou, C. Mavrommatis, E. Petrakou

University of Athens, Athens, Greece

L. Gouskos, T.J. Mertzimekis, A. Panagiotou[1]

University of Ioánnina, Ioánnina, Greece

I. Evangelou, C. Foudas, P. Kokkas, N. Manthos, I. Papadopoulos, V. Patras,

F.A. Triantis

KFKI Research Institute for Particle and Nuclear Physics, Budapest, Hungary

A. Aranyi, G. Bencze, L. Boldizsar, G. Debreczeni, C. Hajdu[1], D. Horvath[11], A. Kapusi, K. Krajczar[12], A. Laszlo, F. Sikler, G. Vesztergombi[12]

Institute of Nuclear Research ATOMKI, Debrecen, Hungary

N. Beni, J. Molnar, J. Palinkas, Z. Szillasi, V. Veszpremi

University of Debrecen, Debrecen, Hungary

P. Raics, Z.L. Trocsanyi, B. Ujvari

Panjab University, Chandigarh, India

S. Bansal, S.B. Beri, V. Bhatnagar, N. Dhingra, M. Jindal, M. Kaur, J.M. Kohli, M.Z. Mehta, N. Nishu, L.K. Saini, A. Sharma, A.P. Singh, J.B. Singh, S.P. Singh

University of Delhi, Delhi, India

S. Ahuja, S. Bhattacharya, B.C. Choudhary, P. Gupta, S. Jain, S. Jain, A. Kumar, R.K. Shivpuri

Bhabha Atomic Research Centre, Mumbai, India

R.K. Choudhury, D. Dutta, S. Kailas, S.K. Kataria, A.K. Mohanty[1], L.M. Pant, P. Shukla, P. Suggisetti

Tata Institute of Fundamental Research - EHEP, Mumbai, India

T. Aziz, M. Guchait[13], A. Gurtu, M. Maity[14], D. Majumder, G. Majumder, K. Mazumdar, G.B. Mohanty, A. Saha, K. Sudhakar, N. Wickramage

Tata Institute of Fundamental Research - HECR, Mumbai, India

S. Banerjee, S. Dugad, N.K. Mondal

Institute for Studies in Theoretical Physics & Mathematics (IPM), Tehran, Iran

H. Arfaei, H. Bakhshiansohi, S.M. Etesami, A. Fahim, M. Hashemi, A. Jafari, M. Khakzad, A. Mohammadi, M. Mohammadi Najafabadi, S. Paktinat Mehdiabadi, B. Safarzadeh, M. Zeinali

INFN Sezione di Bari [a], Università di Bari [b], Politecnico di Bari [c], Bari, Italy

M. Abbrescia[a,b], L. Barbone[a,b], C. Calabria[a,b], A. Colaleo[a], D. Creanza[a,c], N. De Filippis[a,c], M. De Palma[a,b], A. Dimitrov[a], L. Fiore[a], G. Iaselli[a,c], L. Lusito[a,b,1], G. Maggi[a,c], M. Maggi[a], N. Manna[a,b], B. Marangelli[a,b], S. My[a,c], S. Nuzzo[a,b], N. Pacifico[a,b], G.A. Pierro[a], A. Pompili[a,b], G. Pugliese[a,c], F. Romano[a,c], G. Roselli[a,b], G. Selvaggi[a,b], L. Silvestris[a], R. Trentadue[a], S. Tupputi[a,b], G. Zito[a]

INFN Sezione di Bologna [a], Università di Bologna [b], Bologna, Italy

G. Abbiendi[a], A.C. Benvenuti[a], D. Bonacorsi[a], S. Braibant-Giacomelli[a,b], P. Capiluppi[a,b], A. Castro[a,b], F.R. Cavallo[a], M. Cuffiani[a,b], G.M. Dallavalle[a], F. Fabbri[a], A. Fanfani[a,b], D. Fasanella[a], P. Giacomelli[a], M. Giunta[a], C. Grandi[a], S. Marcellini[a], M. Meneghelli[a,b], A. Montanari[a], F.L. Navarria[a,b], F. Odorici[a], A. Perrotta[a], A.M. Rossi[a,b], T. Rovelli[a,b], G. Siroli[a,b], R. Travaglini[a,b]

INFN Sezione di Catania [a], Università di Catania [b], Catania, Italy

S. Albergo[a,b], G. Cappello[a,b], M. Chiorboli[a,b,1], S. Costa[a,b], A. Tricomi[a,b], C. Tuve[a]

INFN Sezione di Firenze [a], Università di Firenze [b], Firenze, Italy

G. Barbagli[a], V. Ciulli[a,b], C. Civinini[a], R. D'Alessandro[a,b], E. Focardi[a,b], S. Frosali[a,b], E. Gallo[a], C. Genta[a], P. Lenzi[a,b], M. Meschini[a], S. Paoletti[a], G. Sguazzoni[a], A. Tropiano[a,1]

INFN Laboratori Nazionali di Frascati, Frascati, Italy

L. Benussi, S. Bianco, S. Colafranceschi[15], F. Fabbri, D. Piccolo

INFN Sezione di Genova, Genova, Italy

P. Fabbricatore, R. Musenich

INFN Sezione di Milano-Biccoca [a], Università di Milano-Bicocca [b], Milano, Italy

A. Benaglia[a,b], G.B. Cerati[a,b], F. De Guio[a,b,1], L. Di Matteo[a,b], A. Ghezzi[a,b,1], M. Malberti[a,b], S. Malvezzi[a], A. Martelli[a,b], A. Massironi[a,b], D. Menasce[a], L. Moroni[a], M. Paganoni[a,b], D. Pedrini[a], S. Ragazzi[a,b], N. Redaelli[a], S. Sala[a], T. Tabarelli de Fatis[a,b], V. Tancini[a,b]

INFN Sezione di Napoli [a], Università di Napoli "Federico II" [b], Napoli, Italy

S. Buontempo[a], C.A. Carrillo Montoya[a], A. Cimmino[a,b], A. De Cosa[a,b], M. De Gruttola[a,b], F. Fabozzi[a,16], A.O.M. Iorio[a], L. Lista[a], M. Merola[a,b], P. Noli[a,b], P. Paolucci[a]

INFN Sezione di Padova [a], Università di Padova [b], Università di Trento (Trento) [c], Padova, Italy

P. Azzi[a], N. Bacchetta[a], P. Bellan[a,b], M. Bellato[a], D. Bisello[a,b], A. Branca[a], P. Checchia[a], E. Conti[a], M. De Mattia[a,b], T. Dorigo[a], F. Gasparini[a,b], P. Giubilato[a,b], A. Gresele[a,c], S. Lacaprara[a,17], I. Lazzizzera[a,c], M. Margoni[a,b], G. Maron[a,17], A.T. Meneguzzo[a,b], M. Nespolo[a], M. Passaseo[a], L. Perrozzi[a,1], N. Pozzobon[a,b], P. Ronchese[a,b], F. Simonetto[a,b], E. Torassa[a], M. Tosi[a,b], A. Triossi[a], S. Vanini[a,b], P. Zotto[a,b], G. Zumerle[a,b]

INFN Sezione di Pavia [a], Università di Pavia [b], Pavia, Italy

P. Baesso[a,b], U. Berzano[a], C. Riccardi[a,b], P. Torre[a,b], P. Vitulo[a,b], C. Viviani[a,b]

INFN Sezione di Perugia [a], Università di Perugia [b], Perugia, Italy

M. Biasini[a,b], G.M. Bilei[a], B. Caponeri[a,b], L. Fanò[a,b], P. Lariccia[a,b], A. Lucaroni[a,b,1], G. Mantovani[a,b], M. Menichelli[a], A. Nappi[a,b], A. Santocchia[a,b], L. Servoli[a], S. Taroni[a,b], M. Valdata[a,b], R. Volpe[a,b,1]

INFN Sezione di Pisa [a], Università di Pisa [b], Scuola Normale Superiore di Pisa [c], Pisa, Italy

P. Azzurri[a,c], G. Bagliesi[a], J. Bernardini[a,b], T. Boccali[a,1], G. Broccolo[a,c], R. Castaldi[a], R.T. D'Agnolo[a,c], R. Dell'Orso[a], F. Fiori[a,b], L. Foà[a,c], A. Giassi[a], A. Kraan[a], F. Ligabue[a,c], T. Lomtadze[a], L. Martini[a], A. Messineo[a,b], F. Palla[a], F. Palmonari[a], S. Sarkar[a,c], G. Segneri[a], A.T. Serban[a], P. Spagnolo[a], R. Tenchini[a], G. Tonelli[a,b,1], A. Venturi[a,1], P.G. Verdini[a]

INFN Sezione di Roma [a], Università di Roma "La Sapienza" [b], Roma, Italy

L. Barone[a,b], F. Cavallari[a], D. Del Re[a,b], E. Di Marco[a,b], M. Diemoz[a], D. Franci[a,b], M. Grassi[a], E. Longo[a,b], G. Organtini[a,b], A. Palma[a,b], F. Pandolfi[a,b,1], R. Paramatti[a], S. Rahatlou[a,b]

INFN Sezione di Torino [a], Università di Torino [b], Università del Piemonte Orientale (Novara) [c], Torino, Italy

N. Amapane[a,b], R. Arcidiacono[a,c], S. Argiro[a,b], M. Arneodo[a,c], C. Biino[a], C. Botta[a,b,1], N. Cartiglia[a], R. Castello[a,b], M. Costa[a,b], N. Demaria[a], A. Graziano[a,b,1], C. Mariotti[a], M. Marone[a,b], S. Maselli[a], E. Migliore[a,b], G. Mila[a,b], V. Monaco[a,b], M. Musich[a,b], M.M. Obertino[a,c], N. Pastrone[a], M. Pelliccioni[a,b,1], A. Romero[a,b], M. Ruspa[a,c], R. Sacchi[a,b], V. Sola[a,b], A. Solano[a,b], A. Staiano[a], D. Trocino[a,b], A. Vilela Pereira[a,b,1]

INFN Sezione di Trieste [a], Università di Trieste [b], Trieste, Italy

F. Ambroglini[a,b], S. Belforte[a], F. Cossutti[a], G. Della Ricca[a,b], B. Gobbo[a], D. Montanino[a,b], A. Penzo[a]

Kangwon National University, Chunchon, Korea

S.G. Heo

Kyungpook National University, Daegu, Korea

S. Chang, J. Chung, D.H. Kim, G.N. Kim, J.E. Kim, D.J. Kong, H. Park, D. Son, D.C. Son

Chonnam National University, Institute for Universe and Elementary Particles, Kwangju, Korea

Zero Kim, J.Y. Kim, S. Song

Korea University, Seoul, Korea

S. Choi, B. Hong, M. Jo, H. Kim, J.H. Kim, T.J. Kim, K.S. Lee, D.H. Moon, S.K. Park, H.B. Rhee, E. Seo, S. Shin, K.S. Sim

University of Seoul, Seoul, Korea

M. Choi, S. Kang, H. Kim, C. Park, I.C. Park, S. Park, G. Ryu

Sungkyunkwan University, Suwon, Korea

Y. Choi, Y.K. Choi, J. Goh, J. Lee, S. Lee, H. Seo, I. Yu

Vilnius University, Vilnius, Lithuania

M.J. Bilinskas, I. Grigelionis, M. Janulis, D. Martisiute, P. Petrov, T. Sabonis

Centro de Investigacion y de Estudios Avanzados del IPN, Mexico City, Mexico

H. Castilla Valdez, E. De La Cruz Burelo, R. Lopez-Fernandez, A. Sánchez Hernández,

L.M. Villasenor-Cendejas

Universidad Iberoamericana, Mexico City, Mexico

S. Carrillo Moreno, F. Vazquez Valencia

Benemerita Universidad Autonoma de Puebla, Puebla, Mexico

H.A. Salazar Ibarguen

Universidad Autónoma de San Luis Potosí, San Luis Potosí, Mexico

E. Casimiro Linares, A. Morelos Pineda, M.A. Reyes-Santos

University of Auckland, Auckland, New Zealand

P. Allfrey, D. Krofcheck, J. Tam

University of Canterbury, Christchurch, New Zealand

P.H. Butler, R. Doesburg, H. Silverwood

National Centre for Physics, Quaid-I-Azam University, Islamabad, Pakistan

M. Ahmad, I. Ahmed, M.I. Asghar, H.R. Hoorani, W.A. Khan, T. Khurshid, S. Qazi

Institute of Experimental Physics, Faculty of Physics, University of Warsaw, Warsaw, Poland

M. Cwiok, W. Dominik, K. Doroba, A. Kalinowski, M. Konecki, J. Krolikowski

Soltan Institute for Nuclear Studies, Warsaw, Poland

T. Frueboes, R. Gokieli, M. Górski, M. Kazana, K. Nawrocki, K. Romanowska-Rybinska, M. Szleper, G. Wrochna, P. Zalewski

Laboratório de Instrumentação e Física Experimental de Partículas, Lisboa, Portugal

N. Almeida, A. David, P. Faccioli, P.G. Ferreira Parracho, M. Gallinaro, P. Martins,

P. Musella, A. Nayak, P.Q. Ribeiro, J. Seixas, P. Silva, J. Varela[1], H.K. Wöhri

Joint Institute for Nuclear Research, Dubna, Russia

I. Belotelov, P. Bunin, M. Finger, M. Finger Jr., I. Golutvin, A. Kamenev, V. Karjavin, G. Kozlov, A. Lanev, P. Moisenz, V. Palichik, V. Perelygin, S. Shmatov, V. Smirnov, A. Volodko, A. Zarubin

Petersburg Nuclear Physics Institute, Gatchina (St Petersburg), Russia

N. Bondar, V. Golovtsov, Y. Ivanov, V. Kim, P. Levchenko, V. Murzin, V. Oreshkin, I. Smirnov, V. Sulimov, L. Uvarov, S. Vavilov, A. Vorobyev

Institute for Nuclear Research, Moscow, Russia

Yu. Andreev, S. Gninenko, N. Golubev, M. Kirsanov, N. Krasnikov, V. Matveev, A. Pashenkov, A. Toropin, S. Troitsky

Institute for Theoretical and Experimental Physics, Moscow, Russia

V. Epshteyn, V. Gavrilov, V. Kaftanov†, M. Kossov[1], A. Krokhotin, N. Lychkovskaya, G. Safronov, S. Semenov, V. Stolin, E. Vlasov, A. Zhokin

Moscow State University, Moscow, Russia

E. Boos, M. Dubinin[18], L. Dudko, A. Ershov, A. Gribushin, O. Kodolova, I. Lokhtin, S. Obraztsov, S. Petrushanko, L. Sarycheva, V. Savrin, A. Snigirev

P.N. Lebedev Physical Institute, Moscow, Russia

V. Andreev, M. Azarkin, I. Dremin, M. Kirakosyan, S.V. Rusakov, A. Vinogradov

State Research Center of Russian Federation, Institute for High En-

ergy Physics, Protvino, Russia

I. Azhgirey, S. Bitioukov, V. Grishin[1], V. Kachanov, D. Konstantinov, A. Korablev, V. Krychkine, V. Petrov, R. Ryutin, S. Slabospitsky, A. Sobol, L. Tourtchanovitch, S. Troshin, N. Tyurin, A. Uzunian, A. Volkov

University of Belgrade, Faculty of Physics and Vinca Institute of Nuclear Sciences, Belgrade, Serbia

P. Adzic[19], M. Djordjevic, D. Krpic[19], J. Milosevic

Centro de Investigaciones Energéticas Medioambientales y Tecnológicas (CIEMAT Madrid, Spain

M. Aguilar-Benitez, J. Alcaraz Maestre, P. Arce, C. Battilana, E. Calvo, M. Cepeda, M. Cerrada, N. Colino, B. De La Cruz, C. Diez Pardos, C. Fernandez Bedoya, J.P. Fernández Ramos, A. Ferrando, J. Flix, M.C. Fouz, P. Garcia-Abia, O. Gonzalez Lopez, S. Goy Lopez, J.M. Hernandez, M.I. Josa, G. Merino, J. Puerta Pelayo, I. Redondo, L. Romero, J. Santaolalla, C. Willmott

Universidad Autónoma de Madrid, Madrid, Spain

C. Albajar, G. Codispoti, J.F. de Trocóniz

Universidad de Oviedo, Oviedo, Spain

J. Cuevas, J. Fernandez Menendez, S. Folgueras, I. Gonzalez Caballero, L. Lloret Iglesias, J.M. Vizan Garcia

Instituto de Física de Cantabria (IFCA), CSIC-Universidad de Cantabria, Santander, Spain

J.A. Brochero Cifuentes, I.J. Cabrillo, A. Calderon, M. Chamizo Llatas, S.H. Chuang, J. Duarte Campderros, M. Felcini[20], M. Fernandez, G. Gomez, J. Gonzalez Sanchez,

R. Gonzalez Suarez, C. Jorda, P. Lobelle Pardo, A. Lopez Virto, J. Marco, R. Marco, C. Martinez Rivero, F. Matorras, F.J. Munoz Sanchez, J. Piedra Gomez[21], T. Rodrigo, A. Ruiz Jimeno, L. Scodellaro, M. Sobron Sanudo, I. Vila, R. Vilar Cortabitarte

CERN, European Organization for Nuclear Research, Geneva, Switzerland

D. Abbaneo, E. Auffray, G. Auzinger, P. Baillon, A.H. Ball, D. Barney, A.J. Bell[22], D. Benedetti, C. Bernet[3], W. Bialas, P. Bloch, A. Bocci, S. Bolognesi, H. Breuker, G. Brona, K. Bunkowski, T. Camporesi, E. Cano, G. Cerminara, T. Christiansen, J.A. Coarasa Perez, R. Covarelli, B. Curé, D. D'Enterria, T. Dahms, A. De Roeck, F. Duarte Ramos, A. Elliott-Peisert, W. Funk, A. Gaddi, S. Gennai, G. Georgiou, H. Gerwig, D. Gigi, K. Gill, D. Giordano, F. Glege, R. Gomez-Reino Garrido, M. Gouzevitch, P. Govoni, S. Gowdy, L. Guiducci, M. Hansen, J. Harvey, J. Hegeman, B. Hegner, C. Henderson, H.F. Hoffmann, A. Honma, V. Innocente, P. Janot, E. Karavakis, P. Lecoq, C. Leonidopoulos, C. Lourenço, A. Macpherson, T. Mäki, L. Malgeri, M. Mannelli, L. Masetti, F. Meijers, S. Mersi, E. Meschi, R. Moser, M.U. Mozer, M. Mulders, E. Nesvold[1], M. Nguyen, T. Orimoto, L. Orsini, E. Perez, A. Petrilli, A. Pfeiffer, M. Pierini, M. Pimiä, G. Polese, A. Racz, G. Rolandi[23], T. Rommerskirchen, C. Rovelli[24], M. Rovere, H. Sakulin, C. Schäfer, C. Schwick, I. Segoni, A. Sharma, P. Siegrist, M. Simon, P. Sphicas[25], D. Spiga, M. Spiropulu[18], F. Stöckli, M. Stoye, P. Tropea, A. Tsirou, A. Tsyganov, G.I. Veres[12], P. Vichoudis, M. Voutilainen, W.D. Zeuner

Paul Scherrer Institut, Villigen, Switzerland

W. Bertl, K. Deiters, W. Erdmann, K. Gabathuler, R. Horisberger, Q. Ingram,

H.C. Kaestli, S. König, D. Kotlinski, U. Langenegger, F. Meier, D. Renker, T. Rohe, J. Sibille[26], A. Starodumov[27]

Institute for Particle Physics, ETH Zurich, Zurich, Switzerland

P. Bortignon, L. Caminada[28], Z. Chen, S. Cittolin, G. Dissertori, M. Dittmar, J. Eugster, K. Freudenreich, C. Grab, A. Hervé, W. Hintz, P. Lecomte, W. Lustermann, C. Marchica[28], P. Martinez Ruiz del Arbol, P. Meridiani, P. Milenovic[29], F. Moortgat, P. Nef, F. Nessi-Tedaldi, L. Pape, F. Pauss, T. Punz, A. Rizzi, F.J. Ronga, L. Sala, A.K. Sanchez, M.-C. Sawley, B. Stieger, L. Tauscher†, A. Thea, K. Theofilatos, D. Treille, C. Urscheler, R. Wallny[20], M. Weber, L. Wehrli, J. Weng

Universität Zürich, Zurich, Switzerland

E. Aguiló, C. Amsler, V. Chiochia, S. De Visscher, C. Favaro, M. Ivova Rikova, B. Millan Mejias, C. Regenfus, P. Robmann, A. Schmidt, H. Snoek, L. Wilke

National Central University, Chung-Li, Taiwan

Y.H. Chang, K.H. Chen, W.T. Chen, S. Dutta, A. Go, C.M. Kuo, S.W. Li, W. Lin, M.H. Liu, Z.K. Liu, Y.J. Lu, J.H. Wu, S.S. Yu

National Taiwan University (NTU), Taipei, Taiwan

P. Bartalini, P. Chang, Y.H. Chang, Y.W. Chang, Y. Chao, K.F. Chen, W.-S. Hou, Y. Hsiung, K.Y. Kao, Y.J. Lei, R.-S. Lu, J.G. Shiu, Y.M. Tzeng, M. Wang

Cukurova University, Adana, Turkey

A. Adiguzel, M.N. Bakirci, S. Cerci[30], C. Dozen, I. Dumanoglu, E. Eskut, S. Girgis, G. Gokbulut, Y. Guler, E. Gurpinar, I. Hos, E.E. Kangal, T. Karaman, A. Kayis Topaksu, A. Nart, G. Onengut, K. Ozdemir, S. Ozturk, A. Polatoz, K. Sogut[31], B. Tali, H. Topakli, D. Uzun, L.N. Vergili, M. Vergili, C. Zorbilmez

Middle East Technical University, Physics Department, Ankara, Turkey

I.V. Akin, T. Aliev, S. Bilmis, M. Deniz, H. Gamsizkan, A.M. Guler, K. Ocalan, A. Ozpineci, M. Serin, R. Sever, U.E. Surat, E. Yildirim, M. Zeyrek

Bogazici University, Istanbul, Turkey

M. Deliomeroglu, D. Demir[32], E. Gülmez, A. Halu, B. Isildak, M. Kaya[33], O. Kaya[33], M. Özbek, S. Ozkorucuklu[34], N. Sonmez[35]

National Scientific Center, Kharkov Institute of Physics and Technology, Kharkov, Ukraine

L. Levchuk

University of Bristol, Bristol, United Kingdom

P. Bell, F. Bostock, J.J. Brooke, T.L. Cheng, E. Clement, D. Cussans, R. Frazier, J. Goldstein, M. Grimes, M. Hansen, D. Hartley, G.P. Heath, H.F. Heath, B. Huckvale, J. Jackson, L. Kreczko, S. Metson, D.M. Newbold[36], K. Nirunpong, A. Poll, S. Senkin, V.J. Smith, S. Ward

Rutherford Appleton Laboratory, Didcot, United Kingdom

L. Basso, K.W. Bell, A. Belyaev, C. Brew, R.M. Brown, B. Camanzi, D.J.A. Cockerill, J.A. Coughlan, K. Harder, S. Harper, B.W. Kennedy, E. Olaiya, D. Petyt, B.C. Radburn-Smith, C.H. Shepherd-Themistocleous, I.R. Tomalin, W.J. Womersley, S.D. Worm

Imperial College, London, United Kingdom

R. Bainbridge, G. Ball, J. Ballin, R. Beuselinck, O. Buchmuller, D. Colling, N. Cripps, M. Cutajar, G. Davies, M. Della Negra, J. Fulcher, D. Futyan, A. Guneratne Bryer,

G. Hall, Z. Hatherell, J. Hays, G. Iles, G. Karapostoli, L. Lyons, A.-M. Magnan, J. Marrouche, R. Nandi, J. Nash, A. Nikitenko[27], A. Papageorgiou, M. Pesaresi, K. Petridis, M. Pioppi[37], D.M. Raymond, N. Rompotis, A. Rose, M.J. Ryan, C. Seez, P. Sharp, A. Sparrow, A. Tapper, S. Tourneur, M. Vazquez Acosta, T. Virdee, S. Wakefield, D. Wardrope, T. Whyntie

Brunel University, Uxbridge, United Kingdom

M. Barrett, M. Chadwick, J.E. Cole, P.R. Hobson, A. Khan, P. Kyberd, D. Leslie, W. Martin, I.D. Reid, L. Teodorescu

Baylor University, Waco, USA

K. Hatakeyama

Boston University, Boston, USA

T. Bose, E. Carrera Jarrin, A. Clough, C. Fantasia, A. Heister, J. St. John, P. Lawson, D. Lazic, J. Rohlf, D. Sperka, L. Sulak

Brown University, Providence, USA

A. Avetisyan, S. Bhattacharya, J.P. Chou, D. Cutts, S. Esen, A. Ferapontov, U. Heintz, S. Jabeen, G. Kukartsev, G. Landsberg, M. Narain, D. Nguyen, M. Segala, T. Speer, K.V. Tsang

University of California, Davis, Davis, USA

M.A. Borgia, R. Breedon, M. Calderon De La Barca Sanchez, D. Cebra, S. Chauhan, M. Chertok, J. Conway, P.T. Cox, J. Dolen, R. Erbacher, E. Friis, W. Ko, A. Kopecky, R. Lander, H. Liu, S. Maruyama, T. Miceli, M. Nikolic, D. Pellett, J. Robles, T. Schwarz, M. Searle, J. Smith, M. Squires, M. Tripathi, R. Vasquez Sierra, C. Veelken

University of California, Los Angeles, Los Angeles, USA

V. Andreev, K. Arisaka, D. Cline, R. Cousins, A. Deisher, J. Duris, S. Erhan[1], C. Farrell, J. Hauser, M. Ignatenko, C. Jarvis, C. Plager, G. Rakness, P. Schlein†, J. Tucker, V. Valuev

University of California, Riverside, Riverside, USA

J. Babb, R. Clare, J. Ellison, J.W. Gary, F. Giordano, G. Hanson, G.Y. Jeng, S.C. Kao, F. Liu, H. Liu, A. Luthra, H. Nguyen, G. Pasztor[38], A. Satpathy, B.C. Shen†, R. Stringer, J. Sturdy, S. Sumowidagdo, R. Wilken, S. Wimpenny

University of California, San Diego, La Jolla, USA

W. Andrews, J.G. Branson, E. Dusinberre, D. Evans, F. Golf, A. Holzner, R. Kelley, M. Lebourgeois, J. Letts, B. Mangano, J. Muelmenstaedt, S. Padhi, C. Palmer, G. Petrucciani, H. Pi, M. Pieri, R. Ranieri, M. Sani, V. Sharma[1], S. Simon, Y. Tu, A. Vartak, F. Würthwein, A. Yagil

University of California, Santa Barbara, Santa Barbara, USA

D. Barge, R. Bellan, C. Campagnari, M. D'Alfonso, T. Danielson, P. Geffert, J. Incandela, C. Justus, P. Kalavase, S.A. Koay, D. Kovalskyi, V. Krutelyov, S. Lowette, N. Mccoll, V. Pavlunin, F. Rebassoo, J. Ribnik, J. Richman, R. Rossin, D. Stuart, W. To, J.R. Vlimant

California Institute of Technology, Pasadena, USA

A. Bornheim, J. Bunn, Y. Chen, M. Gataullin, D. Kcira, V. Litvine, Y. Ma, A. Mott, H.B. Newman, C. Rogan, V. Timciuc, P. Traczyk, J. Veverka, R. Wilkinson, Y. Yang, R.Y. Zhu

Carnegie Mellon University, Pittsburgh, USA

B. Akgun, R. Carroll, T. Ferguson, Y. Iiyama, D.W. Jang, S.Y. Jun, Y.F. Liu, M. Paulini, J. Russ, N. Terentyev, H. Vogel, I. Vorobiev

University of Colorado at Boulder, Boulder, USA

J.P. Cumalat, M.E. Dinardo, B.R. Drell, C.J. Edelmaier, W.T. Ford, B. Heyburn, E. Luiggi Lopez, U. Nauenberg, J.G. Smith, K. Stenson, K.A. Ulmer, S.R. Wagner, S.L. Zang

Cornell University, Ithaca, USA

L. Agostino, J. Alexander, A. Chatterjee, S. Das, N. Eggert, L.J. Fields, L.K. Gibbons, B. Heltsley, W. Hopkins, A. Khukhunaishvili, B. Kreis, V. Kuznetsov, G. Nicolas Kaufman, J.R. Patterson, D. Puigh, D. Riley, A. Ryd, X. Shi, W. Sun, W.D. Teo, J. Thom, J. Thompson, J. Vaughan, Y. Weng, L. Winstrom, P. Wittich

Fairfield University, Fairfield, USA

A. Biselli, G. Cirino, D. Winn

Fermi National Accelerator Laboratory, Batavia, USA

S. Abdullin, M. Albrow, J. Anderson, G. Apollinari, M. Atac, J.A. Bakken, S. Banerjee, L.A.T. Bauerdick, A. Beretvas, J. Berryhill, P.C. Bhat, I. Bloch, F. Borcherding, K. Burkett, J.N. Butler, V. Chetluru, H.W.K. Cheung, F. Chlebana, S. Cihangir, M. Demarteau, D.P. Eartly, V.D. Elvira, I. Fisk, J. Freeman, Y. Gao, E. Gottschalk, D. Green, K. Gunthoti, O. Gutsche, A. Hahn, J. Hanlon, R.M. Harris, J. Hirschauer, B. Hooberman, E. James, H. Jensen, M. Johnson, U. Joshi, R. Khatiwada, B. Kilminster, B. Klima, K. Kousouris, S. Kunori, S. Kwan, P. Limon, R. Lipton, J. Lykken, K. Maeshima, J.M. Marraffino, D. Mason, P. McBride, T. McCauley,

T. Miao, K. Mishra, S. Mrenna, Y. Musienko[39], C. Newman-Holmes, V. O'Dell, S. Popescu[40], R. Pordes, O. Prokofyev, N. Saoulidou, E. Sexton-Kennedy, S. Sharma, A. Soha, W.J. Spalding, L. Spiegel, P. Tan, L. Taylor, S. Tkaczyk, L. Uplegger, E.W. Vaandering, R. Vidal, J. Whitmore, W. Wu, F. Yang, F. Yumiceva, J.C. Yun

University of Florida, Gainesville, USA

D. Acosta, P. Avery, D. Bourilkov, M. Chen, G.P. Di Giovanni, D. Dobur, A. Drozdetskiy, R.D. Field, M. Fisher, Y. Fu, I.K. Furic, J. Gartner, S. Goldberg, B. Kim, S. Klimenko, J. Konigsberg, A. Korytov, A. Kropivnitskaya, T. Kypreos, K. Matchev, G. Mitselmakher, L. Muniz, Y. Pakhotin, C. Prescott, R. Remington, M. Schmitt, B. Scurlock, P. Sellers, N. Skhirtladze, D. Wang, J. Yelton, M. Zakaria

Florida International University, Miami, USA

C. Ceron, V. Gaultney, L. Kramer, L.M. Lebolo, S. Linn, P. Markowitz, G. Martinez, J.L. Rodriguez

Florida State University, Tallahassee, USA

T. Adams, A. Askew, D. Bandurin, J. Bochenek, J. Chen, B. Diamond, S.V. Gleyzer, J. Haas, S. Hagopian, V. Hagopian, M. Jenkins, K.F. Johnson, H. Prosper, S. Sekmen, V. Veeraraghavan

Florida Institute of Technology, Melbourne, USA

M.M. Baarmand, B. Dorney, S. Guragain, M. Hohlmann, H. Kalakhety, R. Ralich, I. Vodopiyanov

University of Illinois at Chicago (UIC), Chicago, USA

M.R. Adams, I.M. Anghel, L. Apanasevich, Y. Bai, V.E. Bazterra, R.R. Betts, J. Callner, R. Cavanaugh, C. Dragoiu, E.J. Garcia-Solis, C.E. Gerber, D.J. Hofman,

S. Khalatyan, F. Lacroix, C. O'Brien, C. Silvestre, A. Smoron, D. Strom, N. Varelas

The University of Iowa, Iowa City, USA

U. Akgun, E.A. Albayrak, B. Bilki, K. Cankocak[41], W. Clarida, F. Duru, C.K. Lae, E. McCliment, J.-P. Merlo, H. Mermerkaya, A. Mestvirishvili, A. Moeller, J. Nachtman, C.R. Newsom, E. Norbeck, J. Olson, Y. Onel, F. Ozok, S. Sen, J. Wetzel, T. Yetkin, K. Yi

Johns Hopkins University, Baltimore, USA

B.A. Barnett, B. Blumenfeld, A. Bonato, C. Eskew, D. Fehling, G. Giurgiu, A.V. Gritsan, Z.J. Guo, G. Hu, P. Maksimovic, S. Rappoccio, M. Swartz, N.V. Tran, A. Whitbeck

The University of Kansas, Lawrence, USA

P. Baringer, A. Bean, G. Benelli, O. Grachov, M. Murray, D. Noonan, V. Radicci, S. Sanders, J.S. Wood, V. Zhukova

Kansas State University, Manhattan, USA

T. Bolton, I. Chakaberia, A. Ivanov, M. Makouski, Y. Maravin, S. Shrestha, I. Svintradze, Z. Wan

Lawrence Livermore National Laboratory, Livermore, USA

J. Gronberg, D. Lange, D. Wright

University of Maryland, College Park, USA

A. Baden, M. Boutemeur, S.C. Eno, D. Ferencek, J.A. Gomez, N.J. Hadley, R.G. Kellogg, M. Kirn, Y. Lu, A.C. Mignerey, K. Rossato, P. Rumerio, F. Santanastasio, A. Skuja, J. Temple, M.B. Tonjes, S.C. Tonwar, E. Twedt

Massachusetts Institute of Technology, Cambridge, USA

B. Alver, G. Bauer, J. Bendavid, W. Busza, E. Butz, I.A. Cali, M. Chan, V. Dutta, P. Everaerts, G. Gomez Ceballos, M. Goncharov, K.A. Hahn, P. Harris, Y. Kim, M. Klute, Y.-J. Lee, W. Li, C. Loizides, P.D. Luckey, T. Ma, S. Nahn, C. Paus, C. Roland, G. Roland, M. Rudolph, G.S.F. Stephans, K. Sumorok, K. Sung, E.A. Wenger, S. Xie, M. Yang, Y. Yilmaz, A.S. Yoon, M. Zanetti

University of Minnesota, Minneapolis, USA

P. Cole, S.I. Cooper, P. Cushman, B. Dahmes, A. De Benedetti, P.R. Dudero, G. Franzoni, J. Haupt, K. Klapoetke, Y. Kubota, J. Mans, V. Rekovic, R. Rusack, M. Sasseville, A. Singovsky

University of Mississippi, University, USA

L.M. Cremaldi, R. Godang, R. Kroeger, L. Perera, R. Rahmat, D.A. Sanders, D. Summers

University of Nebraska-Lincoln, Lincoln, USA

K. Bloom, S. Bose, J. Butt, D.R. Claes, A. Dominguez, M. Eads, J. Keller, T. Kelly, I. Kravchenko, J. Lazo-Flores, C. Lundstedt, H. Malbouisson, S. Malik, G.R. Snow

State University of New York at Buffalo, Buffalo, USA

U. Baur, A. Godshalk, I. Iashvili, A. Kharchilava, A. Kumar, S.P. Shipkowski, K. Smith

Northeastern University, Boston, USA

G. Alverson, E. Barberis, D. Baumgartel, O. Boeriu, M. Chasco, K. Kaadze, S. Reucroft, J. Swain, D. Wood, J. Zhang

Northwestern University, Evanston, USA

A. Anastassov, A. Kubik, N. Odell, R.A. Ofierzynski, B. Pollack, A. Pozdnyakov, M. Schmitt, S. Stoynev, M. Velasco, S. Won

University of Notre Dame, Notre Dame, USA

L. Antonelli, D. Berry, M. Hildreth, C. Jessop, D.J. Karmgard, J. Kolb, T. Kolberg, K. Lannon, W. Luo, S. Lynch, N. Marinelli, D.M. Morse, T. Pearson, R. Ruchti, J. Slaunwhite, N. Valls, J. Warchol, M. Wayne, J. Ziegler

The Ohio State University, Columbus, USA

B. Bylsma, L.S. Durkin, J. Gu, C. Hill, P. Killewald, K. Kotov, T.Y. Ling, M. Rodenburg, G. Williams

Princeton University, Princeton, USA

N. Adam, E. Berry, P. Elmer, D. Gerbaudo, V. Halyo, P. Hebda, A. Hunt, J. Jones, E. Laird, D. Lopes Pegna, D. Marlow, T. Medvedeva, M. Mooney, J. Olsen, P. Piroué, X. Quan, H. Saka, D. Stickland, C. Tully, J.S. Werner, A. Zuranski

University of Puerto Rico, Mayaguez, USA

J.G. Acosta, X.T. Huang, A. Lopez, H. Mendez, S. Oliveros, J.E. Ramirez Vargas, A. Zatserklyaniy

Purdue University, West Lafayette, USA

E. Alagoz, V.E. Barnes, G. Bolla, L. Borrello, D. Bortoletto, A. Everett, A.F. Garfinkel, Z. Gecse, L. Gutay, Z. Hu, M. Jones, O. Koybasi, A.T. Laasanen, N. Leonardo, C. Liu, V. Maroussov, P. Merkel, D.H. Miller, N. Neumeister, K. Potamianos, I. Shipsey, D. Silvers, A. Svyatkovskiy, H.D. Yoo, J. Zablocki, Y. Zheng

Purdue University Calumet, Hammond, USA

P. Jindal, N. Parashar

Rice University, Houston, USA

C. Boulahouache, V. Cuplov, K.M. Ecklund, F.J.M. Geurts, J.H. Liu, J. Morales, B.P. Padley, R. Redjimi, J. Roberts, J. Zabel

University of Rochester, Rochester, USA

B. Betchart, A. Bodek, Y.S. Chung, P. de Barbaro, R. Demina, Y. Eshaq, H. Flacher, A. Garcia-Bellido, P. Goldenzweig, Y. Gotra, J. Han, A. Harel, D.C. Miner, D. Orbaker, G. Petrillo, D. Vishnevskiy, M. Zielinski

The Rockefeller University, New York, USA

A. Bhatti, L. Demortier, K. Goulianos, G. Lungu, C. Mesropian, M. Yan

Rutgers, the State University of New Jersey, Piscataway, USA

O. Atramentov, A. Barker, D. Duggan, Y. Gershtein, R. Gray, E. Halkiadakis, D. Hidas, D. Hits, A. Lath, S. Panwalkar, R. Patel, A. Richards, K. Rose, S. Schnetzer, S. Somalwar, R. Stone, S. Thomas

University of Tennessee, Knoxville, USA

G. Cerizza, M. Hollingsworth, S. Spanier, Z.C. Yang, A. York

Texas A&M University, College Station, USA

J. Asaadi, R. Eusebi, J. Gilmore, A. Gurrola, T. Kamon, V. Khotilovich, R. Montalvo, C.N. Nguyen, J. Pivarski, A. Safonov, S. Sengupta, A. Tatarinov, D. Toback, M. Weinberger

Texas Tech University, Lubbock, USA

N. Akchurin, C. Bardak, J. Damgov, C. Jeong, K. Kovitanggoon, S.W. Lee, P. Mane,

Y. Roh, A. Sill, I. Volobouev, R. Wigmans, E. Yazgan

Vanderbilt University, Nashville, USA

E. Appelt, E. Brownson, D. Engh, C. Florez, W. Gabella, W. Johns, P. Kurt, C. Maguire, A. Melo, P. Sheldon, J. Velkovska

University of Virginia, Charlottesville, USA

M.W. Arenton, M. Balazs, S. Boutle, M. Buehler, S. Conetti, B. Cox, B. Francis, R. Hirosky, A. Ledovskoy, C. Lin, C. Neu, R. Yohay

Wayne State University, Detroit, USA

S. Gollapinni, R. Harr, P.E. Karchin, M. Mattson, C. Milstène, A. Sakharov

University of Wisconsin, Madison, USA

M. Anderson, M. Bachtis, J.N. Bellinger, D. Carlsmith, S. Dasu, J. Efron, L. Gray, K.S. Grogg, M. Grothe, R. Hall-Wilton[1], M. Herndon, P. Klabbers, J. Klukas, A. Lanaro, C. Lazaridis, J. Leonard, D. Lomidze, R. Loveless, A. Mohapatra, W. Parker, D. Reeder, I. Ross, A. Savin, W.H. Smith, J. Swanson, M. Weinberg

†: Deceased

1: Also at CERN, European Organization for Nuclear Research, Geneva, Switzerland

2: Also at Universidade Federal do ABC, Santo Andre, Brazil

3: Also at Laboratoire Leprince-Ringuet, Ecole Polytechnique, IN2P3-CNRS, Palaiseau, France

4: Also at Suez Canal University, Suez, Egypt

5: Also at Fayoum University, El-Fayoum, Egypt

6: Also at Soltan Institute for Nuclear Studies, Warsaw, Poland

7: Also at Massachusetts Institute of Technology, Cambridge, USA

8: Also at Université de Haute-Alsace, Mulhouse, France

9: Also at Brandenburg University of Technology, Cottbus, Germany

10: Also at Moscow State University, Moscow, Russia

11: Also at Institute of Nuclear Research ATOMKI, Debrecen, Hungary

12: Also at Eötvös Loránd University, Budapest, Hungary

13: Also at Tata Institute of Fundamental Research - HECR, Mumbai, India

14: Also at University of Visva-Bharati, Santiniketan, India

15: Also at Facolta' Ingegneria Università di Roma "La Sapienza", Roma, Italy

16: Also at Università della Basilicata, Potenza, Italy

17: Also at Laboratori Nazionali di Legnaro dell' INFN, Legnaro, Italy

18: Also at California Institute of Technology, Pasadena, USA

19: Also at Faculty of Physics of University of Belgrade, Belgrade, Serbia

20: Also at University of California, Los Angeles, Los Angeles, USA

21: Also at University of Florida, Gainesville, USA

22: Also at Université de Genève, Geneva, Switzerland

23: Also at Scuola Normale e Sezione dell' INFN, Pisa, Italy

24: Also at INFN Sezione di Roma; Università di Roma "La Sapienza", Roma, Italy

25: Also at University of Athens, Athens, Greece

26: Also at The University of Kansas, Lawrence, USA

27: Also at Institute for Theoretical and Experimental Physics, Moscow, Russia

28: Also at Paul Scherrer Institut, Villigen, Switzerland

29: Also at University of Belgrade, Faculty of Physics and Vinca Institute of Nu-

clear Sciences, Belgrade, Serbia

30: Also at Adiyaman University, Adiyaman, Turkey

31: Also at Mersin University, Mersin, Turkey

32: Also at Izmir Institute of Technology, Izmir, Turkey

33: Also at Kafkas University, Kars, Turkey

34: Also at Suleyman Demirel University, Isparta, Turkey

35: Also at Ege University, Izmir, Turkey

36: Also at Rutherford Appleton Laboratory, Didcot, United Kingdom

37: Also at INFN Sezione di Perugia; Università di Perugia, Perugia, Italy

38: Also at KFKI Research Institute for Particle and Nuclear Physics, Budapest, Hungary

39: Also at Institute for Nuclear Research, Moscow, Russia

40: Also at Horia Hulubei National Institute of Physics and Nuclear Engineering (IFIN-HH), Bucharest, Romania

41: Also at Istanbul Technical University, Istanbul, Turkey

Bibliography

[1] A. Lahiri and P.B. Pal, *A First Book of Quantum Field Theory*, second edition; Alpha Science International (2005)

[2] Sakurai, J.J., *Modern Quantum Mechanics*, revised edition, Addison-Wesley (1994).

[3] Perkins, D.H., *Introduction to High Energy Physics*, Cambridge University Press (2000).

[4] K. Nakamura et al. (Particle Data Group), *J. Phys. G* **37** (2010) 075021, doi:10.1088/0954-3899/37/7A/075021.

[5] Tata, X., "What Is Supersymmetry And How Do We Find It?", arXiv:hep-ph/9706307v1 (1997).

[6] T. Jittoh, J. Sato, T. Shimomura, and M. Yamanaka, "Long Life Stau in the Minimum Supersymmetric Standard Model", *Phys. Rev. D* **73** (2006) 055009, arXiv:hep-ph/0512197. doi:10.1103/PhysRevD.73.055009.

[7] S. Dimopoulis, M. Dine, S. Raby, and S. Thomas, "Experimental Signatures of Low Energy Gauge Mediated Supersymmetry Breaking", *Phys. Rev. Lett.* **76** (1996) 3494-3497, arXiv:hep-ph/9601367. doi:10.1103/PhysRevLett.76.3494.

[8] M.J. Strassler and K.M. Zurek, "Echoes of a Hidden Valley at Hadron Colliders", *Phys. Lett. B* **651** (2007) 374-379, arXiv:hep-ph/0604261. doi:10.1016/j.physletb.2007.06.055.

[9] M.J. Strassler, "Possible Effects of a Hidden Valley on Supersymmetric Phenomenology", arXiv:hep-ph/0607160 (2006).

[10] A. Arvanitaki et al., "Astrophysical Probes of Unification", *Phys. Rev. D* **79** (2009) 105022, arXiv:0812.2075. doi:10.1103/PhysRevD.79.105022.

[11] Jedamzik, K., "Did Something Decay, Evaporate, or Annihilate During Big Bang Nucleosynthesis?", *Phys. Rev. D* **70** (2004) 063524, doi:10.1103/PhysRevD.70.063524.

[12] K. Jedamzik, K. Choi, L. Roszkowski, and R. Ruiz de Austri, "Solving the Cosmic Lithium Problems with Gravitino Dark Matter in the Constrained Minimal

Supersymmetric Standard Model", *J. Cosmol. Astropart. Phys.* **07** (2006) 007, doi:10.1088/1475-7516/2006/07/007.

[13] S. Bailey, K. Jedamzik, and G. Moultaka, "Gravitino Dark Matter and the Cosmic Lithium Abundances", *Phys. Rev. D* **80** (2009) 063509, doi:10.1103/PhysRevD.80.063509.

[14] DØ Collaboration, "Search for Stopped Gluinos from $p\bar{p}$ Collisions at $\sqrt{s}$ = 1.96-TeV", *Phys. Rev. Lett.* **99** (2007) 131801, arXiv:0705.0306. doi:10.1103/PhysRevLett.99.131801.

[15] CMS Collaboration, "Reference Page for Top-Quark Analyses: Samples and Cross-Sections", collaboration-internal web page: https://twiki.cern.ch/twiki/bin/viewauth/CMS/CrossSections_3XSeries. Retrieved Jan. 2011.

[16] A.D. Martin, R.G. Roberts, W.J. Sterling, and R.S. Thorne, "Parton Distributions and the LHC: W and Z Production", *Eur. Phys. J. C* **14** (2000) 133-145, arXiv:hep-ph/9907231v1. doi:10.1007/s100520000324.

[17] LHC Design Report, Vol. I, Ch. 2 *Beam Parameters and Definitions*

[18] LHC Design Report, Vol. I, Ch. 3 *Layout and Performance*

[19] LHC Design Report, Vol. I, Ch. 7 *Main Magnets in the Arcs*

[20] LHC Design Report, Vol. III, Ch. 1 *Introduction, The Proton Pre-Injectors*

[21] LHC Design Report, Vol. III, Ch. 7 *Bunch Splitting and Bunch Rotation in the PS*

[22] LHC Design Report, Vol. III, Ch. 9 *Transverse Emittance Conservation and Measurement*

[23] LHC Design Report, Vol. III, Ch. 11 *Introduction, The SPS as LHC Injector*

[24] C.E. Hill et al., "CERN Hadron Linacs", http://linac2.home.cern.ch/linac2/default.htm. Retrieved Dec. 2007.

[25] R. Bailey and P. Collier, "Standard Filling Schemes for Various Operation Modes (Revised)", LHC Project Note 323 (2003).

[26] LHC Program Coordinator, "LHC Filling Schemes". http://lpc.web.cern.ch/lpc/fillingschemes.htm. Retrieved Jan. 2011.

[27] M. Ferro-Luzzi, W. Herr, and T. Pieloni, "LHC Bunch Filling Schemes for Commissioning and Initial Luminosity Optimization", LHC Project Note 415 (2008).

[28] The ATLAS Experiment, http://atlas.ch. Retrieved Jan. 2008.

[29] The Compact Muon Solenoid Experiment, http://cms.cern.ch. Retrieved Jan. 2008.

[30] The ALICE Experiment Public Pages, http://aliceinfo.cern.ch/Public. Retrieved Jan. 2008.

[31] LHCb Public Home Webpage, http://lhcb-public.web.cern.ch/lhcb-public/. Retrieved Jan. 2008.

[32] CERN Press Office, "CERN Announces New Start-Up Schedule for Worlds Most Powerful Particle Accelerator", http://press.web.cern.ch/press/PressReleases/Releases2007/PR06.07E.html. Jun. 22, 2007.

[33] DeSalvo, Riccardo, "Why People Like the Hybrid Photodiode", *Nucl. Instrum. Meth. A* **387** (1997) 92-96, doi:10.1016/S0168-9002(96)00969-2.

[34] P. Cushman, A. Heering and A. Ronzhin, "Custom HPD Read-out for the CMS HCAL", *Nucl. Instrum. Meth. A* **442** (2000) 289, doi:10.1016/S0168-9002(99)01236-X.

[35] CMS Collaboration, "The CMS Experiment at the CERN LHC", *JINST* **3** (2008) S08004, doi:10.1088/1748-0221/3/08/S08004.

[36] CMS Collaboration, "Identification and Filtering of Uncharacteristic Noise in the CMS Hadron Calorimeter", *JINST* **5** (2010) T03014, arXiv:0911.4881v3. doi:10.1088/1748-0221/5/03/T03014.

[37] CMS Collaboration, "Performance of Jet Algorithms in CMS", CMS Physics Analysis Summary JME-07-003 (2008).

[38] M Cacchiari, G. Salam, and G. Soyez, "The Anti-kt Jet Clustering Algorithm", *JHEP* **04** (2008) 063, doi:10.1088/1126-6708/2008/04/063.

[39] CMS Collaboration, "Measurement of CMS Luminosity", CMS Physics Analysis Summary EWK-10-004 (2010).

[40] CMS Collaboration, "Performance of CMS Muon Reconstruction in Cosmic-Ray Events", *JINST* **5** (2010) T03022, doi:10.1088/1748-0221/5/03/T03022.

[41] T. Sjostrand, S. Mrenna, and P. Z. Skands, "PYTHIA 6.4 Physics and Manual", *JHEP* **05** (2006) 026, arXiv:hep-ph/0603175. doi:10.1088/1126-6708/2006/05/026.

[42] GEANT4 Collaboration, "GEANT4: A Simulation Toolkit", *Nucl. Instrum. Meth. A* **506** (2003) 250-303, doi:10.1016/S0168-9002(03)01368-8.

[43] CMS Collaboration, "CMS Computing: Technical Design Report", CERN-LHCC-2005-023

[44] R. Mackeprang and A. Rizzi, "Interactions of Coloured Heavy Stable Particles in Matter", *Eur. Phys. J. C* **50** (2007) 353-362, arXiv:hep-ph/0612161. doi:10.1140/epjc/s10052-007-0252-4.

[45] R. D. Cousins and V.L. Highland, "Incorporating Systematic Uncertainties into an Upper Limit", *Nucl. Instrum. Meth. A* **320** (1992) 331-335, doi:10.1016/0168-9002(92)90794-5.

[46] W. Beenakker, S. Brensing, M. Kramer, A. Kulesza, E. Laenen and I. Niessen, "Soft-Gluon Resummation for Squark and Gluino Hadroproduction", *JHEP* **0912** (2009) 041, arXiv:0909.4418v1. doi:10.1088/1126-6708/2009/12/041.

[47] W. Beenakker, S. Brensing, M. Kramer, A. Kulesza, E. Laenen and I. Niessen, private communication. 2010.

[48] F. Buccella, G.R. Farrar and A. Pugliese, "R-Baryon Masses", *Phys. Lett. B* **153** (1985) 311, doi:10.1016/0370-2693(85)90555-6.

[49] https://twiki.cern.ch/twiki/bin/view/RooStats

[50] CMS Collaboration, "Search for Heavy Stable Charged Particles in pp Collisions at 7 TeV", CMS Physics Analysis Summary EXO-10-004 (2010).